BEHAVIOR AND ANALYSIS OF AN INTEGRAL ABUTMENT BRIDGE

Paul J. Barr
Marv W. Halling
Conner Huffaker
Hugh Boyle

Utah State University
Department of Civil and Environmental Engineering
Logan, Utah

September 2013

Acknowledgements

The authors acknowledge the Utah Department of Transportation (UDOT) for funding this research, and the following individuals from UDOT on the Technical Advisory Committee for helping to guide the research:

- Abdul Wakil
- Hugh Boyle
- Russ Scovil
- Joshua Sletten
- Carmen Swanwick

Disclaimer

The authors alone are responsible for the preparation and accuracy of the information, data, analysis, discussions, recommendations, and conclusions presented herein. The contents do not necessarily reflect the views, opinions, endorsements, or policies of the Utah Department of Transportation or the U.S. Department of Transportation. The Utah Department of Transportation makes no representation or warranty of any kind, and assumes no liability therefore.

TABLE OF CONTENTS

LIST OF FIGURES

EXECUTIVE SUMMARY

As part of a study to develop design guidelines for integral abutment bridges, a study was undertaken in which the bridge movement of the 400 South Street Bridge was surveyed for one year to quantify changes in bridge movement due to temperature variations. These quantitative bridge movements were compared to predicted behavior from a finite-element model. The model was subsequently used to determine likely causes of cracking stresses in the 400 South Street Bridge north abutment. The modeling scheme was further implemented to investigate the influence that various bridge parameters have on the integral abutment stresses. This final report presents the survey and finite element analyses of the investigation. These findings will be used to develop design guidelines for integral abutment bridges.

In order to quantify the influence of temperature changes on the 400 South Street Bridge, 32 Sokkia RS30N reflective targets were strategically attached to the bridge at various locations along its length. Eight targets were attached near the joints at the approach slab such that one target was positioned on each side of the joint at all four corners of the bridge. Three targets in a vertical line were used on each of the exterior girders directly adjacent to each abutment. The remaining 12 targets were implemented by attaching three targets in a vertical line at the middle of the pier diaphragm directly above each side of both bents. The targets placed in groups of three were approximately located at the top, middle, and bottom of the section. These targets were surveyed every month for 12 consecutive months during the early morning hours. The average difference between the maximum recorded length measured and the minimum recorded length measured was 17.52 mm (0.690 in.) for the east side of Span 1, 18.42 mm (0.725 in.) for the west side of Span 1, 10.51 mm (0.414 in.) for the west side of Span 3, and 10.67 mm (0.420 in.) for the east side of Span 3. These changes in length coincided with restraint conditions between purely fixed and simply supported. Movement of expansion joints was also recorded. The movements of the expansion gaps at opposite corners appear to exhibit similar movements. This behavior indicates a type of twisting motion occurring within the bridge as a result of unequal movements at the east and west sides of each abutment. This motion suggests that the bridge abutments experience forces that incite weak axis bending in the abutments, especially in the north abutment.

A detailed finite-element model of the bridge was created using SAP2000 (Computers and Structures, Inc.) software. A detailed model was developed using solid elements for all components of the bridge except piles and bents. Longitudinal surface springs were placed at the abutment elements in order to simulate the soil-abutment interaction. A typical temperature load was assigned to the bridge deck and girder elements to compare the calculated stress concentrations in the model with the observed cracking on the abutment on the 400 South Street Bridge. The model produced high stress concentrations in the abutment adjacent to the bottom girder flange, which was the same location of observed cracking. The finite-element model also showed lateral movement of the abutment. This lateral abutment explains the unequal movements of the bridge spans.

Once the comparison between the measured bridge behavior of the survey and the findings of the detailed finite element model was completed, a simplified model was used to evaluate the bending moment and stresses in the abutment of the 400 South Street Bridge. The model was also used to perform a parametric study on the influence of skew, span length, and temperature gradient. The study provided the basis for the following conclusions:

1. Bridge Movement - In general, expansion and contraction of the 400 South Street Bridge was observed as temperature increased and decreased, respectively. The observed movements were unequal when comparing the east and west sides of the bridge. Through finite-element analyses, this unequal movement is believed to be a result of lateral movement at the skewed support of the north abutment. Reduction of the lateral movement would reduce tensile stress in the abutment.

2. Skew – As little as a 5º increase in skew angle can significantly increase the weak axis bending moment of the bridge abutment.
3. Length – As the span length increases by a factor of 2, an approximate 60% increase in weak-axis bending moment in the bridge abutments was observed.
4. Temperature Gradient – Temperature gradients, in combination with uniform temperature changes, influence the stresses in the bridge abutments. A 20 °F increase in temperature difference between the girders and deck of the bridge can cause an increase in the stresses observed in the bridge abutments. The influence of temperature gradients on abutment stresses should be investigated.
5. The abutment cracking of the 400 South Street Bridge is likely a result of a combination of bridge parameters. These properties include a combination of skew, curvature, span length, and detailing. Integral abutment bridges with more than one of these conditions require additional design checks.
6. Finite element models can predict localized and global increases in demand on integral abutments.

1. INTRODUCTION

1.1 CONTEXT

Integral abutment bridges possess a number of unique design details that make them desirable in many applications. Integral abutment bridges can be single-span or multi-span. These bridges are constructed without expansion joints within the superstructure of the bridge. The superstructure is constructed integrally with the abutments. Normally these abutments are supported by rows of vertically driven piles.

Integral abutment bridges eliminate the use of moveable joints and the expensive maintenance or replacement costs that go with them. The overall design of integral abutment bridges is simpler than that of their non-integral counterparts. The simplicity of these bridges allows for rapid construction. These bridges have proven themselves in earthquakes and performance studies. The advantages of integral abutment bridges make them the preferred choice for many departments of transportation throughout the United States.

The Utah Department of Transportation (UDOT) has successfully used integral abutment bridges for a variety of applications throughout the state. One such bridge exists over 400 South Street in Salt Lake City. This bridge has curved and skewed geometry. The north abutment of this bridge began to show signs of cracking and spalling adjacent to the bridge girders. UDOT initiated a study of this bridge in order to better understand the source of the cracking and spalling of the north abutment. Consequently, a year-long bridge survey was conducted and a parametric study was performed using a series of finite element models. These serve to explain the observed behavior of the 400 South Street Bridge and develop guidelines for future applications of integral abutment bridges in the state of Utah.

1.2 400 SOUTH STREET BRIDGE

The bridge investigated is situated over 400 South Street in Salt Lake City just east of the Interstate-15 corridor. The bridge facilitates flow of traffic from 500 South Street and from northbound I-15 onto Interstate-80 westbound toward Sat Lake City International Airport. The three-span bridge exceeds 300 feet in length and has a curved and skewed geometry. This bridge was selected for study due to the presence of cracking at the north abutment.

1.3 RESEARCH OBJECTIVES

The general objectives of this report are as follows:

- Develop a comprehensive literature review concerning implementation of integral abutment bridges.
- Document the findings of a monthly-obtained year-long survey taken of the 400 South Street Bridge.
- Present the development and results of a finite element model of the 400 South Street Bridge.
- Outline the effects of skew, bridge length, and soil conditions as obtained by a parametric study finite element model.
- Provide conclusions and recommendations useful in the future application of integral abutment bridges in the state of Utah.

1.4 OUTLINE OF REPORT

The organization of this report is as follows:

Section 2 presents a literature review containing information about integral abutment bridges in general, as well as research that has been done regarding integral abutment bridge behavior.

Section 3 describes the dimensions and properties of the bridge used in this study. It also presents the details and results of the thermal analysis study conducted through surveying and the finite-element model of the bridge.

Section 4 describes the finite element model developed for the bridge used in this study. A parametric study is also contained therein.

Section 5 includes a summary of the content of this report, as well as conclusions and recommendations regarding this bridge and the future application of integral abutment bridges.

2. LITERATURE REVIEW

2.1 HISTORICAL BACKGROUND

Integral abutment bridges have been built throughout the United States since the 1930s and have since become more common, especially for bridges with short, continuous spans. An integral abutment bridge is designed without the use of expansion joints in the bridge deck. This requires the bridge and abutment to be detailed so that the developed loads during expansion and contraction will be resisted by its members. This jointless design allows for lower installation and maintenance costs by avoiding costly bearings and the inevitable maintenance they require. This design philosophy has evolved since its introduction in the United States and has improved through the individual experience of various states in constructing these integral bridges.

Current trends regarding integral construction originated in 1930 when Professor Hardy Cross presented a method for analysis of integral-type structures following a publication on distributing fixed end moments for continuous frames. Based on Cross's methods, bridge design began moving toward continuous construction. The Ohio Highway Department, now Ohio DOT, was one of the first agencies to embrace the use of continuous construction. Methods for achieving continuity evolved from riveted field splices to field butt welding and then to high-strength bolting, which became the method of choice for the Ohio DOT in 1963. These various methods have given the Ohio DOT more than 70 years of experience in continuous construction. In conjunction with their practice of continuous construction, the Ohio DOT was the first state to routinely eliminate deck joints at abutments. This configuration implemented the use of flexible piles as abutment supports instead of movable deck joints and was designated as an integral abutment. The Ohio DOT used a modified version of this design in several hundred bridges and applied the integral abutment concept to a steel beam bridge in the early 1960s. Since that time, most steel beam and girder bridges with skew angles less than 30° and lengths less than approximately 300 feet were designed with integral construction when conditions permitted. The Ohio DOT also pioneered the use of prestressed concrete girders for highway bridges. Subsequently, other states followed suit by implementing integral abutments for continuous construction and by 1987, 87% (26 of 30) of responding transportation departments indicated that they were using continuous construction for short- and moderate-length bridges. Gradual design changes in the Ohio DOT and other state agencies allowed for longer integral abutment bridges based upon the positive maintenance performance. The Tennessee DOT currently is regarded as the leader in continuous integral abutment bridge construction, building a continuous bridge in 1980 with a length of 2,700 feet center-to-center of the abutment bearings. Continuous integral abutment bridges with concrete substructure members ranging from 500- to 800-ft long have also been constructed in Kansas, California, Colorado, and Tennessee. Continuous integral bridges with steel substructure members in the 300-feet range have had few maintenance problems for years in such states as North Dakota, South Dakota, and Tennessee (Burke, 2009).

In conventionally designed bridges, expansion joints and bearing details are required in the bridge deck and at the abutments as shown in Figures 2.1 and 2.2 (Soltani 1992). These details have been found to have a tendency to deteriorate and freeze up, leading to large maintenance and/or replacement costs. Failure of these expansion devices can also introduce large stresses that were not considered in the design and can damage the superstructure. In many cases (Burke 2009), "significantly more damage and distress have been caused by the use of movable deck joints at piers and abutments than the secondary stresses that these joints were intended to prevent." These expansion details are the primary source of maintenance and performance issues in this type of bridge. Thus, the main goal of an integral abutment bridge is to eliminate the expansion joints and bearings completely. Eliminating bearings decreases installation costs and the long-term maintenance costs that have been found to be associated with conventional bridges. The complete removal of these components is accomplished by creating a structural connection between the

bridge superstructure and abutments. The connection details between the superstructure and abutments vary depending on the individual states or agencies and according to the bridge material. Some examples of abutment configuration for various states are shown in Figure 2.3 (Soltani 1992). The abutments can be supported on spread footings or on driven piles or drilled shafts. It is also common to structurally connect an approach slab to many integral abutment bridges. This connection allows for a smooth transition between the bridge and approach embankment. A notable variation of the integral abutment bridge design is a semi-integral abutment bridge. In this bridge configuration, expansion joints in the deck are still eliminated but girder bearings are still placed at the abutments. The important improvement from a conventional bridge is that the superstructure extends over the top of the abutment, thus protecting the bearing and reducing long-term maintenance costs (Horvath 2000).

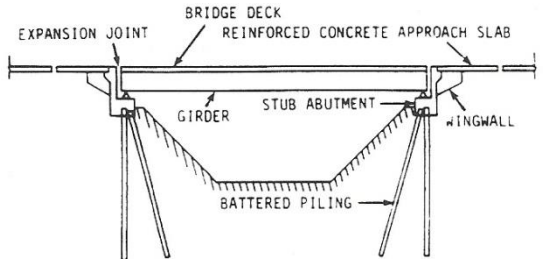

Figure 2.1 Cross Section of Bridge with Expansion Joints

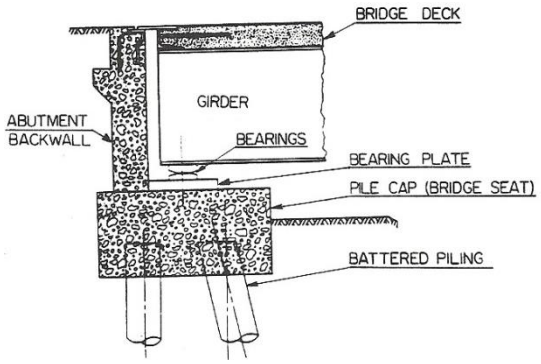

Figure 2.2 Abutment Detail of Bridge with Expansion Joints

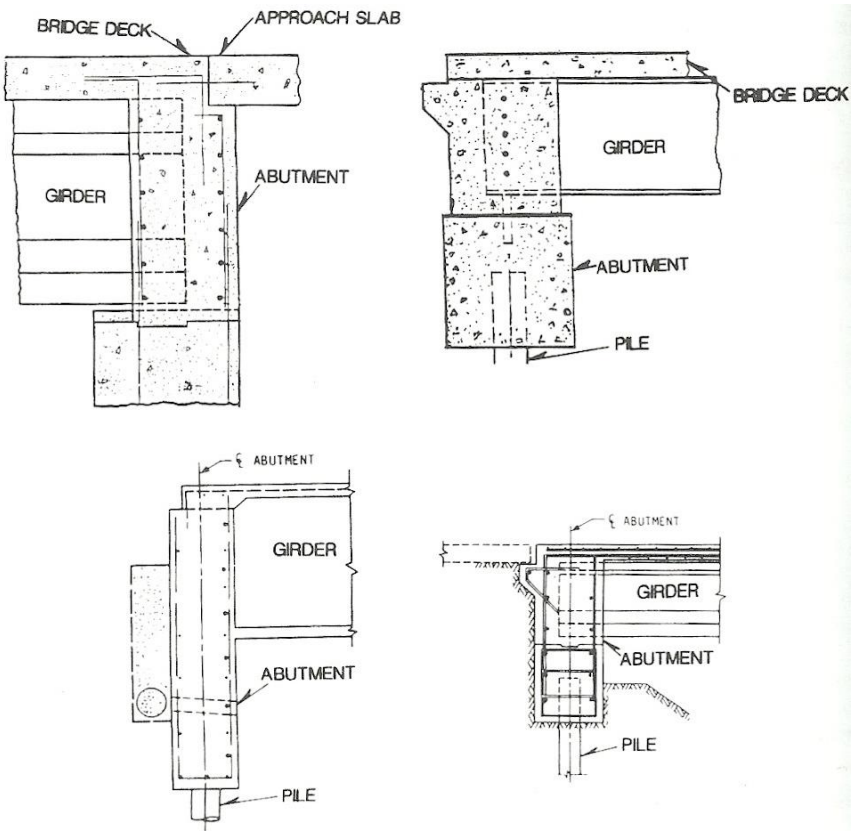

Figure 2.3 Integral Abutment Details

The desirable attributes of integral bridges are accompanied by some concerns about relatively high unit stresses. Many integral bridge components function under loading conditions that result in high stress levels. However, many bridge engineers would still rather build a cheaper integral bridge and design for the higher stresses rather than design and build costly jointed bridges with lower stress levels. The Tennessee DOT, for example, applies integral abutment bridge designs whenever bridge conditions will permit. The Tennessee DOT's design policy states, "When the total anticipated movement at an abutment is less than two (2) inches [50 mm] and the abutment is not restrained against movement, no joint will be required and the superstructure and abutment beam will be constructed integrally." They have determined that the toleration of these high stresses in some cases results in relatively minor structural distress. Some causes of concern due to these high stresses include visible distress in steel piles, minor cracks in bridge abutment wingwalls, and pile cap cracking. These problems have been found to be correctable with more generous wingwall reinforcement, providing more substantial pile cap connection reinforcement, and orienting steel H-piles with the weak axis normal to the direction of the bridge longitudinal movement. In addition, precast prestressed concrete and prefabricated steel superstructures are a viable way to overcome problems associated with the initial concrete shrinkage of superstructures that exists in cast-in-place bridges. Some additional damage may be caused by the pavement growth/pressure phenomenon that should be appropriately considered in the design of an integral bridge. When properly designed, these bridges can usually withstand the pressures generated by both pavements and bridges (Burke 2009).

2.2 GEOTECHNICAL ISSUES WITH INTEGRAL ABUTMENT BRIDGES

According to John S. Horvath of The Manhattan College School of Engineering (2000), there are two commonly encountered problems inherent in the design of integral abutment bridges that are not structural in nature but, rather, geotechnical. The cyclic loading of the bridge superstructure due to daily changes in temperature causes the abutments to rotate about the base and translate into the soil, thus developing considerable lateral earth pressure on the abutments. The magnitude of these soil pressures can approach or reach the passive state in the summer when bridge expansion is highest. Passive earth pressures are large in magnitude and may exceed the normally consolidated at-rest state for which an abutment should normally be designed by at least an order of magnitude. Failure to design the abutment for the larger pressures that develop during bridge thermal expansion can cause structural damage to the abutment. Adversely, the cost to properly design the abutment subjected to these higher forces will increase. In winter months, the bridge contracts and the pressure on the abutments can develop into the active condition. As the abutment moves away from the soil, a wedge of soil is commonly displaced near the top of the abutment. As a result, a void may form beneath the approach slab (if used) and settlement results in a bump at the end of the bridge. Over time, the movement of the soil toward the abutment results in a buildup of lateral earth pressure as the soil becomes effectively wedged behind the abutment. This phenomenon is referred to as "ratcheting" and may result in eventual failure of the abutment or the approach slab. Both these problems have a common source to which Horvath proposes possible geotechnical solutions involving a "compressible inclusion" behind the abutment. This compressible inclusion would create an allowance for expansion and lateral earth pressure without the problems caused by movement and settlement of the backfill material. A simply structural solution would be to shorten the abutment height. In this case, the lateral earth pressures would continue to increase in the summer, but the total resultant force and flexural stresses would be lessened. Some experiences with the application of a compressible inclusion show that this does not eliminate the tendency for the material to slump toward the abutment in the winter months when the bridge contracts and the abutment moves away from the backfill. In order to eliminate both problems, Horvath proposes the use of a mechanically stabilized earth wall or a geofoam compressible inclusion. In his opinion, the best way to apply the geofoam is described as a wedge-shaped mass that would effectively create a geofoam wall next to the abutment. Using this geofoam configuration would help with both the settlement behind the abutment and the tendency toward ratcheting behavior (Horvath 2000).

A number of limitations and guidelines that have been presented in order to avoid passive pressure as well as relatively high-pile stresses, are available. Practices to minimize the development of passive pressure include limiting the length, skew, abutment type, abutment details, and backfill material. The use of approach slabs is encouraged, in addition to the use of a well-drained granular backfill protected by approach slab curbs, turn-back wingwalls, and embankment-supported stub abutment types. The issue of high-pile stresses is addressed by using a single row of slender vertical piles, with steel H-piles expressed as the most suitable for longer applications (>300 ft). Orienting these piles with the weak axis normal to the direction of flexure, as well as providing pre-bored holes filled with granular material, also help control this issue. The use of an abutment hinge, and limiting the pile type, bridge length, and skew (typically less than 30°) of the structure, are encouraged to limit pile flexure. Most of the usual steel or well-reinforced prestressed concrete piles can be used for short integral bridges (<300 ft). The use of semi-integral abutments is a viable solution to limit these effects. Other slight concerns include minor wingwall cracks, which can be corrected with more generous wingwall reinforcement, and pile cap cracking, which has been eliminated by providing greater pile cap connection reinforcement and by rotating steel H-piles to place the weak axis normal to the direction of longitudinal bridge movement (Burke 2009).

2.3 DESIGN DETAILS

In 1992, the Transportation Research Record contained a "Performance Evaluation of Integral Abutment Bridges" by Alan A. Soltani and Anant R. Kukreti, which focused specifically on bridges with no skew (90º bridges). It contains a questionnaire issued to every department of transportation across the United States in which 29 of the 38 responding states indicated use of integral abutment bridges. Most of these states had developed their own specific guidelines regarding allowable bridge lengths, but these guidelines are largely empirical and based on observed past performance. The study shows that design practices used by many states may be too conservative, and much longer bridges could be constructed with little impact to their performance. The design and construction details of five states considered to be pioneers in their implementation of integral abutment bridges were further evaluated and will be discussed below.

2.3.1 Tennessee

Tennessee has had extensive experience and is the apparent forerunner in the use of relatively long-span integral abutment bridges. The longest of these, constructed around 1992, consisted of a 416-ft steel bridge, a 460-ft cast-in-place concrete bridge, and a 927-ft prestressed concrete bridge. The performance of these bridges is noted to be better than expected. When designing a bridge, the Tennessee DOT reports, "We design Tennessee bridges in concrete for a temperature range of 20 to 90° F, and steel superstructure bridges for a range of 0 to 120° F. Based on these ranges and thermal coefficients of expansion for respective materials, we design for 0.505 inch of movement per 100 feet of span in concrete, and 0.936 inch of movement per 100 feet of span in steel." Another design detail that is employed by the Tennessee DOT is the use of a compression seal between the approach slab and deck if the interface is concrete pavement approaching a concrete deck. No special treatment is used where the interface is asphalt to concrete. The Tennessee DOT acknowledges that this may result in some local pavement failure and a bump at the end of the bridge, but considers this a minor problem in comparison with joint maintenance.

The Tennessee DOT also offers these explanations about its efforts regarding how to eliminate expansion joints:

1. "We take advantage of pile translation and rotation capabilities."
2. "By modifying foundation conditions, if feasible."
3. "By taking advantage of reduced modulus of elasticity of concrete for long-term loads (1,000,000 versus 3,000,000 psi)."
4. "By allowing hinges to form naturally or constructing them."
5. "Employing expansion bearing, where necessary."

Figure 2.4 illustrates typical details of integral abutment bridge construction in Tennessee (Soltani 1992).

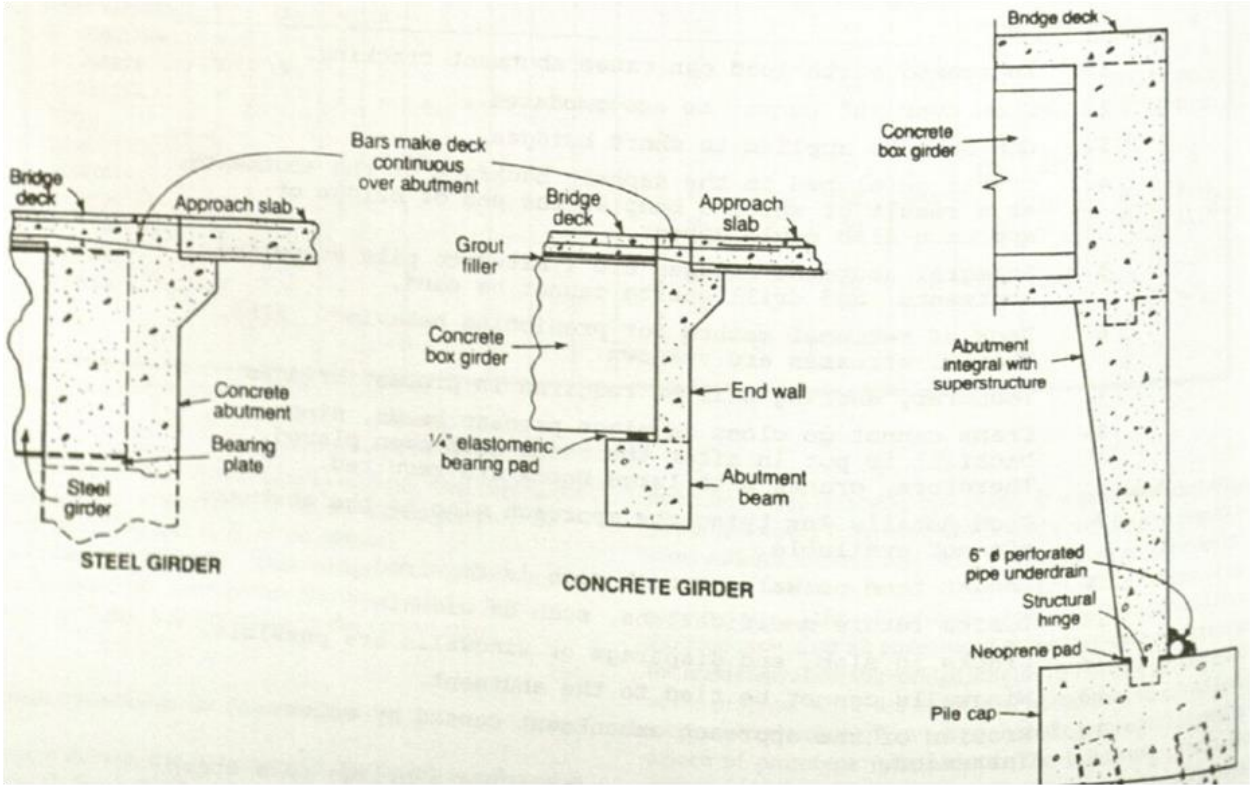

Figure 2.4 Tennessee Abutment Details

2.3.2 California

The performance of integral abutment bridges in the state of California during the 1971 San Fernando earthquake contributed greatly to their increased popularity. During this earthquake, integral abutment bridges suffered less damage and performed better overall in comparison with bridges with jointed abutments. Consequently, since 1971, it has been general practice in California to implement jointless design in highway structures. As a result, most structures shorter than 350 feet since that time have been jointless. California also has over 100 jointless structures with lengths greater than 350 feet. Even on most structures with expansion joints, the abutments are designed without joints. Because water intrusion is the main problem with this design in California, the California DOT designs the connection of the approach slab directly to the abutment and extends it over the wingwalls. An underlying drainage system is also typically provided (Soltani 1992).

2.3.3 South Dakota

South Dakota has extensive experience using integral abutment bridges, particularly for steel bridges. They are also one of the first states to conduct a full-scale testing program to evaluate the performance of integral abutment bridges. A full-scale model was constructed and tested to simulate different stages of construction. At each stage, the specimen was subjected to a series of movements designed to simulate expansion and contraction caused by daily temperature variations. Based on the test results, the following conclusions were obtained:

1. The induced movement and shear force in the girder, caused by temperature changes alone, are usually smaller than the overstress allowance made by AASHTO for combine loadings.

2. The integral abutment acts as if it were a rigid body.
3. Thermal movements larger than 0.5 inches may cause yielding in the steel piling.

The researchers stated that the last conclusion may require further experimentation to verify as it contradicts the successful practices of Tennessee and North Dakota, which recommend 7 inches and 4 inches of expansion, respectively. In addition, one notable conclusion was that the stresses at various parts of the specimen were of greater magnitude during expansion than during contraction. This is attributed to the passive resistance of the backfill to expansion as well as the fact that the active soil pressure actually helps contraction (Soltani 1992).

2.3.4 North Dakota

North Dakota has been constructing integral abutment bridges for more than 30 years. They were also the only state as of 1992 to attempt to eliminate the passive soil pressure behind the abutments. A field study was conducted in which a compressible material was placed in the webs of the abutment piles as shown in Figure 2.5 (Soltani 1992). The bridge was 450-ft long, made up of six 75-ft spans, had integral abutments, piers, concrete box girders, and a concrete deck. The North Dakota DOT used the following equations to calculate temperature change and the resultant change in length.

$$\Delta T = T_1 - T_2 + \frac{(T_3 - T_1)}{3} \quad and \quad \Delta L = L \propto \Delta T$$

Where

T_1 = air temperature at dawn on the hottest day
T_2 = air temperature at dawn on the coldest day
T_3 = maximum air temperature on the hottest day.
L = original length of the bridge and
α = coefficient of thermal expansion of the bridge deck material

Observations from this study led to conclusions by the North Dakota DOT that the total change in bridge length did not result in equal movement at each abutment and that the stress at the top of the pile is sufficient to initiate yield stress in the steel but not enough to cause a plastic hinge to form (Soltani 1992).

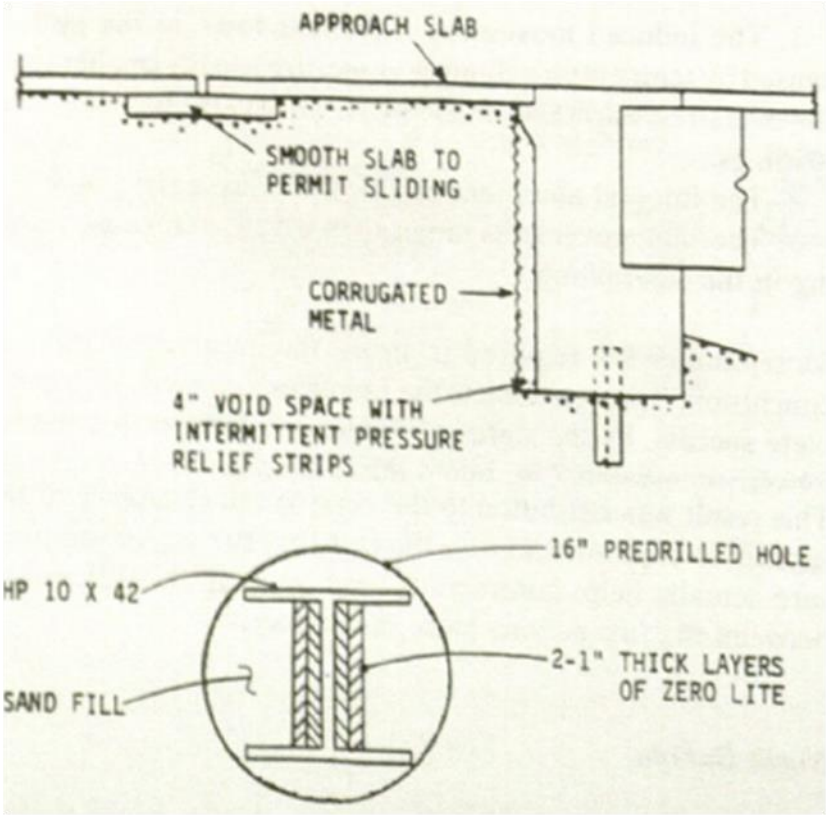

Figure 2.5 North Dakota Integral Abutment System with Pressure Relief Strips

2.3.5 Iowa

Iowa has been constructing integral abutments on concrete bridges since 1964. One of the first bridges built in this state was a 230-ft long bridge with no skew. Inspection of this bridge shows no major cracks or apparent distress in the abutment walls, wingwalls, and beams caused by thermal movement. The Iowa DOT reported that inspection on 20 integral abutment bridges was performed approximately five years after construction. Some bridges had skew angle of up to 23 degrees. Inspections were terminated because no problems were found related to lack of expansion joints in the superstructure. Iowa's designs are based on an allowable bending stress of 55% of yield plus a 30% overstress, because the loading is caused by temperature effects. The movement in the piles is found by a rigid joint analysis, which considers the relative stiffness of the superstructure and the piling. The piles are assumed to have an effective length of 10.5 feet. The soil resistance is not considered. The Iowa DOT analysis shows that the pile deflection is approximately ⅜ inch (Soltani 1992).

2.4 COMPARISON OF EUROPEAN AND U.S. INTEGRAL ABUTMENT BRIDGE DESIGN

An international survey conducted in 2007 gathered information from seven European countries to compare the various design requirements and restrictions of various countries. England, Finland, France, Ireland, Luxembourg, Germany, and Sweden responded to the survey. The responses from France were excluded because they did not construct bridges that were considered to be true fully integral abutment bridges. Luxembourg was also excluded from the survey results due to their small size and limited bridge population. The summarized results of this survey are shown in Figure 2.6 (White 2007).

Criteria	England	Finland	Ireland	Germany	Sweden
Use Fully Integral Abutment Bridges?	Yes	Yes	Yes	Yes	Yes
Maximum Skew Angle?	30°+	30°	30°+	None	None
Steel Pile Foundation Used?	Yes	Yes	Yes	Rarely	Yes
Steel Pipe Pile Filled with Reinforced Concrete?	Rarely	No	Yes	Rarely	Yes
Reinforced Concrete Pile Foundation Used?	Yes	Rarely	Yes	Yes	No
Prestressed Piles Used?	Rarely	No	Rarely	No	Yes
Spread Footing Used?	Yes	No	Yes	Yes	Yes
Use Active Soil Pressure, Full Passive Soil Pressure, or Other Requirement?	Other Reqmt.	Depends on Span length	Other Reqmt.	Passive	Depends on Span length
Approach Slabs Recommended?	No	Yes	No	Yes	Varies
Wingwalls Permitted to be Cast Rigidly with Abutment Stem?	Yes	Yes	Yes	Yes	Yes
Use Semi-Integral Abutment Bridges?	Yes	Yes	Yes	No	Yes
Maximum Skew Angle?	30°+	30°	30°+	-	None
Steel Pile Foundation Used?	Yes	Yes	Yes	-	Yes
Steel Pipe Pile Filled with Reinforced Concrete?	Rarely	No	Yes	-	Yes
Reinforced Concrete Pile Foundation Used?	Yes	Rarely	Yes	-	-
Prestressed Piles Used?	Rarely	No	Rarely	-	Yes
Spread Footing Used?	Yes	Yes	Yes	-	Yes
Use Active Soil Pressure, Full Passive Soil Pressure, or Other Requirement?	Other Reqmt.	Depends on Span length	Other Reqmt.	-	Depends on Span length
Approach Slabs Recommended?	No	Yes	No	-	Varies
Wingwalls Permitted to be Cast Rigidly with Abutment Stem?	Yes	Yes	Yes	-	Yes

Figure 2.6 Summary of European Integral Abutment Bridge Survey

The European survey data were compared with recent survey data of state agencies within the United States. This comparison provides useful insight into design requirements and restrictions based on the field experience of different countries. Integral abutment design details regarding the foundation, backfill, approach slabs, wingwalls, and beam design were extensively compared and are further explained below.

2.4.1 Foundation

None of the responses to the European survey indicated that pile foundations are always required for fully integral abutment bridges. When spread footings were used, however, no problems were reported due to the rotational restraint of the abutment stem. The survey also indicated that steel piles were rarely used in Europe. When steel piles were used, they were typically symmetrical cross-shaped piles with the

exception of England and Ireland, which typically used steel H-piles oriented with the strong axis perpendicular to the direction of bridge expansion. The most common piles used in European integral abutment bridges were steel pipe piles filled with reinforced concrete. This is in stark contrast to the requirements of many state agencies within the United States. In the United States, where more than 70% of state agencies reported steel H-piles to be the most commonly used pile for integral abutment bridges. Regarding pile orientation, 33% of state agencies required the H-piles to be oriented with the strong axis perpendicular to the direction of bridge expansion, while 46% required the weak axis of H-piles to be oriented perpendicular to the direction of bridge expansion (White 2007).

2.4.2 Backfill

The most common backfill material both in Europe and in the United States is well compacted gravel or sand. In the United States, 69% of responding state agencies required a well compacted granular backfill, while 15% require the backfill to be loose in an effort to reduce forces on the moving abutment stem. None of the European countries required the use of an elastic material behind the abutments. However, in the United States, 23% of respondents indicated the use of some type of compressible material behind the abutment stem. The responses of European countries varied concerning the design soil pressure behind the abutment. Some adopted a similar policy to the U.S. and account for the full passive pressure, while others employ formulas in their design codes that estimate the soil pressure behind an integral abutment bridge to be between the at rest pressure and the full passive pressure. In the United States, 59% of the states surveyed accounted for the full passive pressure in their design (White 2007).

2.4.3 Approach Slabs

According to the European survey, approach slabs are not required to be used with integral abutment bridges, but were indicated by most countries to be desirable. The length of the approach slab used in those countries ranged from 10-25 feet. Most state agencies in the United States require approach slabs to be used with integral abutment bridges in order to reduce the impact forces on the bridge. Of those states that require use of an approach slab, 46% reported that settlement of the approach slab is a maintenance problem. Use of a buried approach slab or ‘drag plate’ makes this settlement easier to repair and may eliminate this concern. An example of a drag plate used in Germany is shown in Figure 2.7 (White 2007).

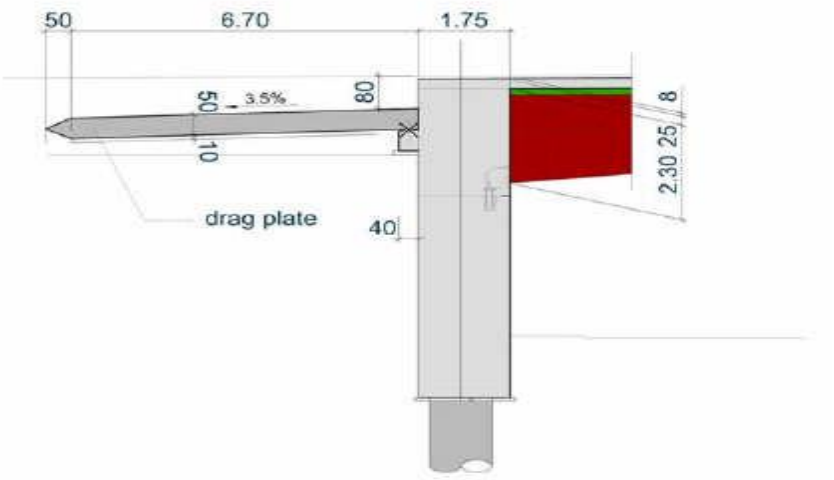

Figure 2.7 Example of a “Drag Plate” Used in Germany

2.4.4 Beam Design

In the European survey, respondents indicated that steel beams, cast-in-place concrete beams, and precast/prestressed concrete beams were all permitted for integral abutment bridges. The predominate beam used was said to be made of precast/prestressed concrete. Cast-in-place reinforced concrete beams were seldom used, except for short-span 3-sided frame structures. These types of structures are seldom constructed in the United States. In the European survey, only Finland reported a maximum span length or total bridge length with steel beams or precast/prestressed concrete beams. The maximum limit for both these types of beams was reported to be 230 feet. In European countries, the maximum skew angle varied for different types of beams when limits were given. For steel beams and cast-in-place concrete beams, the maximum allowable skew angle was reported to be 30°, and for precast/prestressed concrete beams the maximum allowable skew angle was reported to be 60°. Sweden was the only European country surveyed to indicate a maximum roadway grade, which was given to be 4% for all three types of beams considered. State agencies in the United States specified more limits to length and skew angle than European countries. For steel beams, maximum span lengths ranged from 225-1000 feet and maximum total bridge length ranged from 500-2000 feet. For precast/prestressed concrete beams, agencies reported maximum span lengths between 20-650 feet and maximum total bridge length from 500-3800 feet. For both steel and precast/prestressed beams, state agencies reported maximum skew angles ranging from 15°-70°, and maximum degree of curvature ranging from 0°-10°. Most European countries permit the use of line girder analysis techniques to design the bridge beams, although they are analyzed for both a simple span condition and a fixed condition to determine the maximum positive moment at the mid-span and the maximum end moments at the abutments, respectively. 3-D modeling is also used in varying degrees among European countries. In the United States, state agencies are split between the use of line-girder techniques and 3-D modeling.

The design details of semi-integral abutment bridges were also compared between European countries and the United States with a very similar comparison observed to that of fully integral abutment bridges (White 2007).

2.5 GENERAL BEHAVIOR OF INTEGRAL ABUTMENT BRIDGES

In a publication for the Virginia Transportation Research Council (VTRC), the general behavior of integral abutment bridges is expressed in an extensive literature review, which will be summarized here. Daily and seasonal variations in ambient temperatures are shown to affect integral abutment bridges. The extreme temperature variations control the extreme displacements of integral abutment bridges. This can be seen in Figure 2.8 (Arsoy 1999). The material and geometry of the bridge are also factors contributing to the displacement of integral bridges.

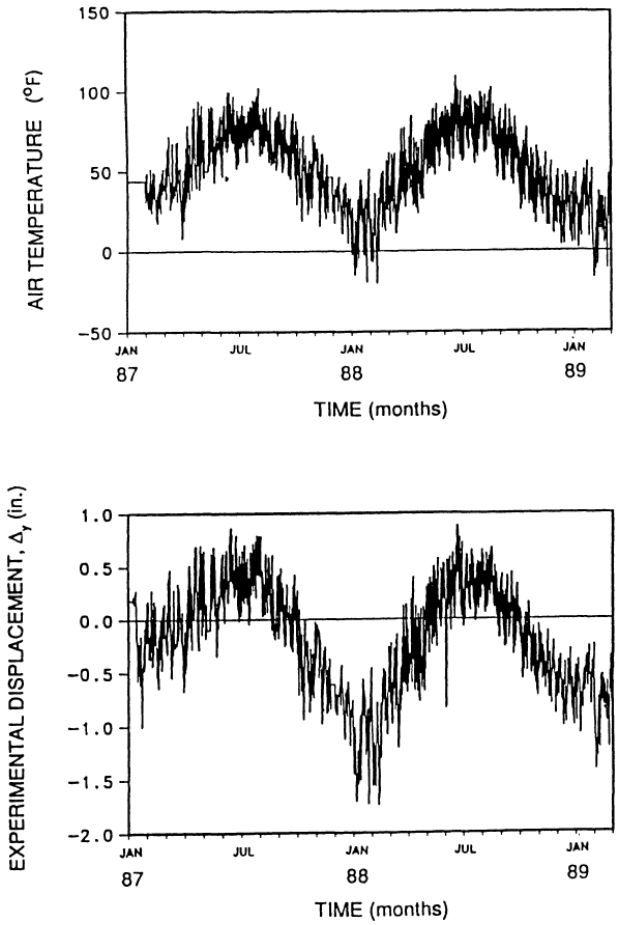

Figure 2.8 Relationship Between Air Temperature and Horizontal Bridge Displacement

In addition to dead and live loads, integral abutment bridges are subject to further secondary loads due to creep, shrinkage, thermal gradients, differential settlements, buoyancy loads, and pavement growth. The effects of shrinkage and creep can be estimated using the Freyermuth method. It has been found that the greatest effect of shrinkage is apparent on the positive moment of single spans and on the continuity connection at abutment of continuous spans. Maximum shrinkage moments take place within 30 days of form removal, but creep effects continue for longer periods of time. In continuous single-span bridges, creep effects are greater than shrinkage effects.

Temperature gradients developed in the bridge cross section may be quite complicated, and these gradients generate secondary bending moments within the cross section of the bridge. The secondary moments generated by temperature gradients can be calculated as prescribed by AASHTO. In the VTRC report, it is stated that in moderate climates, the moments generated by thermal gradients can be neglected.

Differential settlement is an additional source for secondary bending moments in integral abutment bridges. Differential settlements can be estimated using simple procedures as defined by AASHTO. Typically, if the differential settlements are less than 1.5 inches (38mm), then the induced moments can be ignored.

In locations where the bridge may have the possibility of becoming submerged, buoyancy loads may appear. Integral abutment bridges are likely to be subjected to uplift forces when fully submerged. Hence, integral abutment bridges should either be limited to areas where the bridge height is higher than the maximum expected flood level, or the buoyancy loads should be considered in the bridge design.

Pavement growth can introduce an additional longitudinal compressive force into the bridge superstructure. Designers should therefore consider the pressure generated by pavement growth. The pavement growth phenomenon can gradually close pressure relief joints, which then create longitudinal compressive forces as pavement undergoes further expansion cycles. The VTRC report mentioned a case of severe abutment damage in a bridge with no pressure relief joints. According to the numerical analysis performed, the damage was caused by pavement growth, which introduced excessive longitudinal pressures on the abutments.

Steel H-piles are the most common pile type used for integral abutment bridges and they are typically oriented to facilitate weak axis bending. For a given deflection, weak axis bending generated less stress in the piles than strong axis bending does. Foundation piles for integral abutment bridges must also be able to carry the necessary vertical loads while also being subjected to temperature-induced displacements. The vertical load carrying capacity of the piles may be reduced due to lateral displacements. The ability of piles to accommodate lateral displacements plays a crucial role in determining the maximum possible length of integral abutment bridges. The VTRC report expresses the possibility of predrilled, oversized holes filled with loose sand after the piles have been driven as an alternative way to minimize the pile stresses and thereby maintain the vertical load carrying capacity as the bridge displaces. It has been found that predrilling greatly increases the vertical load carrying capacity of the piles. Predrilled length must then be considered. For an HP 10X42 steel H-pile, 6-10 feet of predrilled length was necessary in order to take full advantage of predrilling.

Earth pressures on the abutment are also considered in the VTRC report. Depending on the amount of temperature-induced displacement of the abutments, the earth pressures on the abutment can be as low as the minimum active pressure or as high as the maximum passive pressure. Many engineers prefer to use Rankine or Coulomb calculations for passive pressure because of their simplicity. These methods are generally conservative for bridge abutment applications. Tests have shown that turn-back (U-shaped) wingwalls result in greater earth pressures than transverse wingwalls.

A common problem occurring with integral abutment bridges is the development of a bump at the end of the bridge. This bump can be cause by cyclic compression or settlement of the backfill between the approach and the abutment. This produces a void below the approach at the abutment, which results in a bump at the end of the bridge. The VTRC report gives the following list of measures that have been effective in preventing and mitigating the approach settlement problem (Arsoy 1999).

1. Settlements should receive prime attention during design. Analysis should be performed and sufficient geotechnical data should be obtained.
2. An efficient drainage system should be included in the design.
3. Adequate compaction specifications and procedures should be employed. However, using a very dense backfill in the close proximity of the abutment is not likely to help reduce settlement. This is due to the cyclic nature of the abutment movement that tends to loosen dense backfill and also to densify loose backfill.
4. If significant settlement of the foundation soil is likely, soil improvement should be considered. To reduce loads on the foundation soil, the embankment may be constructed of lightweight materials.

5. Recognize that integral abutment bridges require continuous, yet reduced, maintenance. This maintenance may include asphalt overlays, slab jacking, and approach slab adjustment or replacement.

An additional investigation into the design details of integral abutment bridges focused on the deck-stringer-abutment continuity details. This study produced some useful insights about the behavior of integral abutment bridges in regards to cracking. Both longitudinal and transverse cracking were observed in approach slabs of an integral abutment bridge. The transverse cracking can occur from heavy vehicular live loads, settlement of the backfill soil, and void development under the approach slabs. Longitudinal cracking in the approach slab also develops when voids form under the approach slab. Most backfill materials are not perfectly elastic, which results in void formation with the cyclic movement of the abutments due to daily and annual temperature fluctuations. It was suggested that the performance of integral abutment bridges could be improved by incorporating a compressible elastic material as an incompressible inclusion, as was mentioned previously. Other cracking patterns were also observed in the decks of integral abutment bridges. Diagonal cracks were seen to occasionally develop at the acute corners of the bridge deck, and straight cracks were also observed over previously placed concrete end diaphragms. Transverse cracks at relatively uniform spacing may also occur as a result of insufficient continuous temperature and shrinkage reinforcement in the deck slabs over the end diaphragms.

Connections between the abutments and the bridge superstructure can be stressed and crack if there is a significant change in temperature during the initial concrete setting. To prevent the occurrence of stressing/cracking, the following procedures were suggested (Roman 2002).

1. Place continuity connection at sunrise.
2. Place deck slabs and continuity connections at night.
3. Place continuity connections after deck slab placement.
4. Use crack sealers

2.6 RESEARCH PROJECTS

2.6.1 Fennema, et al. (2005)

This project conducted a comparison between predicted and measured responses of an integral abutment bridge in Pennsylvania. The monitored bridge was a three-span, composite structure with four prestressed, concrete I-girders bearing on reinforced concrete piers and abutments. The south abutment was constructed with no expansion joint at the abutment and bore directly on rock. The north abutment was a standard Pennsylvania DOT integral abutment bearing on a single row of eight HP 12X74 piles. The bridge was thoroughly instrumented with vibrating wire based instruments and monitored between November 24, 2002, and March 24, 2003. Three levels of comparative numerical analysis were employed to determine the movements and behavior of integral abutment bridges due to thermal loads. Level 1 was an analysis of the behavior of the laterally loaded piles alone with no abutment or superstructure. Level 2 consisted of a two-dimensional, three-bent numerical model developed in STAAD Pro composed of frame members and soil springs. Level 3 analysis used a three-dimensional finite element model developed in STAAD Pro consisting of frame members, plate elements, and soil springs. Detail was given regarding the development of each level of analysis and the results obtained. Key conclusions drawn include the following (Fennema 2005):

1. Development of multilinear soil springs from *p-y* curves is a valid approach
2. 2D numerical models are sufficiently accurate to determine pile response

3. The primary mode of movement of the integral abutment is rotation about the base of the abutment, not longitudinal displacement of the abutment
4. The girder-abutment connection is best approximated as hinged

2.6.2 Abendroth, et al. (2007)

The details of the first integral abutment bridge in the state of Iowa to use precast, prestressed concrete (PC) piles in the abutment are contained in this report sponsored by the Iowa Highway Research Board and the Iowa Department of Transportation. The bridge was constructed in 2000 and consists of a 110-ft long, 30-ft wide, single-span precast, prestressed concrete girder superstructure with a 20° skew angle. The top of each pile was wrapped with a double layer of carpet in an attempt to create a pinned type of connection. The bridge was fitted with a variety of strain gauges, displacements sensors, and thermocouples. The data obtained showed that the published AASHTO guidelines regarding thermal gradients were in agreement with the recorded values. The effectiveness of the carpet wrap was debatable, but it was concluded that the connection should not be assumed as a pinned connection for this type of configuration. Data indicated the development of pile cracking and an accompanying change in behavior was evident. Excavation confirmed the presence of a pile crack, suggesting periodic inspection of the abutment piles in order to prevent long-term corrosion of the prestressing strands.

In connection with observation and instrumentation of the bridge, the details of a nationwide survey investigating the use of precast, prestressed concrete piles was included. The survey indicated that out of the 88% of respondents who had designed integral abutment bridges, 23% allowed the use of PC piles with integral abutment bridges. Seventy percent of respondents designed integral abutment bridges but did not allow the use of PC piles. Reasons for not permitting PC piles included lack of ductility from PC piles, insufficient research, PC piles not readily available, PC piles not being economical, and negative opinions of bridge contractors (Abendroth 2007).

2.6.3 Civjan, et al. (2007)

An extensive parametric analysis was performed on a zero skew, three-span bridge in Massachusetts. The bridge was extensively instrumented and subsequently monitored for four years. 2D and 3D finite element models were used to create an equivalent model, which was compared to the field data in a separate publication. Loose and dense backfill conditions were evaluated in this investigation because of their effect on the abutment soil springs used in the model. The assumed soil properties covered a reasonable range of conditions and were meant to provide representative upper and lower bounds of typical backfill material. The effects of the parameters selected relate to deformations of the abutment, pile deformations, maximum moments in the abutment piles, and pressures developed by the abutment backfill. These are descriptors of bridge behavior. Regarding abutment displacement and rotation, it was shown by the finite element model that an applied temperature differential causes an imposed distortion of the bridge at the girder location, while soil conditions control the response of the rest of the structure. When expansion occurs, the deflection at the base of the abutment is largely controlled by the backfill conditions, but during contraction, the soil conditions or construction practices at the abutment piles affect the results most. The study concluded that the behavior of integral abutment bridges was greatly affected by the soil-structure parameters. Due to the variability of final soil conditions, conservative design assumptions are warranted. Another conclusion stated that lower pile restraint results in a decrease in both abutment rotation and pile moment during contraction, but during bridge expansion, the resulting backfill pressures would increase. Also, during expansion, denser backfill properties result in greater abutment rotation, decreased pile moment, and greater soil pressure behind the abutments (Civjan 2007).

2.6.4 Olson, Long, et al. (2009)

Researchers conducted a literature review regarding other states' limitations and guidelines pertaining to the use of integral abutment bridges. A survey of states with similar climates, as well as those states considered well-experienced with integral abutments, was also conducted. Two-dimensional modeling was conducted using FTOOL and LPILE software. Three-dimensional finite element modeling was also performed using SAP 2000. The modeling was based upon the current guidelines of the Illinois DOT. Different pile types and sizes, span lengths, skew angles, and girder material (steel vs. concrete) were compared through modeling to develop useful graphs summarizing allowable lengths and skew angles of details commonly used in the state of Illinois. Based on the modeling conducted, several conclusions and recommendations were made. Notable findings include the recommendation of compacting the granular backfill used directly behind the abutment backwall, as well as suggested maximum lengths and skew angles for some commonly used piles. To increase the length and skew limitations in Illinois, the following options were recommended: (1) Predrill the pile locations to a depth of 8 feet; (2) Reduce the depth of pile embedment in the pile cap to 6 inches, effectively introducing a hinge at the pile-to-pile cap interface; or (3) incorporate a mechanical hinge at the cold joint between the pile cap and the abutment. The Virginia DOT incorporates such a hinge using "strips of high durometer neoprene along either side of the dowels along the centerline of the integral abutment" (Olson 2009).

2.6.5 Shah (2007)

This study focused on the finite element analysis of integral abutment bridges with some emphasis on the complex soil interactions that occur in response to thermally induced deformations. A basic overview of integral abutment bridges, their geometry, history, and advantages, are stated. The soil-structure interaction is considered a critical design issue. A literature review is also contained that focuses on the past numerical models of integral abutment bridges. The studies presented deal heavily with the effects and behavior of the backfill soil that interacts with the integral abutment. A bridge with typical geometry and length for the state of Kansas was selected for finite element modeling with ABAQUS software. The bridge structure was modeled and the soil reaction was modeled using nonlinear springs. The complete details of this model are contained within the report, along with graphical results of different soil properties considered. The study concluded that "the overall behavior of integral abutment bridges is significantly affected by the type of soil adjacent to the abutment." Analysis indicated linear response to the selected temperature ranges. In response to thermal loads considered, an increase in relative compaction of the soil behind the abutment from 90% to 96% decreases the pile top displacement and maximum bending moment, increases the maximum compressive stresses in the girders, and increases the soil pressure on the abutment. Findings also indicated that translation of the abutment is 3.46 times larger than rotation for a relative compaction of 90%, rotation is larger than translation by 1.44 times for a relative compaction of 96% with $\Delta T=60°F$, but that difference entirely diminishes for a compaction of 96% and a $\Delta T=100°F$. The largest difference in maximum bending moments between central and end piles was found to occur for a relative compaction of 96% and a $\Delta T=60°F$. Although the abutment was assumed to be a rigid body, the thermal gradient within the abutment led to bending of the abutment. Throughout all the testing considered, none of the loading scenarios resulted in passive failure of the soil behind the abutment (Shah 2007).

2.6.6 Arenas, et al. (2012)

A study was conducted for the Virginia Center for Transportation Innovation and Research focusing specifically on integral abutment bridges with foundation piling in the backfill of Mechanically Stabilized Earth (MSE) walls with a "U-back" configuration. This indicates that the MSE wall has three faces. The study also focused on several unknowns and points of controversy in the design of integral abutment

bridges. The study included the implementation of many numerical analyses and subsequent monitoring to verify them, as well as a nationwide survey of departments of transportation. The nationwide survey received 21 usable responses from various states. The survey included questions about general bridge issues, piles, MSE walls, abutments, approach slabs, and other miscellaneous details. The Utah Department of Transportation (UDOT) was one of the agencies that responded to the survey. UDOT was identified as one of the agencies that used a combination of active and passive pressures in the calculation of earth pressure behind the abutment. This practice was also used by the majority of those who responded. A few notable conclusions made by this study include (Arenas 2013):

- Steel pipe sleeves filled with sand do not reduce forces and moments in the piles because of the tendency to densify with cyclic loading due to thermal response.
- The peak earth pressure behind the abutment can increase up to 60% after the first year but increases by less than 6 additional percentage points during the following year. The earth pressure buildup is due mainly to soil settlement and rearrangement behind the abutment.
- It was recommended that H-piles oriented for weak-axis bending with webs perpendicular to the bridge alignment be used for bridges with less than 20° skew to decrease bending moment in the longitudinal direction.

3. THERMAL ANALYSIS

The thermal monitoring and analysis that was conducted on a three-span, integral abutment bridge, located in Salt Lake City, Utah, is described in Chapter 3. A description of the test bridge is presented, followed by a description of the survey conducted to obtain data regarding the temperature-induced movement of the bridge. The results obtained through this year-long survey are presented, along with supplementary data from a day-long survey. In addition, a comparison of a three-dimensional survey that was conducted by NV5 is also presented. Chapter 3 concludes with a discussion on average bridge temperature measurements and the guidelines presented in the AASHTO LRFD specifications for a typical Utah bridge, followed by a summary of the thermal analysis.

3.1 400 SOUTH STREET BRIDGE DESCRIPTION

The bridge monitored for this study is a three-span, integral abutment bridge, located in Salt Lake City, Utah. The bridge was built in 1999 and is part of the Lincoln Highway/I-80 that crosses over heavily travelled 400 South Street at approximately 800 West Street, directly east of the I-15 corridor. The bridge accommodates four lanes of traffic: two lanes of northbound traffic that depart from I-15 and two lanes of incoming traffic from 500 South Street. These four lanes of traffic merge into I-80 westbound towards the Salt Lake City International Airport. The Average Daily Traffic (ADT) on the 400 South Street Bridge is approximately 29,447 vehicles with an Average Daily Truck Traffic (ADTT) of 6%. An aerial view of the bridge can be seen in Figure 3.1.

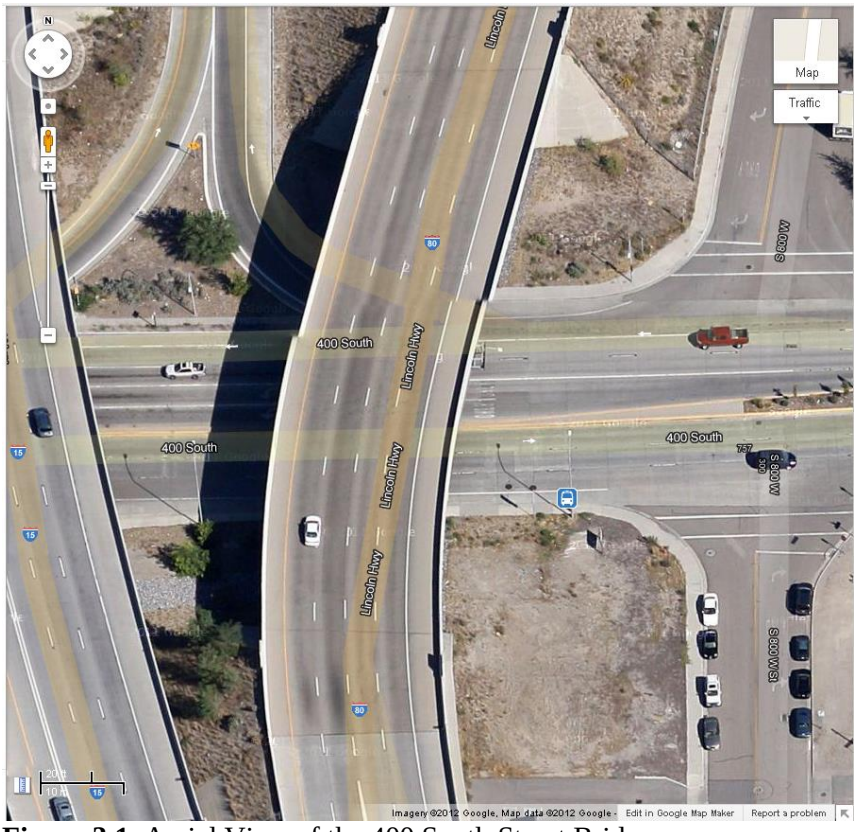

Figure 3.1 Aerial View of the 400 South Street Bridge

The deck of the bridge is curved, while the girders beneath are in three separate, straight segments. The girders in each segment are placed at a skewed angle that accommodates the curved deck above. Three spans comprise the overall bridge and are defined as Span 1, Span 2, and Span 3. Span 1 is defined as the southernmost span, Span 2 is the middle span, and Span 3 is the northern span. Figure 3.2 shows a plan view of the bridge, as well as the nomenclature designated for the spans and corners of the bridge. An elevation view of the full bridge is shown in Figure 3.3.

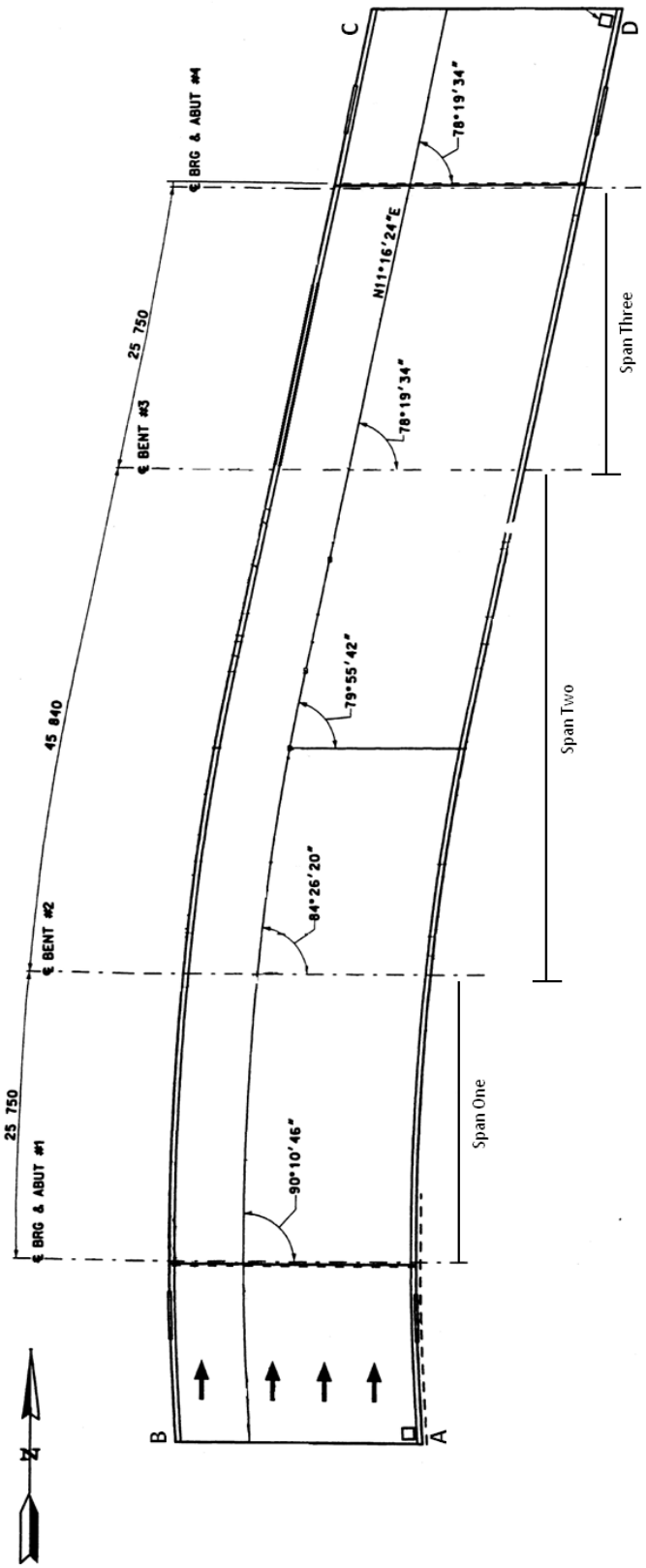

Figure 3.2 Plan View of 400 South Street Bridge (Dimensions in Millimeters)

Figure 3.3 Photograph of 400 South Street Bridge in Elevation View

The overall length of the bridge between the integral abutments is 97.3 m (320 ft). Span 1 (south) and Span 3 (north) each measure 25.8 m (84.5 ft) long and Span 2 (middle) measures 45.8 m (150.4 ft) in length. Span 1 has a skew angle of 0.2 degrees, Span 2 has a skew angle of approximately 5.6 degrees, and Span 3 has a skew angle of approximately 11.7 degrees. The bridge also has an overall angle of curvature of approximately 16 degrees and a radius of curvature of 257 m (843 ft). The total width of the bridge is 21.3 m (70 ft) with an actual road width of 20.4 m (67 ft). Concrete parapets 432 mm (18 in.) wide are located at each side along the full length of the bridge.

The deck of the 400 South Street Bridge is constructed of reinforced concrete. The average deck thickness is 200 mm (8.0 in.). The elevation view of the bridge at the bents, including the bridge deck, is shown in Figure 3.4. The specified concrete compressive strength (f'c) of the bridge deck is 28 MPa (4000 psi).

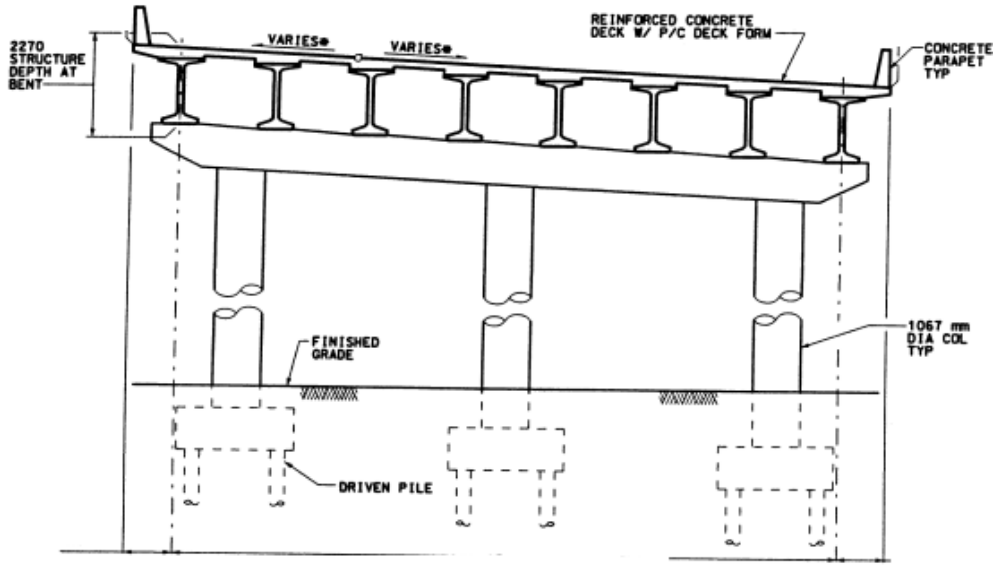

Figure 3.4 Cross-Sectional View of the 400 South Street Bridge at the Bent (Dimensions in Millimeters)

The 400 South Street Bridge consists of eight AASHTO-PCI W1850MG prestressed concrete girders per span, each with a depth of 1850 mm (72 in.). The girders are spaced across the width of the bridge at 2.8 m (9.1 ft) for Span 1, 2.7 m (8.9 ft) for Span 2, and 2.7 m (8.9 ft) for Span 3. The prestressed concrete used a minimum compressive strength at release of 38 MPa (5500 psi) and a 28-day minimum compressive strength of 52 MPa (7500 psi). For the prestressing strands, 15.2 mm (0.6 in.) diameter, seven-wire low relaxation strand with an ultimate stress at failure of 1860 MPa (270 ksi) was used. Figure 3.15 shows a cross-sectional view of the girder with a detailed view of the location of the reinforcement.

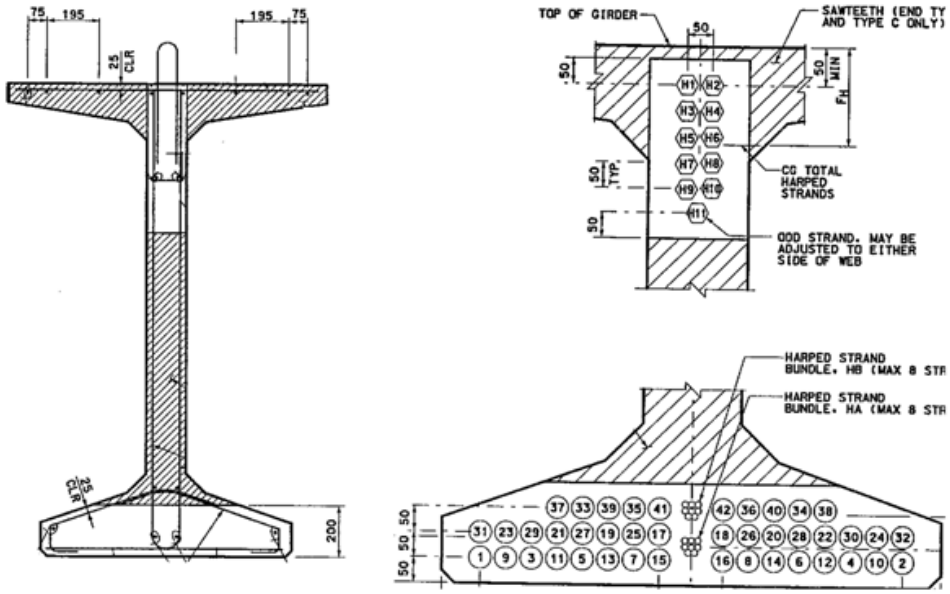

Figure 3.5 Girder Cross Section and Detail View of Prestressing strand Template (Dimensions in Millimeters)

The prestressed concrete girders used contain both harped strands and straight strands. At the girder ends, the centroid of the harped prestressing strands is located 60 mm (2.36 in.) below the top of the girder for girders located in Span 1 and Span 3, and 135 mm (5.31 in.) below the top of the girder for girders located in Span 2. The harping point is located 10.3 m (33.8 ft) from the ends of the girders in Span 1 and Span 3 and 18.34 m (60.16 ft) from the girder ends in Span 2. In Span 1 and Span 3, two strands per bundle were used with a final total harped strand force of 340 kN (76.4 kips) per bundle. In Span 2, eight strands per bundle were used with a final total harped strand force of 1172 kN (263.5 kips) per bundle. At the girder ends, the centroid of the straight prestressing strands is located 50 mm (1.97 in.) above the bottom of the girder for girders located in Span 1 and Span 3 and 100 mm (3.94 in.) above the bottom of the girder for girders located in Span 2. In Span 1 and Span 3, 12 straight strands were used with a final total straight strand force of 2040 kN (458.6 kips). In Span 2, 38 straight strands were used with a final total straight strand force of 5563 kN (1250.6 kips). The location of the harped and straight strands is shown in Figure 3.6.

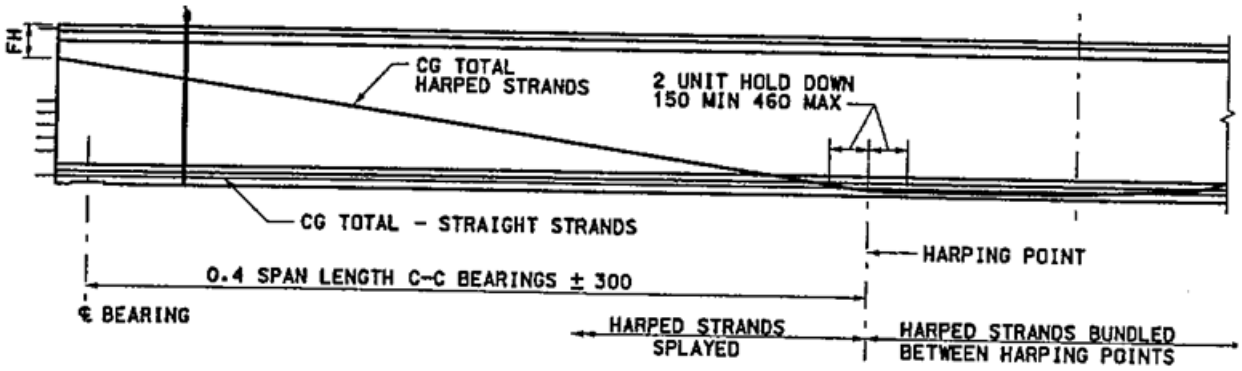

Figure 3.6 Profile View of Girder End with Location of Strands Shown
(Dimensions in Millimeters)

The bridge is supported at the ends using integral abutments with dimensions of 0.9 m (3.0 ft) thick by 3.33 m (11.0 ft) in height. Each abutment is supported by 12 324 mm (12 in.) diameter driven piles spaced at 1.8 m (6 ft). The driven piles supporting the north abutment each have an allowable pile load of 623 kN (140 kips), and those at the south abutment have an allowable pile load of 534 kN (120 kips). Figure 3.7 shows the dimensions of the abutment, as well as the configuration of the reinforcing steel.

The bridge is supported between Span 1 and Span 2 and between Span 2 and Span 3, by two bent caps measuring 1.5 m (5.0 ft) wide by a minimum dimension of 1.5 m (5.0 ft) tall, which are supported on three 1.1 m (3.5 ft) diameter reinforced concrete columns. Each column is supported by a reinforced concrete foundation 1.5 m (5.0 ft) square with a minimum depth of 1.5 m (5.0 ft). The foundations are each supported by eight 406 mm (16 in.) diameter driven steel piles, each with an allowable pile load of 1335 kN (300 kips).

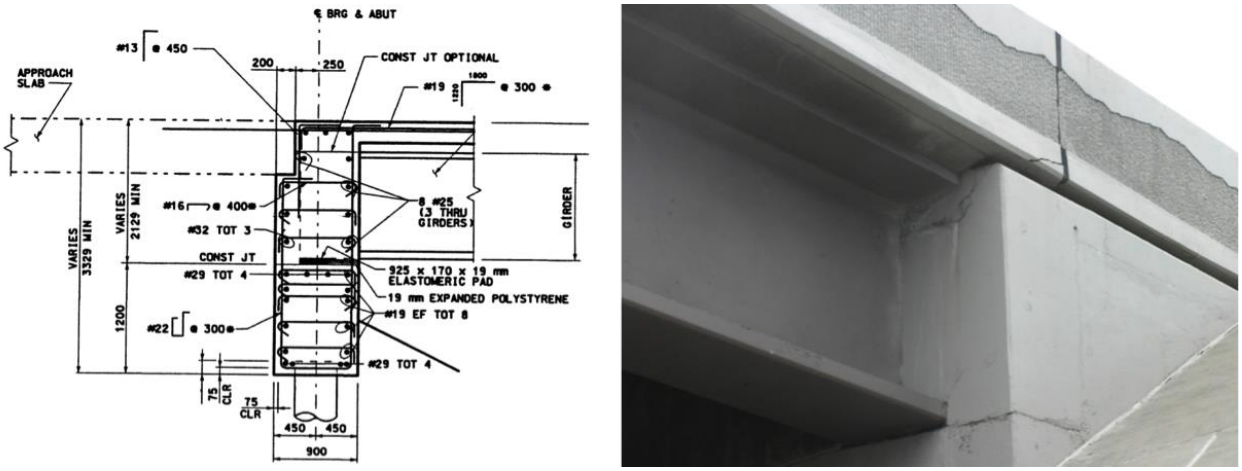

Figure 3.7 Detail View of Abutment with Reinforcing Shown and Photo of Actual Abutment
(Dimensions in Millimeters)

3.2 BRIDGE SURVEY

3.2.1 Monthly Survey

In order to obtain the data required to quantify basic span movement, the bridge was instrumented with 32 Sokkia RS30N reflective targets placed strategically at various locations along the bridge. These targets measure 30 mm (1.18 in.) square. The targets can be seen in Figure 3.8. Eight targets were attached near the joints at the approach slab such that one target was positioned on each side of the joint at all four corners of the bridge. The corners are labeled A, B, C, and D in Figure 3.2. The next 12 targets were used by placing three targets in a vertical line on each of the exterior girders directly adjacent to each abutment. The targets placed in groups of three were approximately located at the top, middle, and bottom of the section. Figure 3.9 shows the arrangement of the survey targets at one location. The locations of these target groups are represented by points 1 and 4, as labeled in Figure 3.10. The remaining 12 targets were used by placing three targets in a vertical line in the middle of the pier diaphragm directly above each side of both bents. The locations of these target groups are marked as points 2 and 3 in Figure 3.10. The configuration shown in Figure 3.10 is of the east side of the bridge. The west side of the bridge is instrumented similarly.

Four specific base stations were identified for measurement readings. Each base station was located so that the survey of the targets placed in each quadrant of the bridge would be obtained. These base stations were permanently located over the duration of the project with a rebar stake and cap. The locations of each station can be seen in Figure 3.11. Station 1 was placed at the southeast corner of the bridge, Station 2 was located near the southwest corner, Station 3 at the northwest corner, and Station 4 at the northeast corner.

Figure 3.8 Survey Target

Figure 3.9 Survey Target Placement

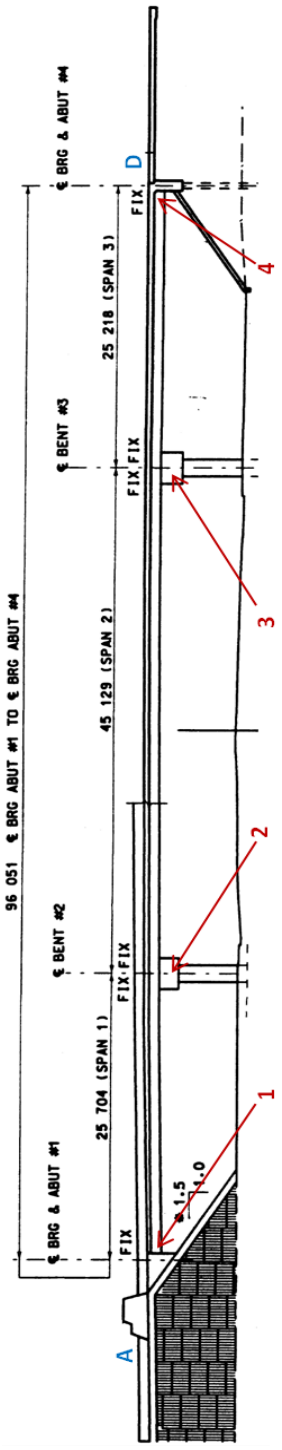

Figure 3.10 Profile View of 400 South Street Bridge with Locations of Survey Targets Shown and Numbered (Dimensions in Millimeters)

Figure 3.11 Locations of Survey Base Stations

The survey of the 36 contact targets was conducted using a Topcon GTS-303D total station and a tripod. At each marked base station, the total station was carefully set up and leveled directly over the rebar caps. The targets attached to the bridge girders and bents were then surveyed. The distances to each survey target for the quadrant of the bridge in question were recorded, as well as the horizontal angle to each target. As there were six targets per quadrant (abutment and bents), six distances and six horizontal angles were recorded at each station surveyed. The survey process was repeated at each of the four base stations, producing 24 measurements of length and 24 horizontal angles. The positioning of the stations was limited by the surroundings of the bridge such that the joints on the approach slab at each corner could not be surveyed using the total station. Instead, starting in January, the distance between the survey targets located on either side of the expansion joint were measured with a measuring tape. These values were recorded in addition to the data collected from the total station at each quadrant of the bridge. An example of the configuration of the survey targets at the expansion joints can be seen in Figure 3.12.

Because the movement of the integral abutment bridge was primarily governed by changes in ambient temperature, a simple configuration was devised in order to collect survey and temperature data for the bridge. The survey was conducted at approximately the same time of morning on a monthly basis. In order to be as consistent and reliable as possible, temperature data were collected from the nearby National Weather Service station at Salt Lake City International Airport. For each monthly reading, the average temperature over the total time required to perform the survey was taken and then recorded.

Figure 3.12 Survey Targets at Approach Slab

3.2.2 Full-Day Survey

A full-day survey was conducted on October 18, 2012, for the east side of the 400 South Street Bridge. The east side was selected because data for Span 2 were desired and could not be collected on the west side. The full-day survey used the same procedure discussed for the monthly surveys and added an additional base station used to calculate values for Span 2.

The full-day survey was conducted using the same total station and base stations used for the monthly surveys. An infrared thermometer was used to measure the temperature of the bridge deck. Once the bridge deck temperature was obtained, a round of survey measurements began. The total station was set up and leveled at Station 1 and the targets for that quadrant were surveyed in the same manner as the monthly surveys. Once the points from Station 1 were measured, the total station was moved to Station 3 and the process was repeated. Following the measurements at Station 3, the total station was moved to a different tripod set up in the median of 400 South Street directly east of the bridge. This tripod remained in the same location for the duration of this survey. From this point, the targets on either side of Span 2 could be seen and measured, providing survey data for Span 2 that were previously unavailable. This completed a round of survey measurements. This was then repeated each hour until there was insufficient daylight to read the targets.

3.3 MEASURED SPAN LENGTH

Using the recorded distances and angles measured from the periodic bridge surveys, a calculation of the changes in lengths of Span 1 and Span 3 was performed using the law of cosines shown as Equation 1.

$$c = \sqrt{a^2 + b^2 + 2abcos\theta}$$

(Eq. 1)

where,

c = distance between targets
a = distance to first target from station
b = distance to second target from station
θ = angle between a and b

This equation was used to calculate the distance between targets (span elongation or shortening) placed on the pier diaphragm and those on the nearest abutment.

The survey only provided the distance between targets. No data were recorded that permitted the determination of direction of movement or determination of the center of gravity of the movement.

3.4 READINGS FROM MONTHLY SURVEY

Calculations using Equation 1 allowed for a direct comparison of change in axial span length with temperature. The results for the monthly survey can be seen for all spans in Figures 3.13 and 3.14 and for each side of Span 1 and Span 3 in Figures 3.15 through 3.18. Figures 3.15 through 3.18 are plotted on an identical scale for ease of comparison.

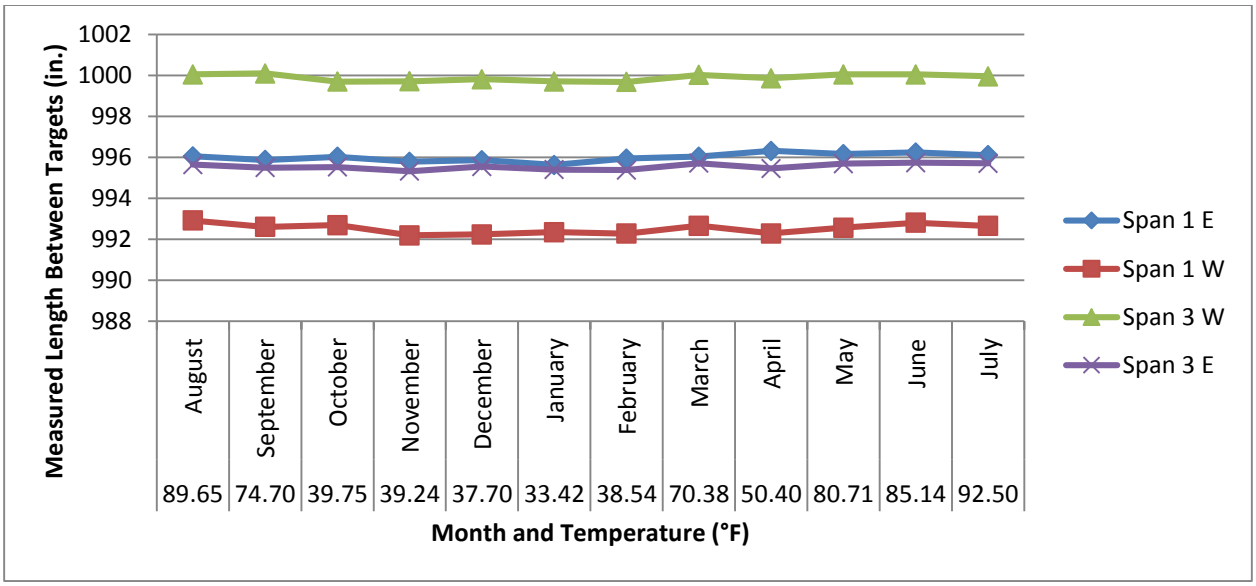

Figure 3.13 Measured Lengths Between Survey Targets in Chronological Order

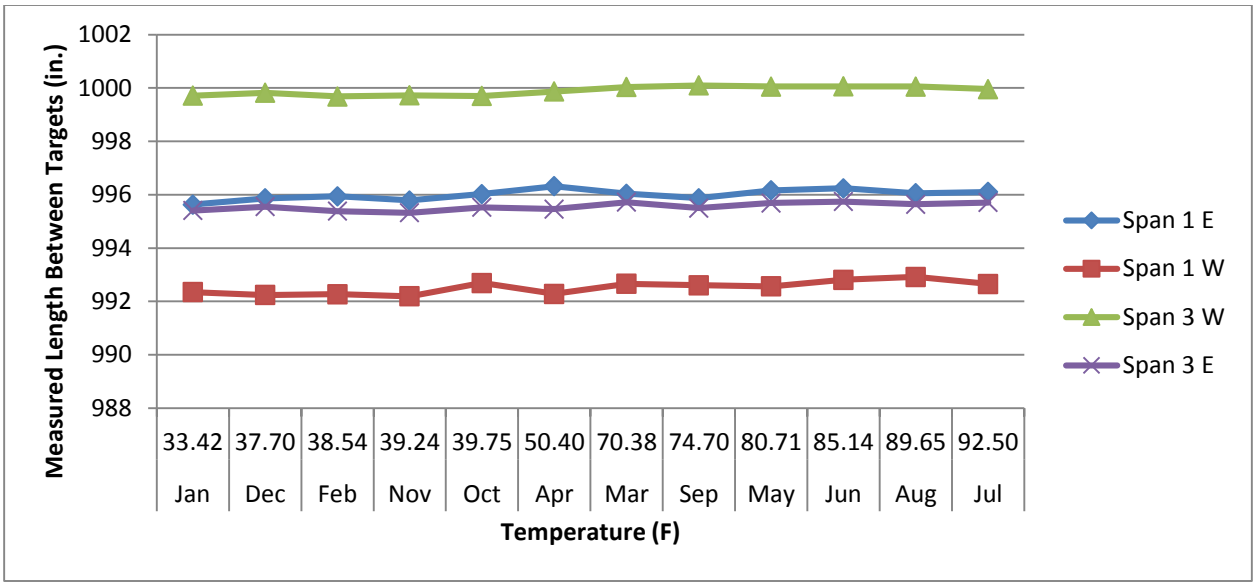

Figure 3.14 Measured Lengths Between Survey Targets in Order of Increasing Temperature

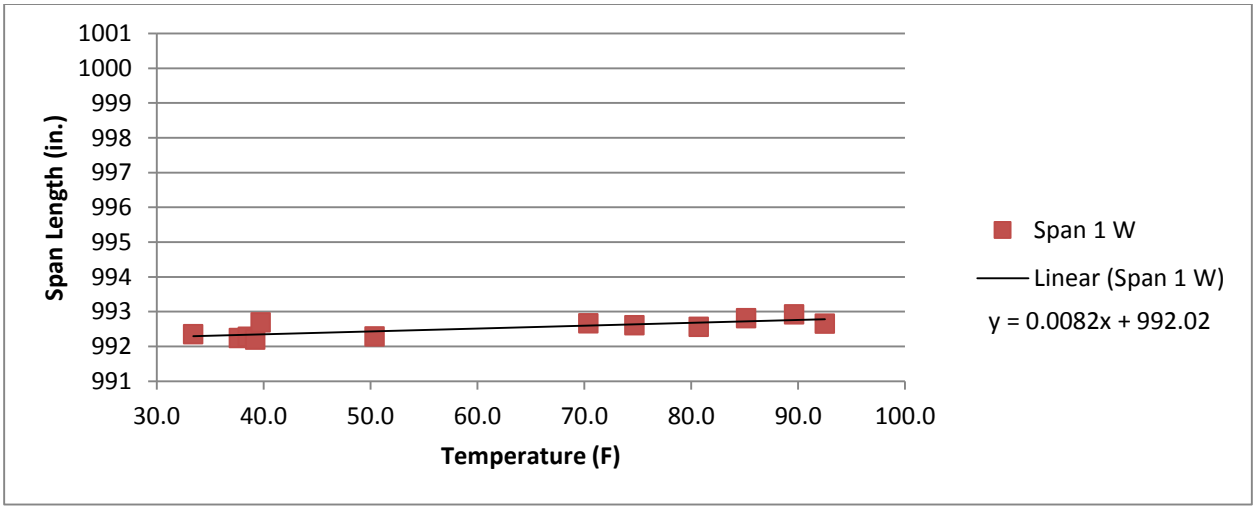

Figure 3.15 Change in Measured Span Length for the West Side of Span 1 in Order of Increasing Temperature

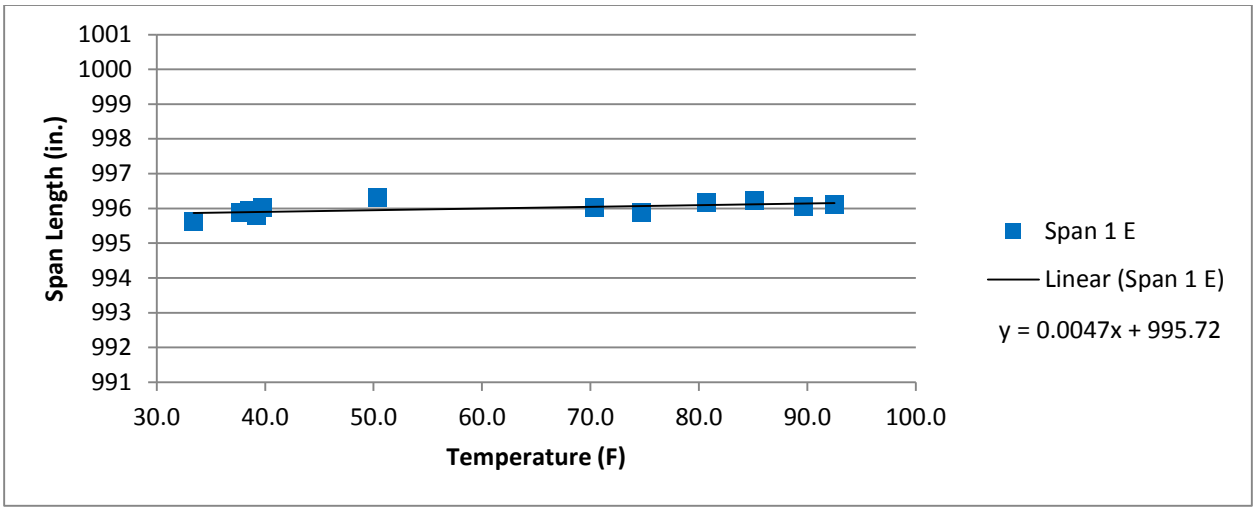

Figure 3.16 Change in Measured Span Length for the East Side of Span 1 in Order of Increasing Temperature

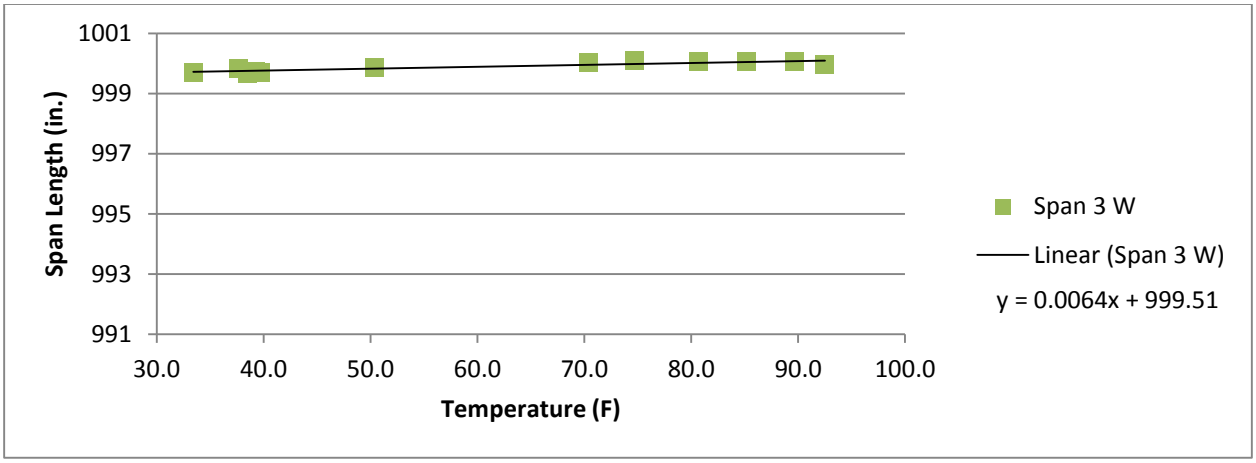

Figure 3.17 Change in Measured Span Length for the West Side of Span 3 in Order of Increasing Temperature

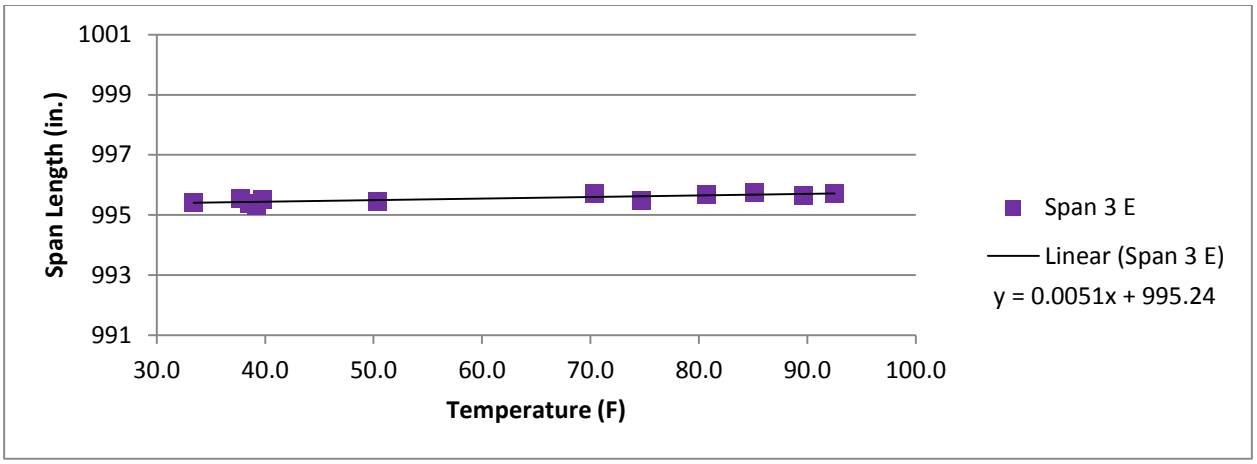

Figure 3.18 Change in Measured Span Length for the East Side of Span 3 in Order of Increasing Temperature

The survey results depicted graphically in Figures 3.13 and 3.14 show that a relatively small amount of movement occurred in the bridge spans. The average difference between the maximum recorded length measured and the minimum recorded length measured was 17.52 mm (0.690 in.) for the east side of Span 1, 18.42 mm (0.725 in.) for the west side of Span 1, 10.51 mm (0.414 in.) for the west side of Span 3, and 10.67 mm (0.420 in.) for the east side of Span 3. In general, the measured lengths obtained increased as the ambient temperature recorded increased.

This same increasing trend can be easily seen in Figures 3.15 through 3.18. The slope of the data trend lines shown in Figures 3.15 through 3.18 indicate that the west side of Span 1 expands more than the east side of Span 1. The same is true for Span 3, in that the west side experienced slightly larger movement than the east side. However, the difference between the magnitudes of the two slopes is smaller for Span 3 in comparison with Span 1. This indicates the presence of a moment in the abutment due to unequal expansion on the east and west sides of the bridge.

As mentioned previously, targets were placed on either side of the expansion gap and measured with a measuring tape at the time of the monthly survey starting in January. Figure 3.12 shows the configuration of the targets at the expansion gaps. A graph of the expansion gap movement recorded for targets placed at corners A, B, C, and D is shown in Figures 3.19 and 3.20.

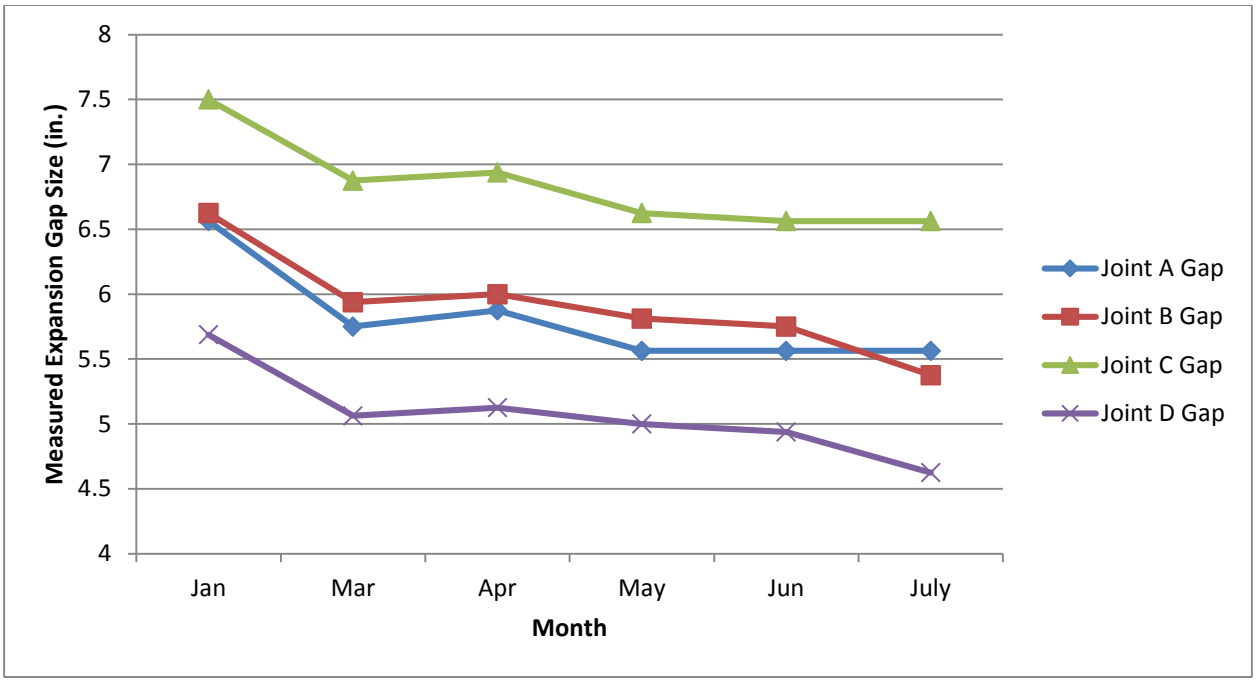

Figure 3.19 Measured Gap at Joints A, B, C, and D in Chronological Order

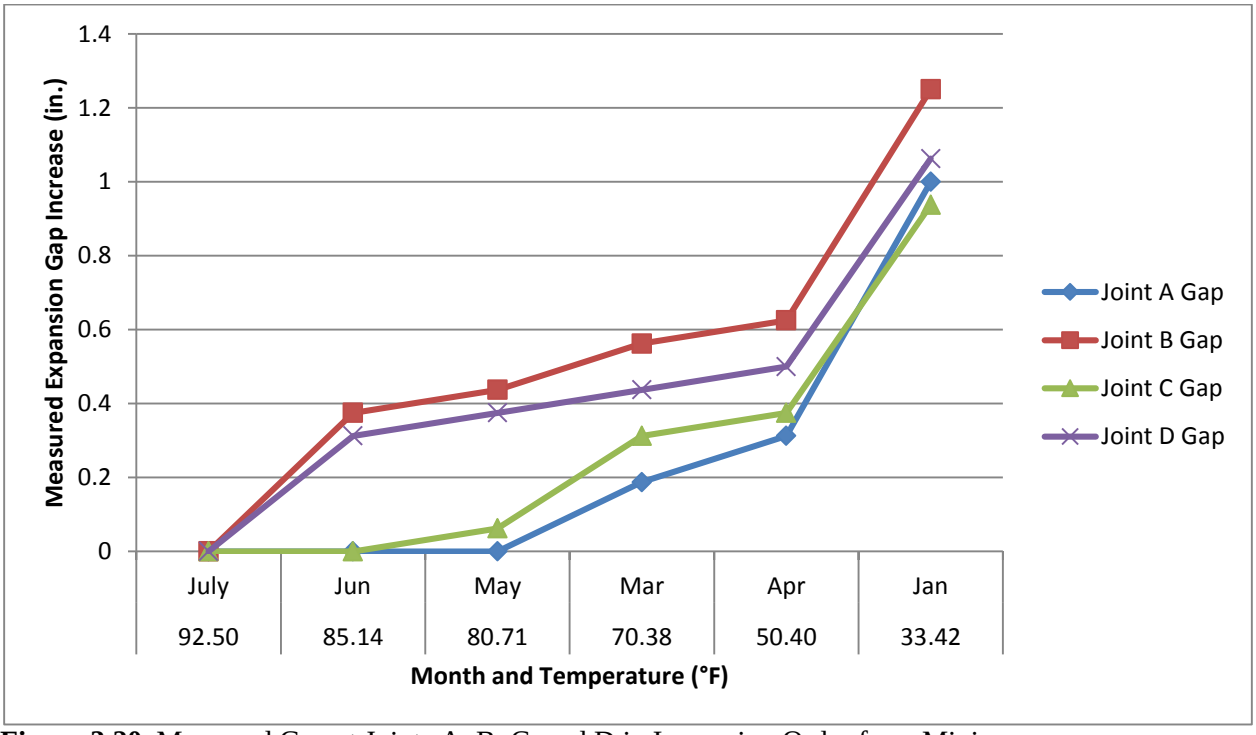

Figure 3.20 Measured Gap at Joints A, B, C, and D in Increasing Order from Minimum

Figure 3.19 clearly shows an increase in expansion gap size measured as the recorded ambient temperature decreases. The movements of the expansion gaps at opposite corners appear to exhibit similar movements. This can be seen in Figure 3.19 when comparing the movement of the Joint B gap with that of Joint D. The same correlation can be made between the Joint B gap and the Joint C gap. The similar

trend line slopes in Figures 3.16 and 3.17 also support this observation. This behavior supports the presence of bending moment occurring within the bridge abutments as a result of unequal movements at the east and west sides of each abutment.

3.5 HOURLY READINGS FROM DAY-LONG SURVEY

Similar calculations were made using Equation 1 with the data collected hourly during the full-day survey. These results are shown graphically in Figures 3.21, 3.22, and 3.23.

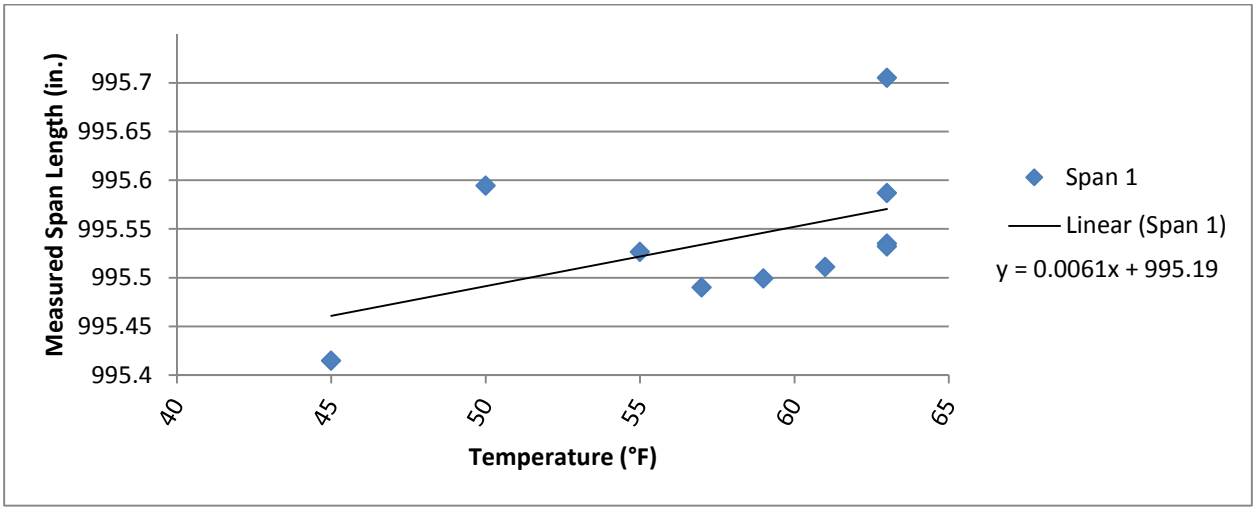

Figure 3.21 Span 1 Measured Lengths Between Survey Targets for Day-Long Survey

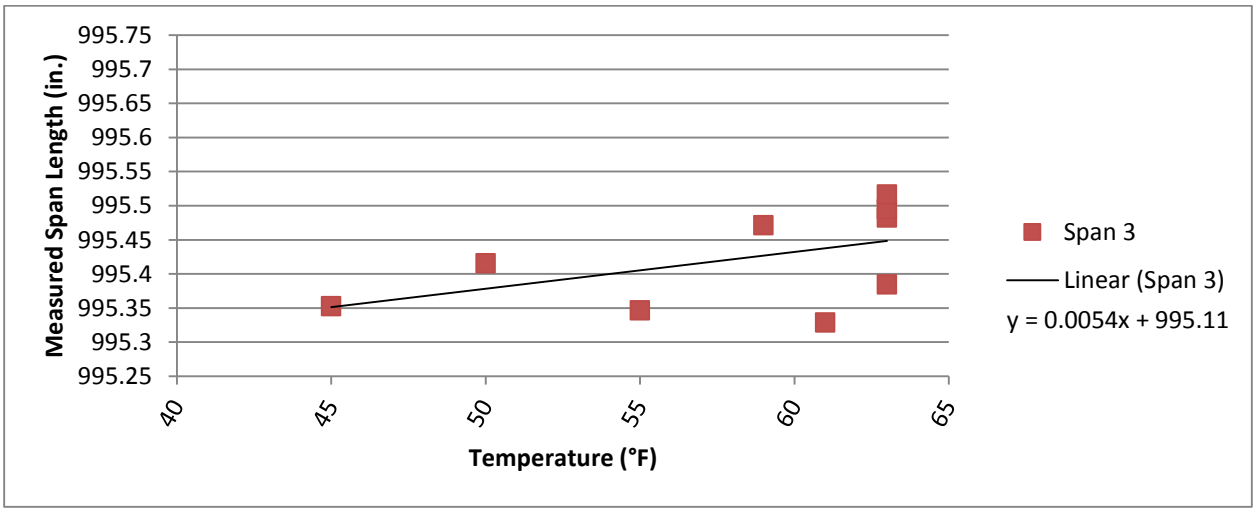

Figure 3.22 Span 3 Measured Lengths Between Survey Targets for Day-Long Survey

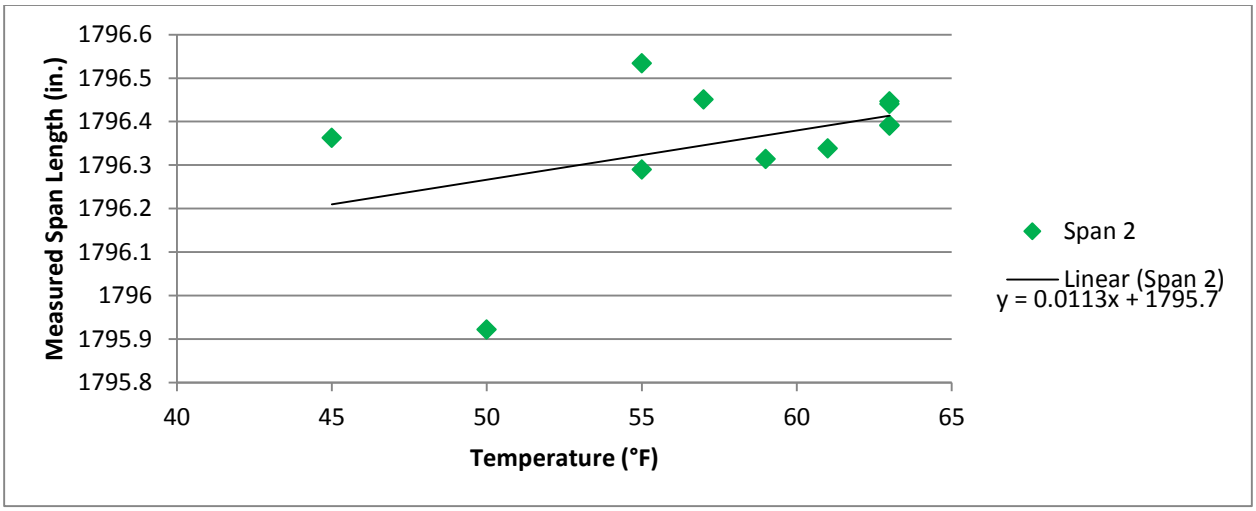

Figure 3.23 Span 2 Measured Length Between Survey Targets for Day-Long Survey

Figures 3.21, 3.22, and 3.23 show a relatively small amount of movement in the bridge spans. For the full-day survey, the measured difference between the maximum recorded length and the minimum recorded length was 7.38 mm (0.29 in.) for Span 1, 15.55 mm (0.61 in.) for Span 2, and 4.78 mm (0.19 in.) for Span 3. In general, the measured lengths obtained increased as the ambient temperature increased throughout the day, with a slight time lag. The slope of the data trend lines shown in Figures 3.15 through 3.18 also indicate greater rate of expansion in Span 3 than observed in Span 1, again indicating that the conditions for Span 3 are different than those of Span 1.

3.6 NV5 MATERIAL

In order to quantify the global bridge movement of the bridge, an investigation by NV5 was performed in which a three-dimensional survey of the bridge was conducted. The three-dimensional survey was performed in conjunction with a standard survey with the level. Both surveys were conducted in February 2012. The goal was to perform two scans of the bridge. The original scan would serve as the baseline scan performed during a relatively cold period of time. It was anticipated that a second scan would be performed during the summer and serve as the bridge condition during a hot period of time. The original scan by NV5 successfully developed a three-dimensional model of the bridge with many more displacement points that could be used for comparison. Figure 3.24 shows the three-dimensional model developed by NV5.

After evaluating the NV5 data and discussing the requirements for the second scan, it was decided to forgo the second scan planned for the summer. This decision was based on the relatively small changes in movement that were measured with the level readings and the precision capabilities of the NV5 system.

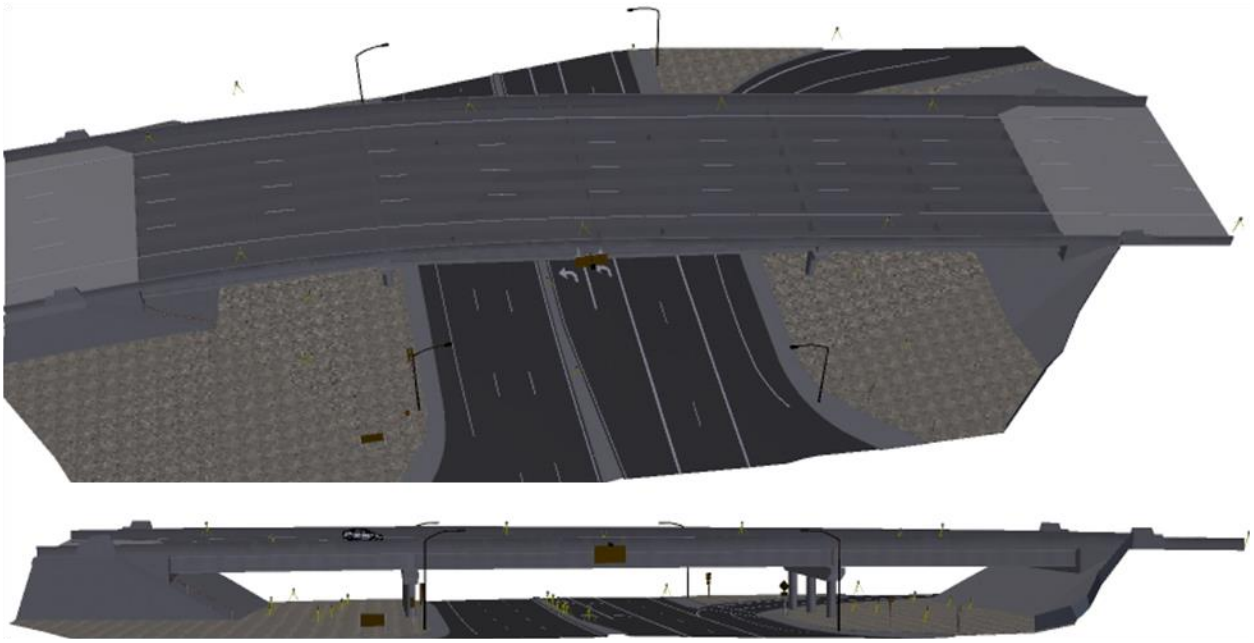

Figure 3.24 3D Bridge Model Developed by NV5

3.7 AVERAGE BRIDGE TEMPERATURE IN UTAH

In parallel with the work on the 400 South Street Bridge, research was also being conducted on a separate bridge (Rodriguez 2012) that helped define average bridge temperatures in the State of Utah. Thermocouples were installed through the depth of an integral abutment bridge located on Interstate 15 over Cannery Road near Perry, Utah. Thermocouples installed throughout the depth of the bridge allowed for the calculation of average maximum and minimum temperatures for a typical Utah bridge. Based on guidelines presented in the AASHTO LRFD Bridge Design Specifications (2010), the average temperature was calculated from recorded temperatures using Equation 2.

$$T_{avg} = \frac{\sum A_i * E_i * \alpha_i * T_i}{\sum A_i * E_i * \alpha_i}$$

(Eq. 2)

where

T_{avg} = average of the bridge temperature over the bridge cross section;
A_i = Area of the bridge cross section of the *i*-th segment;
E_i= Modulus of elasticity of the cross section of the *i*-th segment;
α_i= Coefficient of thermal expansion of the material used for the *i*-th segment;
T_i= Temperature of the cross section of the *i*-th segment.

Using Equation 2, the data collected every 15 minutes from the bridge thermocouples were used to calculate average bridge temperature. The resulting average bridge temperatures obtained are shown in Figure 3.25 (Rodriguez 2012). A comparison of the measured maximum temperature gradient determined for a typical Utah Bridge is also shown in Figure 3.26 (Rodriguez 2012). The figures show that the AASHTO LRFD average bridge temperature limits, as well as the prescribed design temperature gradient,

accurately encompass the measured data. The reader is referred to the publication by Rodriguez (2012) for additional information.

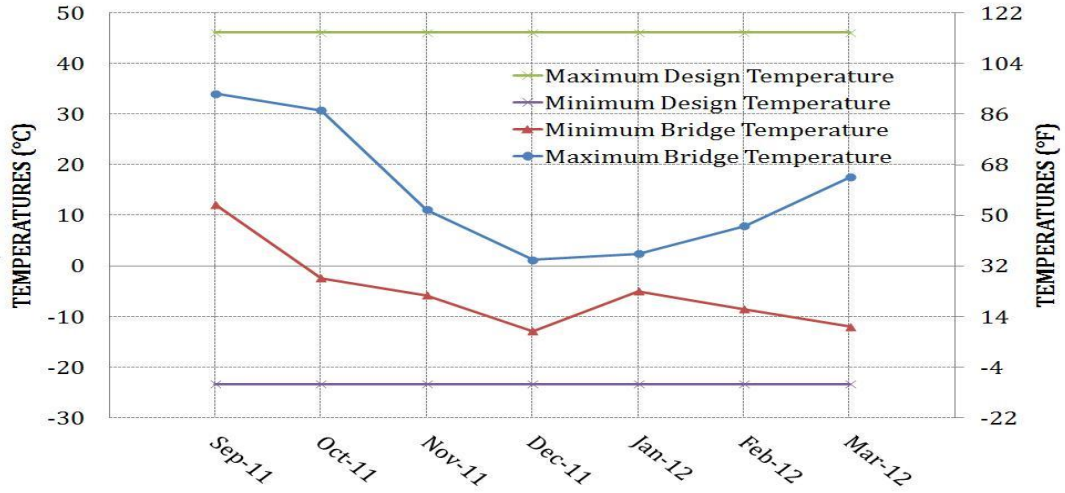

Figure 3.25 Monthly Measured Mean Temperature for a Utah Bridge

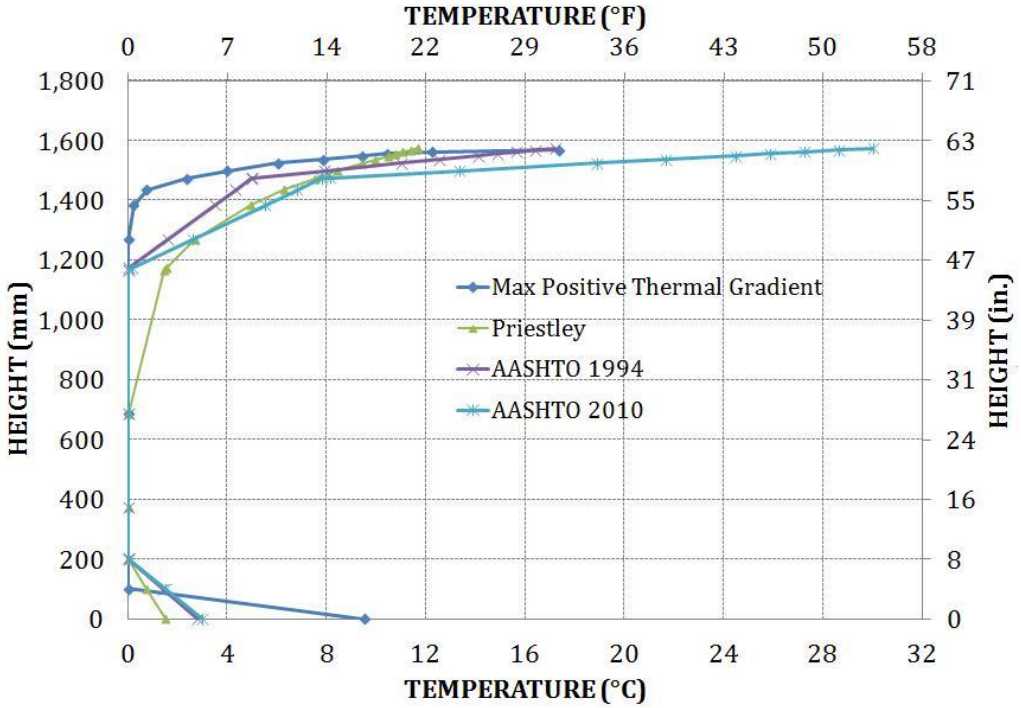

Figure 3.26 Maximum Positive Thermal Gradient for a Utah Bridge on September 25

3.8 SUMMARY

The 400 South Street Bridge in Salt Lake City was monitored for changes in displacement due to temperature. In addition, a full bridge scan by NV5 was conducted. A comparison of measured average bridge temperatures and positive temperature gradients of a typical Utah Bridge with the AASHTO LRFD specifications was performed. A summary of the research findings is provided below.

- Based on the survey data collected, a small amount of movement due to changes in temperature was observed in each of the spans of the 400 South Street Bridge. However, despite the small movement, damage occurred in the north abutment.
- According to the periodic monthly survey, slightly more movement occurs on the west side of Span 1 than on the east side. There was also slightly more movement observed on the east side of Span 3 than on the west side The full-day survey showed similar magnitudes in Span 1 and Span 3.
- The survey data showed that opposite corners of the bridge expanded and contracted differently, indicating the potential presence of an overall twisting motion. This non-uniform expansion and contraction could potentially be inciting a moment at the north abutment.
- According to temperature measurements on a typical Utah bridge, the maximum and minimum average design temperatures are indicative of the average bridge temperatures occurring in Utah. These maximum and minimum temperatures are predicted within the AASHTO LRFD specifications. In addition, temperature gradient measurements are also within the recommendations provided by AASHTO.
- The three-dimensional survey conducted by NV5 did not have enough accuracy to perform a second test.

4. FINITE ELEMENT ANALYSES

4.1 FINITE ELEMENT MODEL

A description of the finite element analyses conducted for the 400 South Street Bridge is contained in Section 4. A description of the initial detailed solid model used to identify locations of stress concentrations is first presented. A simplified model of the 400 South Street Bridge follows. Data concerning change in span length with temperature are then included. A description of a parametric study conducted to further identify bridge parameters influencing the spalling of the abutments is included. The findings of these tests are also presented. A summary of the findings of the finite element analyses concludes Section 4.

4.1.1 Detailed Solid Model

A detailed finite element model of the 400 South Street Bridge was created using SAP2000 (Computers and Structures, Inc.) software. The model was developed using solid elements for the girders, abutments, bents, and bridge deck. The columns and piles were modeled using frame elements. The bridge girders were modeled using the specified prestressed concrete properties with an ultimate compressive strength (f'c) of 52 MPa (7500 psi). The cast-in-place concrete used to model the deck, abutments, bents, and columns was assigned an ultimate compressive strength of 28 MPa (4060 psi). A modulus of elasticity of 24900 MPa (3670 ksi) was used for the cast-in-place concrete and a modulus of Elasticity of 33900 MPa (5000 ksi) was used for the prestressed concrete. The concrete-filled driven piles below the abutments were modeled using frame elements. The piles were modeled using circular steel sections with an outside diameter of 324 mm (12.8 in.). The wall thickness of the piles was increased from the actual pile thickness of 10 mm (0.39 in.) to 31.9 mm (1.26 in.) using transformed section properties and the modular ratio. Surface springs were placed on the abutment face in the longitudinal direction in order to simulate the soil-abutment interaction. A spring stiffness of 150 pcf was used based on typical properties of granular backfill. Springs were assigned as compression and tension springs on the surface of the abutment. No springs were placed on the piles. A view of this model can be seen in Figure 4.1.

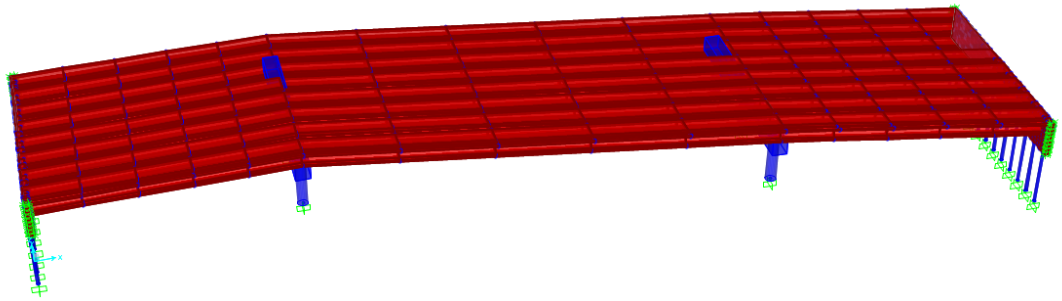

Figure 4.1 3D View of Solid SAP Model

Once the solid version of the SAP model was created, a uniform temperature load of 10° C (50° F) was applied to the concrete girders and deck of the bridge model. The calculated changes in stress for the abutment was then plotted as color contours on each of the solid elements used to model the abutment. These contours show the principal stresses in the abutment. The highest concentrations of stresses appeared as purple and red areas. These calculated stress concentrations were localized about the bottom girder flange, which coincides with the same locations as the observed spalling on the 400 South Street Bridge. An example of the stress contours observed can be seen in Figure 4.2.

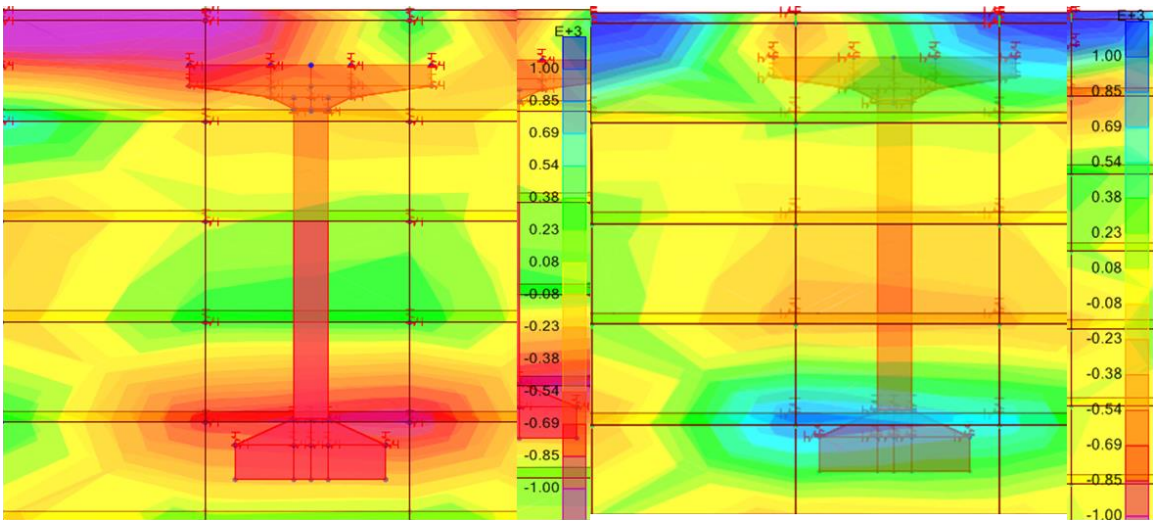

Figure 4.2 View of Model Abutment with Stress Contours Around Girder Bottom

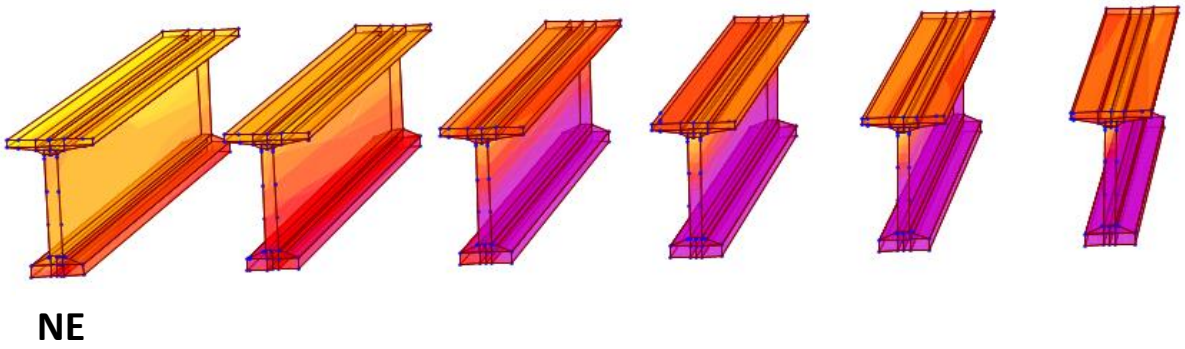

Figure 4.3 View of Stress Contours on Model Girders

Figure 4.3 shows the change in girder stresses at the north abutment of the bridge. For this figure, the girder on the right is at the northwest corner and the girder on the left is at the northeast corner. The figure shows that the calculated girder stresses progressively decrease when moving from the northwest corner to the northeast corner. In comparison, the stresses in the girder at the northwest are more than double those in the northeast girder.

4.1.2 Simplified Finite-Element Model

In order to investigate the important bridge properties that resulted in the observed stress concentrations, a simplified model of the 400 South Street Bridge was constructed using SAP 2000. For the simplified model, frame elements were used to model all of the components of the bridge except the deck, which was modeled using solid elements. This simplified version of the model allowed for parametric studies of bridge parameters that influence the changes in moments in the bridge abutments. The frame elements used to model the bridge abutments were assigned line springs with a stiffness of 29.2 kN/m (2000 lb/ft), which corresponds to the stiffness applied to the detailed model. A graphical representation of this model can be seen in Figure 4.4.

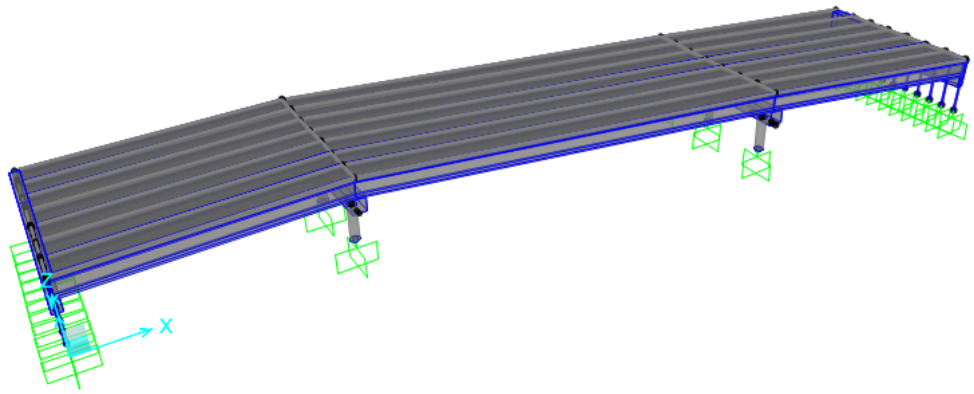

Figure 4.4 View of the Simplified SAP Model Using Frame Elements

Once the simplified finite-element model was developed, a series of temperature loads were applied uniformly on the concrete girders and deck. The applied temperatures corresponded to the measured temperature values recorded during the monthly surveys discussed in Section 3. The minimum recorded temperature was used as a base temperature. The temperature loads were then determined by calculating the difference between the temperature readings for each month compared with the minimum recorded temperature. This resulted in 11 values of temperature changes that were subsequently placed on the bridge model. The change in span length could then be determined using the deflections produced by the simplified SAP model. These changes in span length were compared with theoretical values calculated using Equation 3.

$$\Delta = \alpha * \Delta T * L \qquad \textbf{(Eq. 3)}$$

where,

Δ = change in span length
α = coefficient of thermal expansion
ΔT = change in temperature
L = length of span

This equation was evaluated for spans one and three with $\alpha=6.5*10^{-6}$ $°F^{-1}$and L=84.41 ft for Span 1 and L=84.69 ft for Span 3. The values used for ΔT were the temperature change values (in °F) recorded for each month relative to the minimum recorded temperature. This comparison can be seen in Figures 4.5 through 4.8.

A comparison of trend lines in Figures 4.5 through 4.8 is very similar. In each case, it is observed that the values of change in calculated length obtained in SAP are lower than those predicted by Equation 3. This signifies that the SAP model represents conditions that are slightly restrained. This agrees with the expected conditions of the 400 South Street Bridge. The measured data in each plot are reasonably predicted by the finite-element model and simply supported conditions. Figure 4.9 shows the behavior of the east and west sides of Span 1 and Span 3 compared to one another.

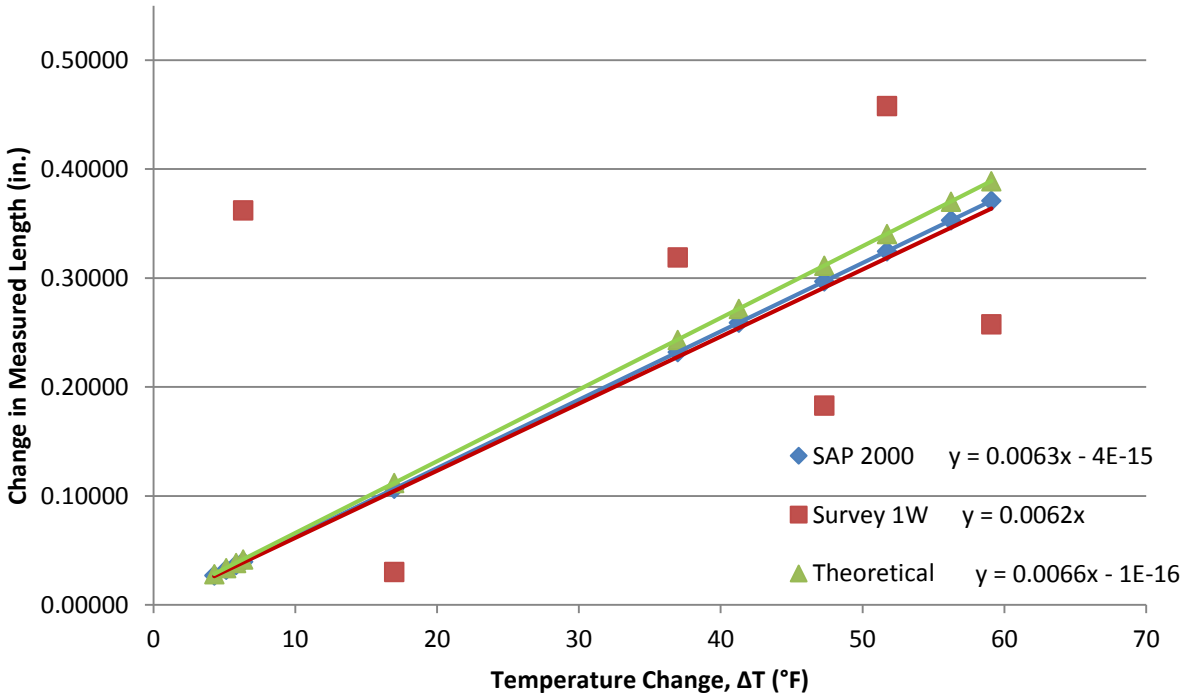

Figure 4.5 Comparison of SAP and Theoretical Values for the West Side of Span 1

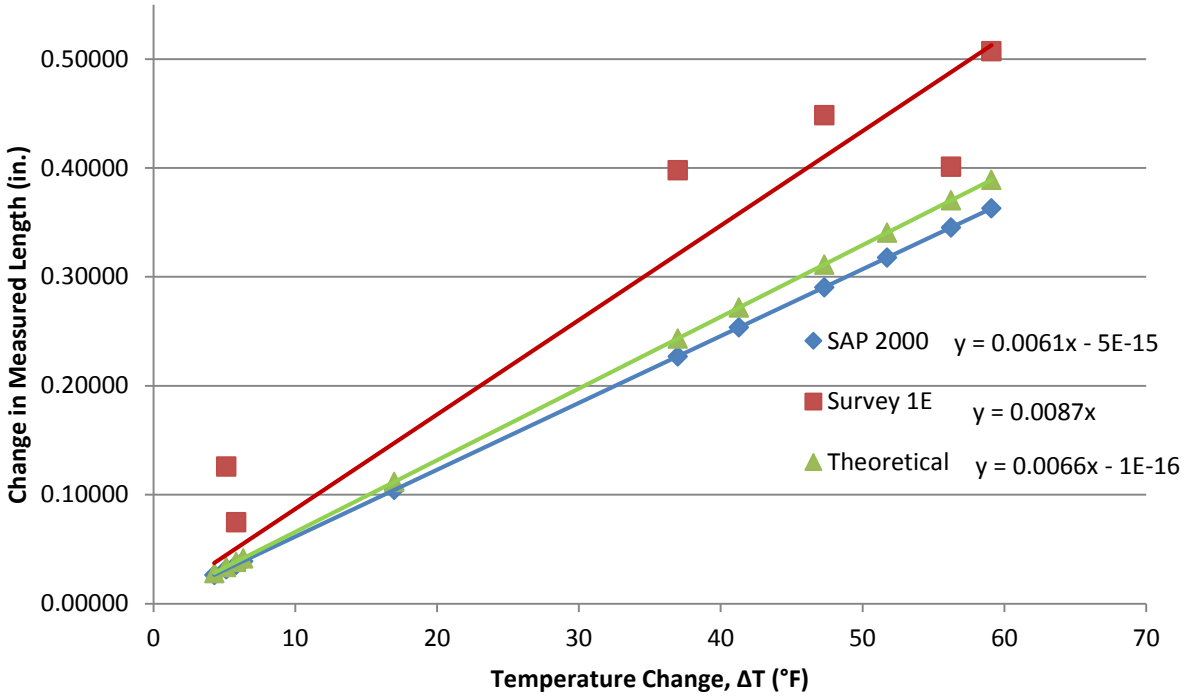

Figure 4.6 Comparison of SAP and Theoretical Values for the East Side of Span 1

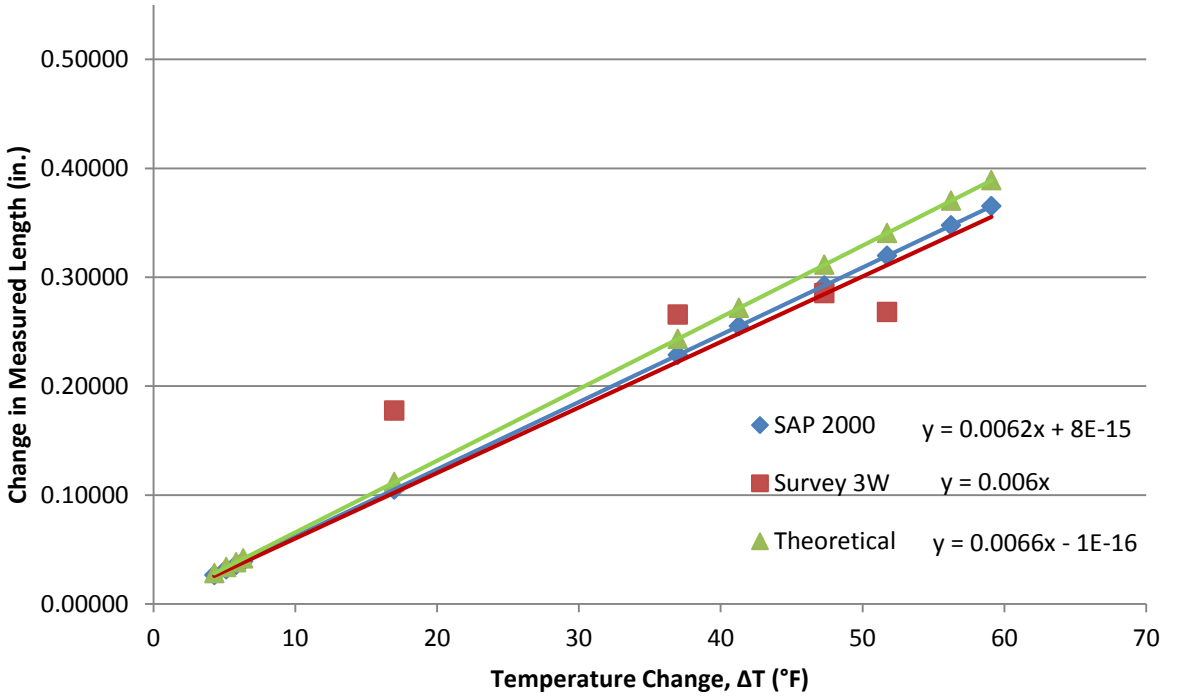

Figure 4.7 Comparison of SAP and Theoretical Values for the West Side of Span 3

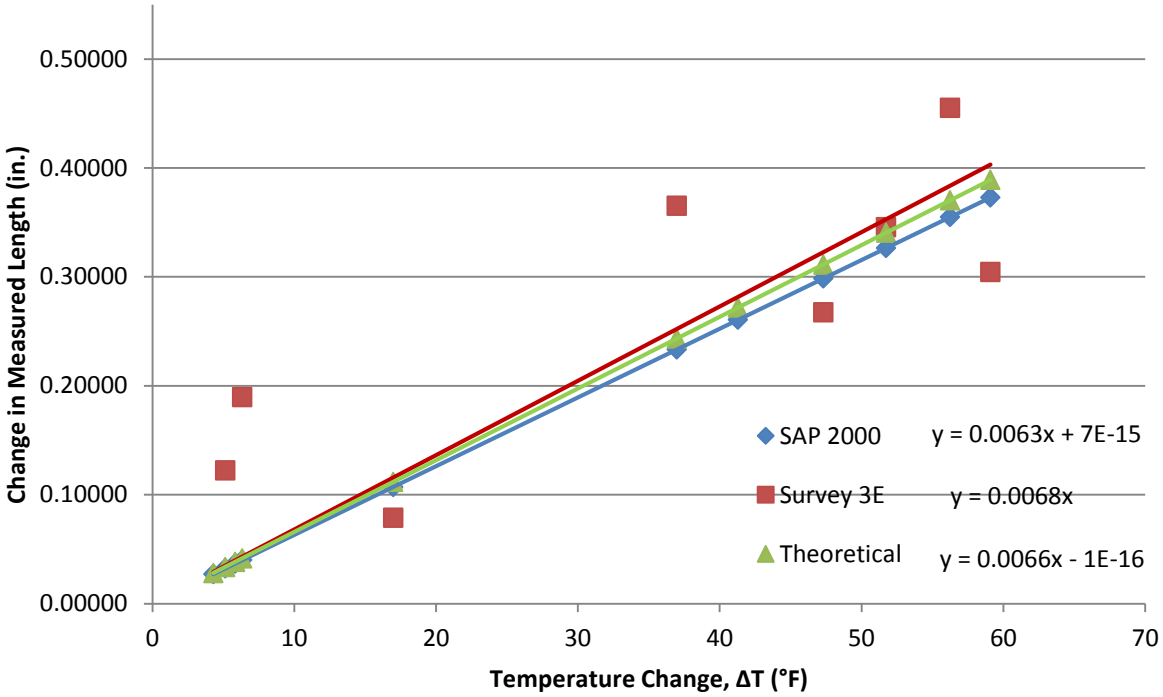

Figure 4.8 Comparison of SAP and Theoretical Values for the East Side of Span 3

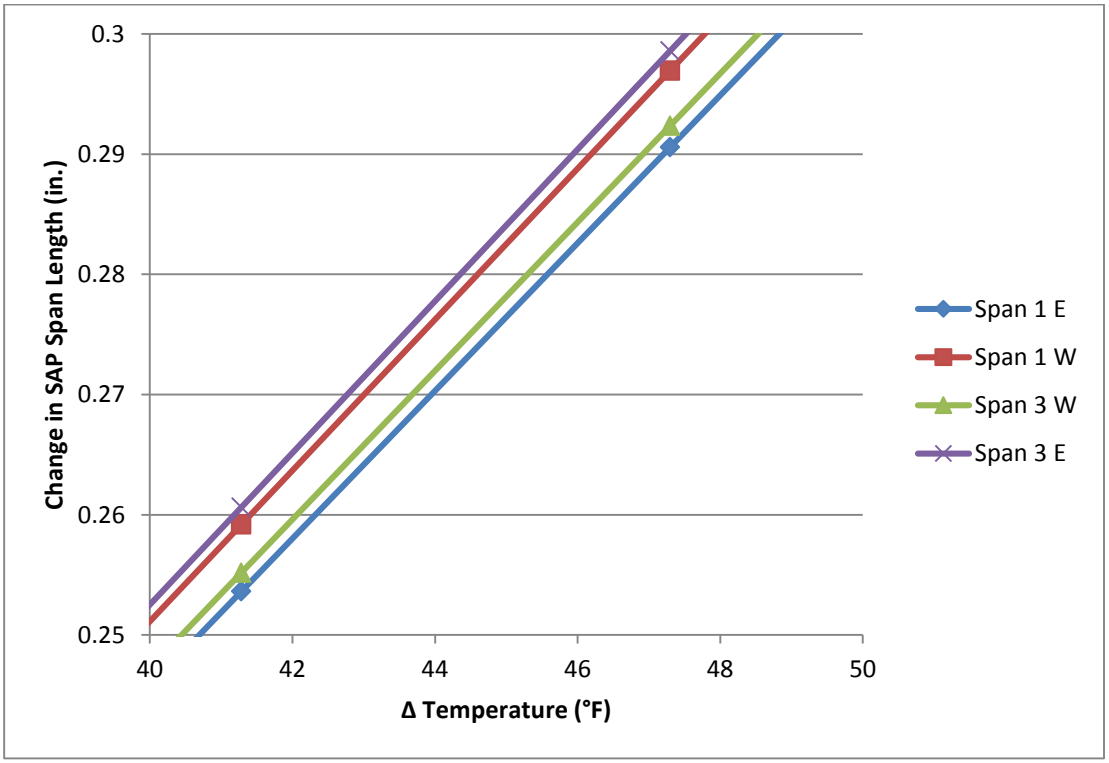

Figure 4.9 Measured Changes in Span Length According to SAP 2000

In Figure 42 it can be seen that the east side of Span 3 and the west side of Span 1 exhibit very similar behavior. This can also be concluded about the west side of Span 3 and The east side of Span 1. This relationship is the same as was observed from the survey data discussed in Chapter 3. As a result, it can be concluded that the same trend of non-uniform expansion and contraction was observed from the SAP model data that was observed in the monthly surveys.

4.1.3 Abutment Lateral Displacement

Calculating the transverse abutment force due to temperature effects can be done using Equations 4 through 8. As the skew angle increases, the transverse abutment force increases.

$$\Delta = \frac{P_l * L}{A * E} \quad \textbf{(Eq. 4)}$$

$$\boldsymbol{P_l = \frac{\Delta * A * E}{L}} \quad \textbf{(Eq. 5)}$$

$$P_l = \frac{\alpha * \Delta T * L * A * E}{L} \quad \textbf{(Eq. 6)}$$

$$\boldsymbol{P_l = \alpha * \Delta T * A * E} \quad \textbf{(Eq. 7)}$$

$$P_l = \alpha * \Delta T * A * E \quad \textbf{(Eq. 8)}$$

where,

- Δ = change in span length
- P_l = lateral force
- L = length of span
- A= Area of abutment
- E= Modulus of elasticity
- α = coefficient of thermal expansion
- ΔT = change in temperature
- P_t = transverse force

Using the same simplified model described in Section 4.1.2, bridge behavior about the lateral deflection of the abutments was obtained. Lateral displacement corresponds to displacement in the transverse

direction of the SAP model. Figure 4.10 shows a comparison of the lateral deflections of the north and south abutments obtained from the SAP model. Figure 4.10 also shows that the north abutment displaces laterally much more than the south abutment does. This unbalanced movement is the main contributing factor to the non-uniform change in span length that can be seen in Figure 4.8.

These observed trends from the SAP model data support the correlation between the survey results and the finite-element model results. Using the same simplified SAP model, a series of parametric studies was then conducted.

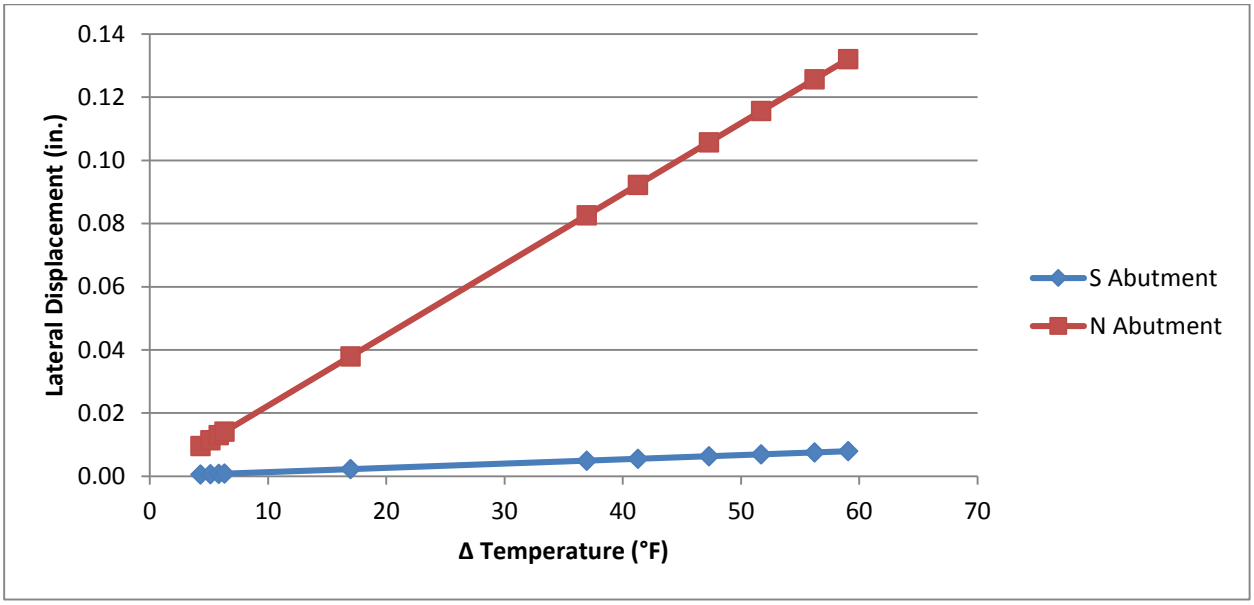

Figure 4.10 Comparison of Modeled Lateral Deflections of the Bridge Abutments

4.2 PARAMETRIC STUDY

In an effort to further identify bridge parameters influencing the spalling observed on the abutment of the actual bridge, a series of parametric studies were conducted using SAP 2000. These studies were used to investigate the influence of skew angle and span length on the weak-axis bending moment in the abutment.

4.2.1 Effect of Abutment and Pier Offset

The first series of parametric tests provided an additional validation of the as-is model, as well as an investigation of the influence of the overall abutment offset of the bridge. This was achieved by a series of evaluations conducted using the simplified model of the bridge that used beam elements for the girders and abutments. The actual abutment offset of the bridge was multiplied by factors ranging from 0.10 to 5.0. The offsets used are labeled as A, B, and C in Figure 4.11. The offset values A, B, and C were multiplied by the factors from 0.1 to 5.0 to produce a series of skew angles occurring in the bridge spans that were factors of the actual bridge geometry. The actual geometry of the bridge was therefore represented by a factor of 1.0. A temperature differential of 50° F was uniformly applied to the girders and deck of the bridge model. For each offset factor, the maximum weak-axis bending moment in the abutment was found obtained the SAP model. Figure 4.12 shows the increase in moment on the skewed (north) abutment. These results agree with the observed spalling of the northern abutment and also serve as a secondary qualitative validation of the SAP model.

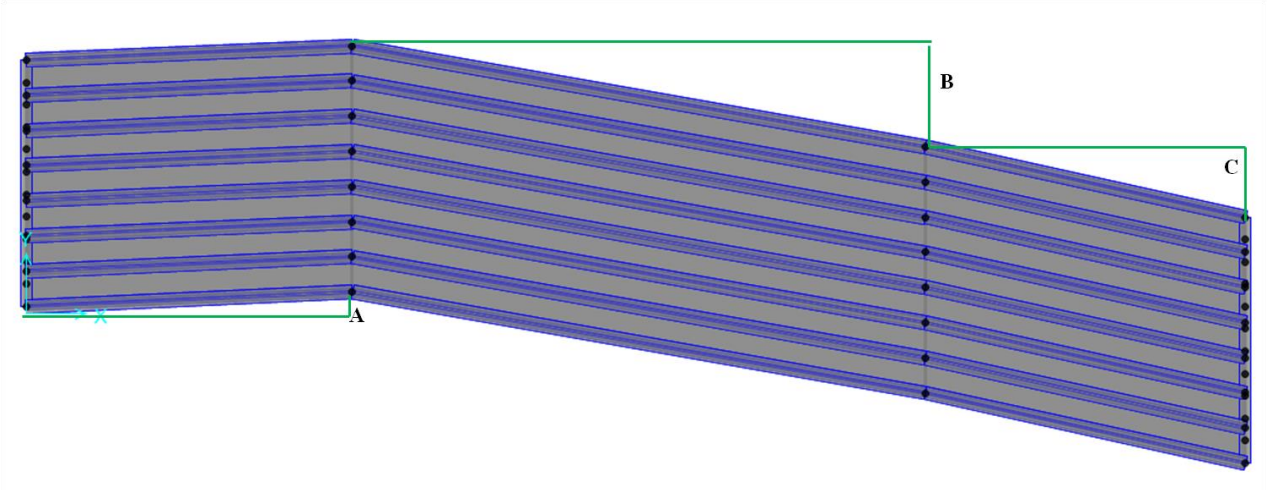

Figure 4.11 Labeled Abutment Offsets of the Bridge

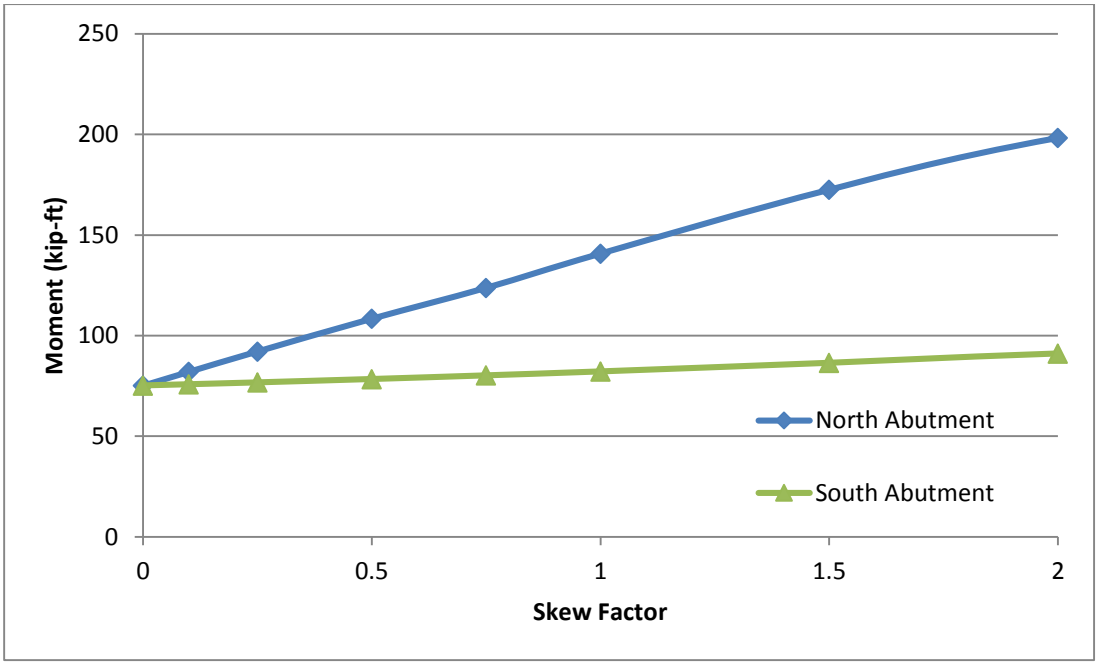

Figure 4.12 Increase in Absolute Maximum Weak-axis Bending Moment of the Abutments for Parametric Study of Full Bridge Geometry

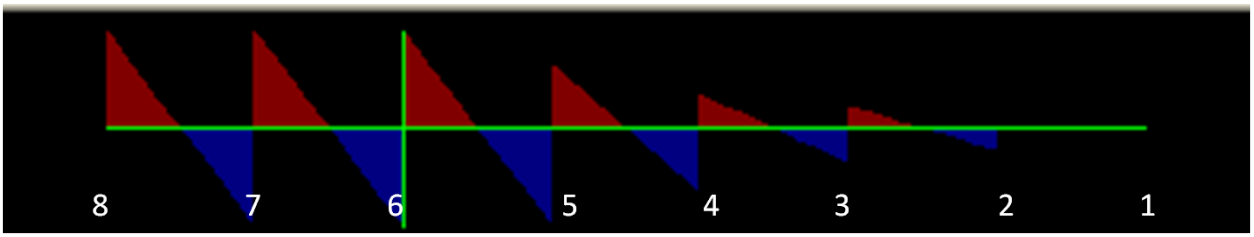

Figure 4.13 Moment Diagram for the North Abutment for the Actual Bridge Geometry

Figure 4.13 shows the moment diagram obtained from the SAP model for the multiplication factor of 1.0, representing the actual bridge geometry. The maximum moment was observed between girders 5 and 6 and between girders 7 and 8. The girders are numbered, with the girder on the east side of the bridge being number 1 and the west most girder being number 8. This agrees with the actual location of the most extreme spalling on the 400 South Street Bridge.

4.2.2 Effect of Skew

Using the same bridge components described for the full-scale model of the bridge, a model was created to test the effects of skew angle. A single span version of the bridge consisting of eight girders and the concrete deck supported by abutments and piles was created. The same configuration of soil springs as previously described was applied to the abutments. The temperature differential applied to the girders and deck was again 50° F. A straight version of this model was evaluated and then the skew angle was increased in 10° increments by rotating the abutments. Figure 4.14 shows an example of this model with a skew angle of 10°.

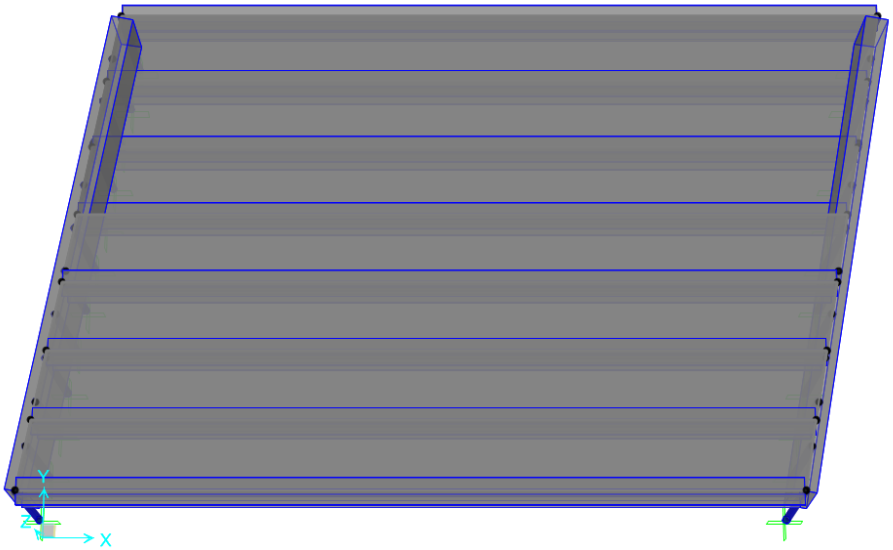

Figure 4.14 Parametric Skew Model with Skew Angle of 10°

The finite-element model results calculated from this study were used to calculate an increase in abutment moment as a function of skew angle. This calculated weak-axis moment could then be compared with the cracking moment of the abutment. The moment values recorded from the skewed models were compared with the moment in the abutments from the straight version of the same model. By dividing the moment from the skewed models by the moment from the zero-skew model, a moment ratio was found. The results from the parametric skew test can be seen graphically in Figures 4.15 and 4.16.

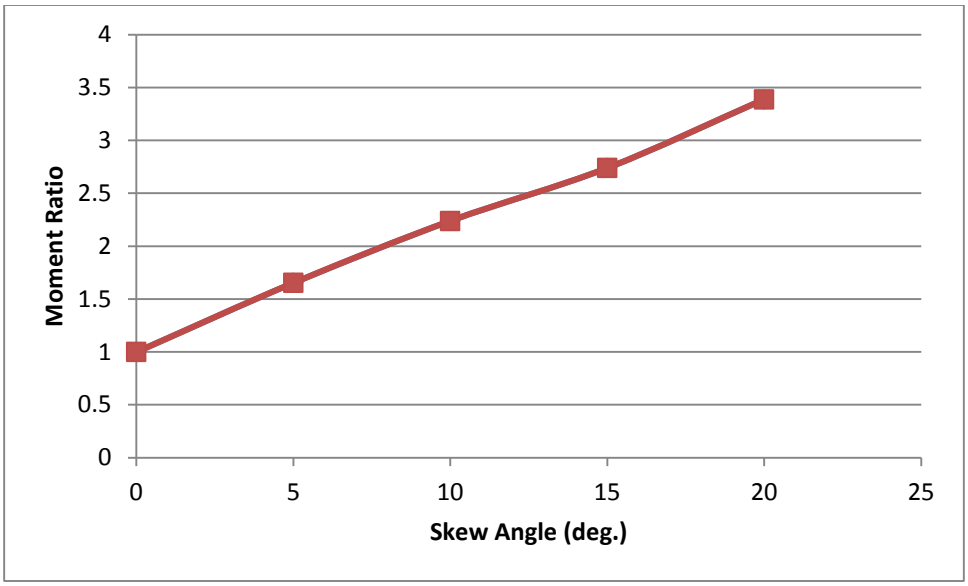

Figure 4.15 Moment Ratio Results of a Parametric Study of Skew Angle

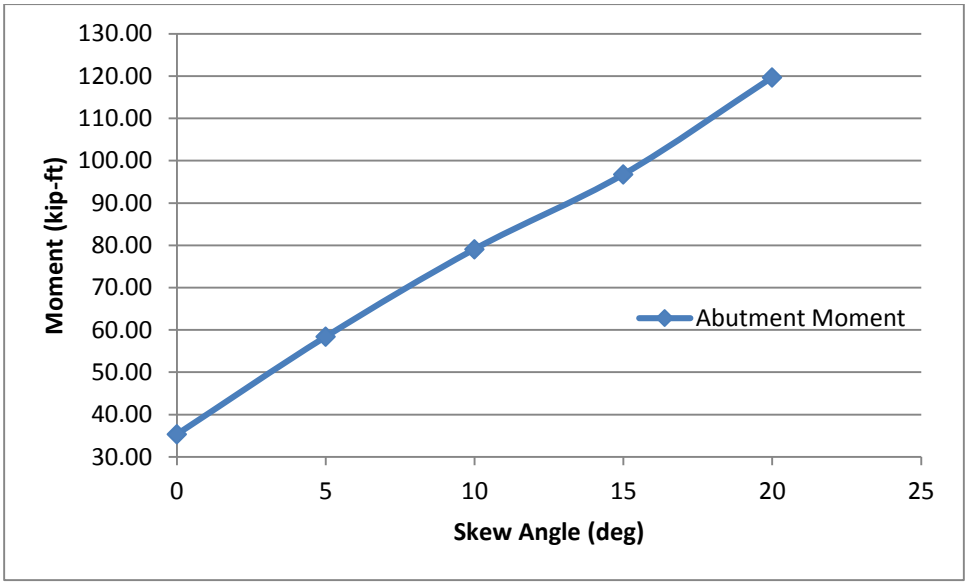

Figure 4.16 Comparison of Absolute Maximum Weak-Axis Bending Moment in the Abutment with Calculated Cracking Moment for a Parametric Study of Skew Angle

Figure 4.15 shows a large increase in moment as skew angle increases. The amount of moment in the 20° skew model is more than three times that of the model without skew. According to this study, for each 5° increase in skew, a 50% to 65% increase in moment is seen in the abutment. This shows a very strong relationship between the amount of moment in the bridge abutments and the skew angle of the abutments. Figure 4.16 shows the increase in weak-axis bending moment in the abutment as skew angle is increased.

4.2.3 Effect of Span Length

A second parametric study was conducted using the same components as the models previously described in a configuration designed to test the effects of span length. A three-span model of similar configuration to that of the actual bridge was used. Each of the three spans was modeled with equal lengths. A sample view of this arrangement can be seen in Figure 4.17.

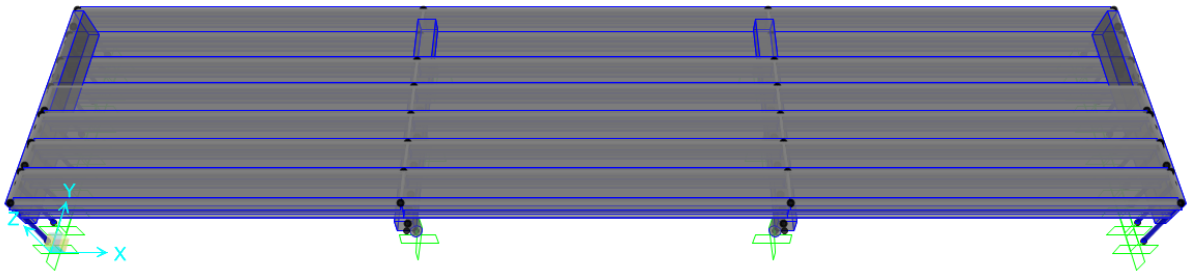

Figure 4.17 Three-span Parametric Length Model

Tests were performed using a range of span lengths from 100 feet to 300 feet in 25-ft increments. The weak-axis bending moment in the abutment was recorded for each configuration and used to calculate a moment ratio for each length test. The results show a clear increase in moment ratio as the span length increases. The results from these tests can be seen in Figures 4.18 and 4.19.

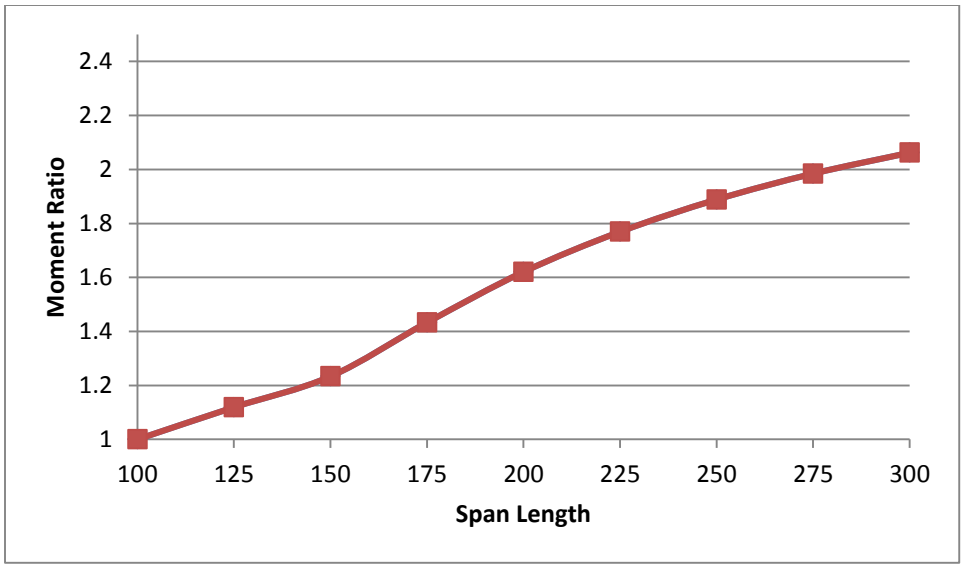

Figure 4.18 Moment Ratio Results of a Parametric Study of Span Length

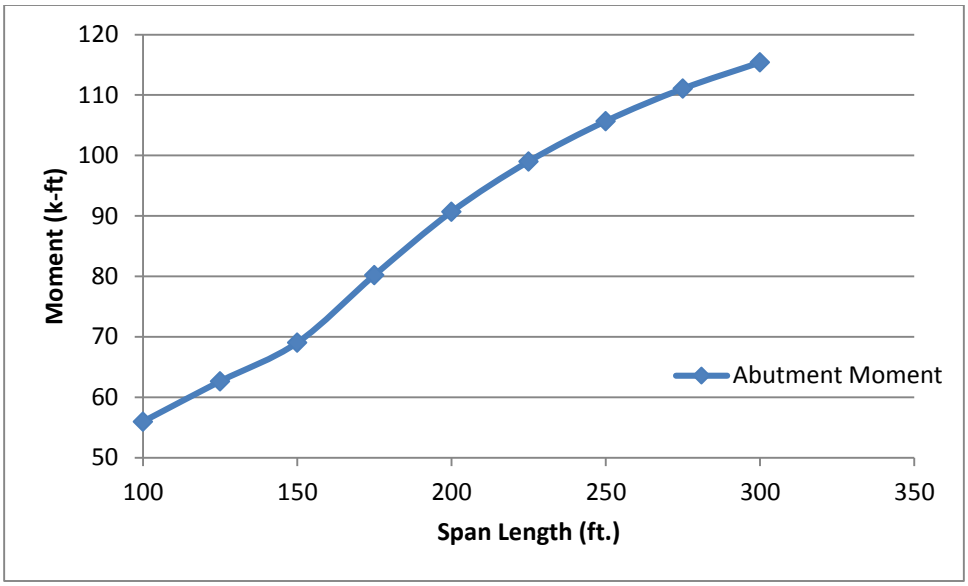

Figure 4.19 Comparison of Absolute Maximum Weak-Axis Bending Moment in the Abutment with Calculated Cracking Moment for a Parametric Study of Length

According to the test results shown in Figure 4.18, by doubling the span length, an approximately 60% increase in moment is seen in the abutment. Figure 4.19 shows the calculated abutment moments from the model.

4.2.4 Effect of Temperature Gradient

An investigation regarding the effect of temperature gradient over the bridge cross-section was carried out using a single-span model of a length of 100 feet. The model was constructed similar to the zero-skew model used in the parametric investigation of skew angle described in Section 4.2.3. The geometry of the bridge model remained constant for this test while the difference between the temperature loads applied to the deck and the girders was increased. The first evaluation was performed without any gradient and a temperature load of 50° F. The temperature load on the deck was then increased in increments of 10° F while the girder temperature loads remained the same. The moment in the abutments as a function of temperature gradient was compared with the values obtained from the uniform temperature loading to get a moment ratio based on temperature gradient. The results from this test are shown in Figures 4.20 and 4.21.

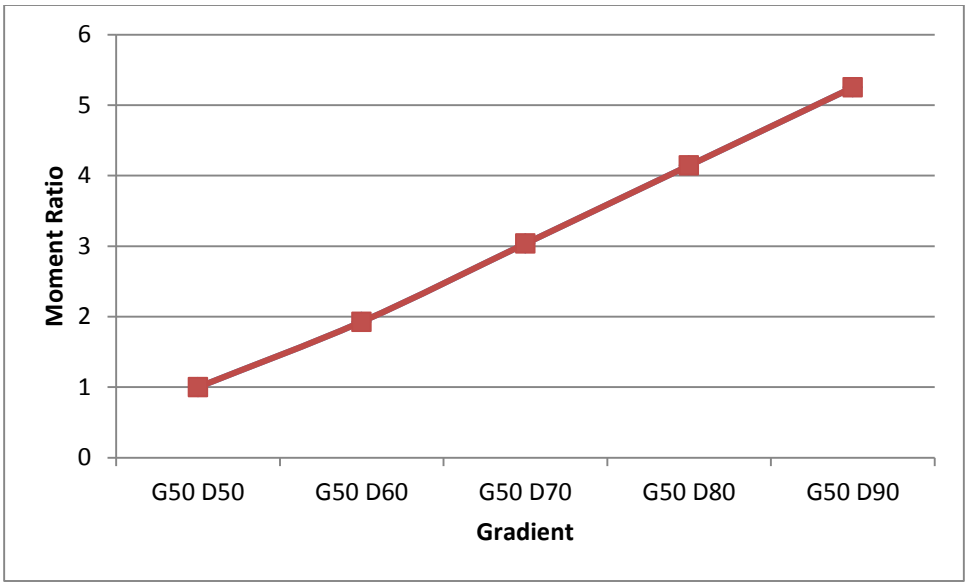

Figure 4.20 Moment Ratio Results from a Parametric Study of Temperature Gradient

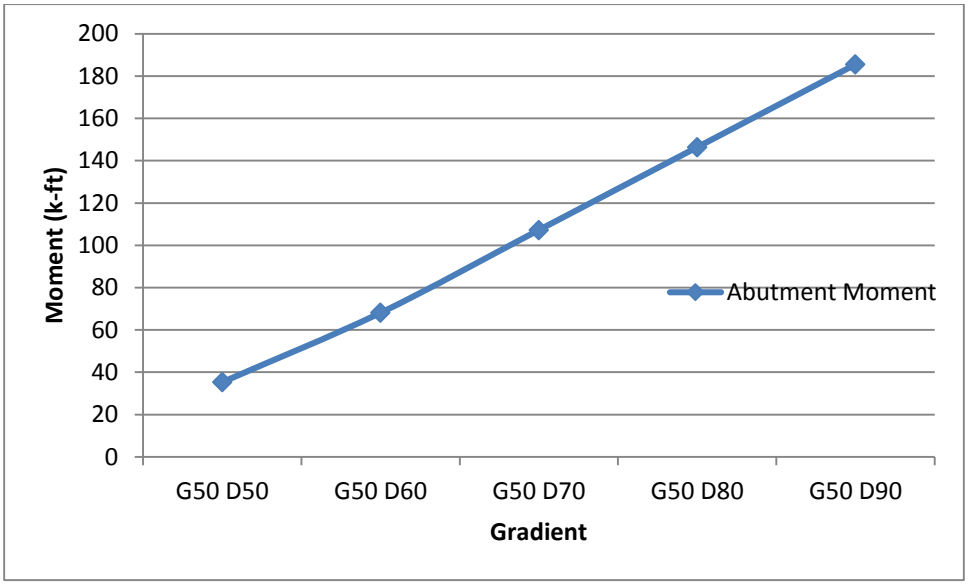

Figure 4.21 Comparison of Absolute Maximum Weak-Axis Bending Moment in the Abutment with Calculated Cracking Moment for a Parametric Study of Length

The results shown in Figure 4.20 show a large increase in the moment in the abutment as the temperature gradient within the bridge increases. According to the data from this test, a 20° F increase in temperature difference between the girders and deck of the bridge causes an approximately 200% increase in the moment observed in the abutment. Figure 4.21 shows that a large temperature gradient can develop moments within the abutments sufficient to cause cracking. In combination with other parameters, even smaller temperature gradients can lead to conditions involving cracking.

4.3 SUMMARY

A solid model was created using SAP 2000 that showed stress concentrations in the same locations that damage occurred on the 400 South Street Bridge. A simplified version of the SAP model was subsequently created using frame elements. This model showed that as overall conditions approach the actual geometry of the 400 South Street Bridge, the moment in the abutment approaches a calculated cracking moment. A parametric study was then performed to attempt to isolate the effects of skew, span length, and temperature gradient. A summary of the research findings is provided below.

- The overall geometry of the 400 South Street Bridge is such that, according to the frame element model, the effects of skew, length, and temperature gradient cause moment in the abutment to approach the calculated cracking moment.
- The study of skew effect showed that for each 5º increase in skew, an approximately 50% to 65% increase in moment was observed in the abutment
- The study of the effects of length indicated that by doubling the span length, an approximately 60% increase in moment was calculated in the abutment.
- The study of temperature gradient effects showed that a 20° F increase in temperature difference between the girders and deck of the bridge causes an approximately 200% increase in the moment observed in the abutment.

5. SUMMARY AND CONCLUSIONS

5.1 SUMMARY

In an effort to understand the cause of the observed spalling at the north abutment of the integral abutment bridge over 400 South Street in Salt Lake City, Utah, the bridge was surveyed monthly to quantify its behavior. Span lengths of the bridge were surveyed monthly and recorded with the accompanying ambient air temperature at the time of the survey.

In addition to the monthly survey, multiple surveys were performed over one day. These two sources of bridge behavior were used to understand the overall response of the bridge to changes in temperature. The overall bridge behavior using the survey data was compared to a detailed finite-element model of the bridge. The finite-element model was shown to exhibit slightly restrained conditions compared with the unrestrained theoretical values. The model showed the same general trends observed in the monthly surveys. Locations of tensile stress concentrations were found to develop at the bottom girder flanges. A simplified modeling scheme was then used to perform a series of parametric studies investigating the effects of skew angle, span length, and temperature gradient on the weak-axis bending moment of the abutment. The relationship between these bridge parameters and the abutment weak-axis moment were obtained. The survey and finite-element results were used to make the following conclusions.

5.2 CONCLUSIONS AND RECOMMENDATIONS

Based on the results from the survey data and finite-element analyses, several conclusions were obtained. Recommendations based on these conclusions are also presented.

1. Bridge Movement – In general, expansion and contraction of the 400 South Street Bridge was observed as temperature increased and decreased, respectively. The observed movements were unequal when comparing the east and west sides of the bridge. Through finite-element analyses, this unequal movement is believed to be a result of lateral movement at the skewed support of the north abutment. Reduction of the lateral movement would reduce tensile stress in the abutment.
2. Skew – As little as a 5º increase in skew angle can significantly increase the weak axis bending moment of the bridge abutment.
3. Length – As the span length increases by a factor of 2, an approximate 60% increase in weak-axis bending moment in the bridge abutments was observed.
4. Temperature Gradient – Temperature gradients, in combination with uniform temperature changes, influence the stresses in the bridge abutments. A 20° F increase in temperature difference between the girders and deck of the bridge can cause an increase in the stresses observed in the bridge abutments. The influence of temperature gradients on abutment stresses should be investigated.
5. The abutment cracking of the 400 South Street Bridge is likely a result of a combination of bridge parameters. These properties include a combination of skew, curvature, span length, and detailing. Integral abutment bridges with more than one of these conditions require additional design checks.
6. Finite element models can predict localized and global increases in demand on integral abutments

REFERENCES

Abendroth, R., G. Lowell, and M. LaViolette. (2007). *An Integral Abutment Bridge with Precast Concrete Piles,* Center for Transportation Research and Education, Iowa State University, Iowa.

Arenas, A., G. Filz, and T. Cousins. (2013) *Thermal Response of Integral Abutment Bridges with Mechanically Stabilized Earth Walls,* Report No. VCTIR 13-R7, Virginia Center for Transportation Innovation and Research, Viginia Polytechnic Institute & State University, Virginia.

Arsoy, S., R. Barker, and J. Duncan. (1999). *The Behavior of Integral Abutment Bridges.* Report No. FHWA/VTRC 00-CR3, Virginian Transportation Research Council, Virginia.

Burke, Martin P. Jr. (2009). *Integral and Semi-Integral Bridges,* 1st Ed., Chapter 1: Integral Bridges, pp. 1-20, Wiley-Blackwell, Iowa.

Civjan, S., C. Bonczar, S. Brena, J. DeJong, and D. Crovo. (2007). "Integral Abutment Bridge Behavior: Parametric Analysis of a Massachusetts Bridge." *Journal of Bridge Engineering*, January/February 2007.

Fennema, J., J. Laman, and D. Linzell. (2005). "Predicted and Measured Response of an Integral Abutment Bridge." *Journal of Bridge Engineering*, November/December 2005.

Horvath, John (2000). *Integral-Abutment Bridges: Problems and Innovative Solutions Using EPS Geofoam and Other Geosynthetics,* Manhattan College Research Report No. CE/GE-00-2, New York.

Olson, S., J. Long, J. Hansen, D. Renekis, and J. LaFave. (2009). *Modification of IDOT Integral Abutment Design Limitations and Details,* Research Report ICT-09-054, Illinois Center for Transportation, University of Illinois at Urbana-Champaign, Illinois.

Rodriguez, Leo (2012). *Temperature Effects on Integral Abutment Bridges for the Long-Term Bridge Performance Program,* Utah State University, Logan, Utah.

Roman, E., Y. Khodair, and S. Hassiotis. (2002). *Design Details of Integral Bridges,* Stevens Institute of Technology, New Jersey.

Shah, Bhavik (2007). *3D Finite Element Analysis of Integral Abutment Bridges Subjected to Thermal Loading,* Kansas State University, Kansas.

Soltani, A. and A. Kukreti. (1992). "Performance Evaluation of Integral Abutment Bridges." *Transportation Research Record* 1371, 17-25.

White, Harry 2nd (2007). *Integral Abutment Bridges: Comparison of Current Practice Between European Countries and the United States of America,* Special Report 152, Transportation Research and Development Bureau, New York State Department of Transportation, New York.

APPENDIX A: MONTHLY SURVEY DATA

400 S Bridge Survey

Date: 26-Aug-11

Prism Height: 6 ft Avg Temp 89.6 F

Station 1	Height:	6.650				
		Dist	**Hz**	**Vert**		
Prism	Reference	175.805	175.805	-0.650		
				Hz Angle		
Target #	**Dist**	**Hz**	**Vert**	**Deg**	**Min**	**Sec**
1				227	52	45
2	124.025	122.425	19.875	228	0	5
3	79.340	77.735	15.865	247	0	25
4	79.080	77.820	14.085	246	56	45
5	78.740	77.795	12.155	246	56	45
6	54.160	49.725	21.465	278	30	0
7	54.975	52.235	17.145	323	25	20
8	54.525	52.425	14.990	323	22	30
9	53.965	52.705	11.595	323	17	35
10				6	43	40
Station 2	Height:	6.030				
		Dist	**Hz**	**Vert**		
Prism	Reference	176.945	176.945	-0.030		
				Hz Angle		
Target #	**Dist**	**Hz**	**Vert**	**Deg**	**Min**	**Sec**
29				**6**	26	35
30	65.355	62.010	20.630	44	46	30
31	64.935	62.135	18.855	44	51	50
32	64.410	62.355	16.130	44	51	25
33	69.500			81	52	25
34	95.110			105	29	30
35	94.810			105	29	40
36	94.405			105	29	40

400 S Bridge Survey						
Prism Height:		6 ft				
Station 3	Height:	7.300				
		Dist	**Hz**	**Vert**		
Prism	Reference	90.880	90.870	-1.300		
				Hz Angle		
Target #	**Dist**	**Hz**	**Vert**	**Deg**	**Min**	**Sec**
20				278	32	50
21				278	39	25
22	95.145	93.380	18.225	297	57	35
23	94.720	93.315	16.275	297	58	35
24	94.335	93.235	14.375	298	0	15
25	74.685	70.765	23.885	321	2	20
26	74.570	72.060	19.180	356	52	20
27	74.185	72.210	17.020	356	47	55
28	73.680	72.380	13.800	356	35	25
29						
Station 4	Height:	6.265				
		Dist	**Hz**	**Vert**		
Prism	Reference	126.340	126.340	-0.265		
				Hz Angle		
Target #	**Dist**	**Hz**	**Vert**	**Deg**	**Min**	**Sec**
10				326	36	55
11	73.050	70.485	19.200	354	41	10
12	72.520	70.655	16.340	354	52	30
13	72.085	70.860	13.235	355	2	55
14	58.875	53.890	23.710	30	50	25
15	72.600	70.185	18.570	67	3	5
16	72.100	70.210	16.415	67	2	50
17	71.670	70.195	14.465	67	2.5	27.5
18				92	42	25
19				92	49	30

400 S Bridge Survey

Date: 30-Sep-11

Prism Height: 6 ft

Avg Temp 74.7 F

Station 1	Height:	6.470				
		Dist	**Hz**	**Vert**		
Prism	Reference	175.685	175.685	-0.470		
				Hz Angle		
Target #	**Dist**	**Hz**	**Vert**	**Deg**	**Min**	**Sec**
1				227	52	15
2	123.970	122.315	20.015	227	59	50
3	79.265	77.635	16.000	247	0	25
4	79.010	77.720	14.220	246	56	35
5	78.660	77.695	12.295	246	56	35
6	54.130	49.640	21.585	278	30	15
7	54.910	52.125	17.270	323	25	40
8	54.455	52.315	15.110	323	23	5
9	53.880	52.590	11.725	323	18	0
10				64	32	20
Station 2	Height:	5.790				
		Dist	**Hz**	**Vert**		
Prism	Reference	176.885	176.880	0.210		
				Hz Angle		
Target #	**Dist**	**Hz**	**Vert**	**Deg**	**Min**	**Sec**
29				**6**	26	25
30	65.355	61.940	20.835	44	45	15
31	64.930	62.065	19.065	44	50	35
32	64.390	62.280	16.335	44	50	30
33	69.485	64.405	26.085	81	51	10
34	95.050	92.860	20.285	105	30	20
35	94.740	92.855	18.795	105	30	0
36	94.325	92.865	16.545	105	30	15

400 S Bridge Survey						
Prism Height:		6 ft				
Station 3	Height:	7.240				
		Dist	**Hz**	**Vert**		
Prism	Reference	90.730	90.720	-1.240		
				Hz Angle		
Target #	**Dist**	**Hz**	**Vert**	**Deg**	**Min**	**Sec**
20				278	32	10
21				278	29	5
22	95.055	93.285	18.265	297	57	25
23	94.630	93.210	16.315	297	58	35
24	94.245	93.135	14.420	298	0	10
25	74.620	70.690	23.900	321	10	0
26	74.495	71.975	19.210	356	52	5
27	74.115	72.125	17.055	356	47	55
28	73.605	72.295	13.830	356	35	10
29						
Station 4	Height:	6.605				
		Dist	**Hz**	**Vert**		
Prism	Reference	126.200	126.200	-0.605		
				Hz Angle		
Target #	**Dist**	**Hz**	**Vert**	**Deg**	**Min**	**Sec**
10				326	37	25
11	72.870	70.395	18.825	354	41	20
12	72.350	70.565	15.965	354	52	50
13	71.930	70.770	12.865	355	3	15
14	58.640	53.805	23.315	30	50	30
15	72.400	70.075	18.190	67	3	50
16	71.915	70.100	16.040	67	3	35
17	71.485	70.085	14.090	67	0	10
18				92	42	35
19				92	50	30

400 S Bridge Survey

Date: 2-Nov-11

Prism Height: 6 ft

Avg Temp 39.75 F

Station 1	Height	6.195				
		Dist	**Hz**	**Vert**		
Prism	Reference	175.820	175.820	-0.195		
				Hz Angle		
Target #	**Dist**	**Hz**	**Vert**	**Deg**	**Min**	**Sec**
1				227	49	15
2	124.055	122.385	20.290	227	57	25
3	79.400	77.710	16.300	246	58	40
4	79.140	77.800	14.515	246	54	25
5	78.785	77.770	12.590	246	54	25
6	54.330	49.725	21.895	278	29	10
7	55.100	52.225	17.575	323	24	25
8	54.630	52.410	15.415	323	21	35
9	54.045	52.690	12.025	323	16	45
10				6	41	25
Station 2	Height	5.755				
		Dist	**Hz**	**Vert**		
Prism	Reference	176.900	176.900	0.245		
				Hz Angle		
Target #	**Dist**	**Hz**	**Vert**	**Deg**	**Min**	**Sec**
29				**6**	25	45
30	65.475	62.055	20.890	44	42	0
31	65.050	62.175	19.120	44	47	20
32	64.510	62.395	16.390	44	47	5
33	69.595	64.500	26.140	81	46	40
34	95.140	92.940	20.335	105	27	50
35	94.835	92.940	18.850	105	27	50
36	94.415	92.945	16.590	105	28	0

400 S Bridge Survey						
Prism Height:		6 ft				
Station 3	Height	7.465				
		Dist	**Hz**	**Vert**		
Prism	Reference	90.865	90.850	-1.465		
				Hz Angle		
Target #	**Dist**	**Hz**	**Vert**	**Deg**	**Min**	**Sec**
20				278	31	25
21				278	39	10
22	95.095	93.360	18.075	297	57	55
23	94.675	93.290	16.125	297	59	0
24	94.295	93.220	14.225	298	0	30
25	74.650	70.785	23.720	321	3	25
26	74.555	72.090	19.020	356	51	35
27	74.175	72.230	16.860	356	47	25
28	73.680	72.405	13.640	356	34	45
29						
Station 4	Height	6.680				
		Dist	**Hz**	**Vert**		
Prism	Reference	126.195	126.190	-0.680		
				Hz Angle		
Target #	**Dist**	**Hz**	**Vert**	**Deg**	**Min**	**Sec**
10				326	35	15
11	72.960	70.500	18.780	354	38	55
12	72.445	70.675	15.925	354	50	10
13	72.030	70.880	12.820	355	0	30
14	58.710	53.895	23.285	30	47	15
15	72.465	70.150	18.150	67	0	40
16	71.980	70.180	15.995	67	0	15
17	71.555	70.165	15.050	66	57	5
18				92	40	5
19				92	48	40

400 S Bridge Survey

Date: 26-Nov-11

Prism Height: 6 ft

Avg Temp 39.24

Station 1	Height	6.395				
		Dist	**Hz**	**Vert**		
Prism	Reference	175.690	175.690	-0.395		
				Hz Angle		
Target #	**Dist**	**Hz**	**Vert**	**Deg**	**Min**	**Sec**
1				227	51	20
2	124.045	122.375	20.265	227	59	30
3	79.400	77.720	16.265	247	0	45
4	79.140	77.800	14.480	246	56	35
5	78.775	77.765	12.559	246	56	45
6	54.320	49.725	21.860	278	30	35
7	55.090	52.225	17.535	323	24	55
8	54.625	52.415	15.380	323	22	10
9	54.040	52.690	11.940	323	17	20
10				6	41	55
Station 2	Height	5.560				
		Dist	**Hz**	**Vert**		
Prism	Reference	177.005	177.005	0.440		
				Hz Angle		
Target #	**Dist**	**Hz**	**Vert**	**Deg**	**Min**	**Sec**
29				6	26	5
30	65.585	62.055	21.230	44	43	55
31	65.150	62.180	19.450	44	49	5
32	64.600	62.395	16.725	44	48	45
33	69.725	64.505	26.475	81	48	5
34	95.215	92.945	20.670	105	27	15
35	94.900	92.940	19.190	105	27	10
36	94.480	92.950	16.930	105	27	20

400 S Bridge Survey						
Prism Height:		6 ft				
Station 3	Height	7.190				
		Dist	**Hz**	**Vert**		
Prism	Reference	90.865	90.860	-1.190		
				Hz Angle		
Target #	**Dist**	**Hz**	**Vert**	**Deg**	**Min**	**Sec**
20				278	30	50
21				278	38	25
22	95.170	93.355	18.495	297	56	50
23	94.740	93.285	16.540	297	58	20
24	94.355	93.210	14.645	297	59	40
25	74.780	70.780	24.140	321	2	50
26	74.660	72.085	19.440	356	50	0
27	74.270	72.230	17.280	356	47	0
28	73.750	72.400	14.055	356	34	25
Station 4	Height	6.655				
		Dist	**Hz**	**Vert**		
Prism	Reference	126.345	126.340	-0.655		
				Hz Angle		
Target #	**Dist**	**Hz**	**Vert**	**Deg**	**Min**	**Sec**
10				326	36	10
11	72.990	70.495	18.905	354	40	0
12	72.465	70.665	16.050	354	51	35
13	72.050	70.875	12.945	355	1	45
14	58.760	53.895	23.410	30	48	10
15	72.495	70.155	18.280	67	1	5
16	72.010	70.180	16.125	67	1	0
17	71.580	70.165	14.180	66	57	40
18				92	40	40
19				92	49	15

400 S Bridge Survey

Date: 2-Jan-12

Prism Height: 6 ft Avg Temp 37.7

Station 1	Height	6.560				
		Dist	**Hz**	**Vert**		
Prism	Reference	175.810	175.810	-0.560		
				Hz Angle		
Target #	**Dist**	**Hz**	**Vert**	**Deg**	**Min**	**Sec**
1				227	50	5
2	124.010	122.370	20.090	227	50	30
3	79.360	77.710	16.100	246	59	35
4	79.100	77.795	14.315	246	56	10
5	78.755	77.775	12.385	246	56	15
6	54.250	49.725	21.690	278	29	20
7	55.040	52.225	17.370	323	25	15
8	54.575	52.415	15.210	323	22	30
9	54.000	52.690	11.820	323	15	50
10				6	41	5
Station 2	Height	5.810				
		Dist	**Hz**	**Vert**		
Prism	Reference	177.020	177.020	0.190		
				Hz Angle		
Target #	**Dist**	**Hz**	**Vert**	**Deg**	**Min**	**Sec**
29				**6**	26	0
30	65.515	62.050	21.015	44	40	25
31	65.075	62.175	19.205	44	41	30
32	64.530	62.390	16.475	44	41	15
33	69.630	64.500	26.230	81	40	50
34	95.155	92.935	20.425	105	20	20
35	94.845	92.935	18.940	105	20	5
36	94.430	92.945	16.680	105	20	20

400 S Bridge Survey						
Prism Height:		6 ft				
Station 3	Height	7.425				
		Dist	**Hz**	**Vert**		
Prism	Reference	90.875	90.865	-1.425		
				Hz Angle		
Target #	**Dist**	**Hz**	**Vert**	**Deg**	**Min**	**Sec**
20				278	30	10
21				278	38	5
22	95.125	93.355	18.250	297	57	5
23	94.700	93.285	16.300	297	57	35
24	94.315	93.210	14.405	297	59	0
25	74.705	70.780	23.895	321	2	20
26	74.600	72.085	19.200	356	50	35
27	74.210	72.230	17.040	356	46	40
28	73.710	72.400	13.815	356	34	5
29						
Station 4	Height	6.705				
		Dist	**Hz**	**Vert**		
Prism	Reference	126.335	126.330	-0.705		
				Hz Angle		
Target #	**Dist**	**Hz**	**Vert**	**Deg**	**Min**	**Sec**
10				326	35	30
11	72.975	70.495	18.880	354	39	5
12	72.455	70.665	16.020	354	50	30
13	72.040	70.870	12.910	355	0	55
14	58.745	53.890	23.380	30	47	35
15	72.480	70.145	18.245	67	1	20
16	71.995	70.175	16.095	67	1	15
17	71.570	70.160	14.140	66	58	0
18				92	41	15
19				92	49	50

400 S Bridge Survey

Date: 31-Jan-12

Prism Height: 6 ft Avg Temp 33.41667

Station 1	Height	6.390		Expansion Gap		6.5625	inches
		Dist	**Hz**	**Vert**			
Prism	Reference	175.805	175.805	-0.390			
				Hz Angle			
Target #	**Dist**	**Hz**	**Vert**	**Deg**	**Min**	**Sec**	
1				227	51	45	
2	124.035	122.370	20.245	227	59	55	
3	79.390	77.710	16.245	247	0	30	
4	79.130	77.795	14.465	246	56	50	
5	78.780	77.775	12.540	246	56	55	
6	54.315	49.725	21.845	278	29	25	
7	55.080	52.220	17.515	323	25	5	
8	54.610	52.410	15.360	323	21	55	
9	54.030	52.685	11.965	323	17	0	
10				6	42	40	
Station 2	Height	5.650		Expansion Gap		6.625	inches
		Dist	**Hz**	**Vert**			
Prism	Reference	177.005	177.005	0.350			
				Hz Angle			
Target #	**Dist**	**Hz**	**Vert**	**Deg**	**Min**	**Sec**	
29				**6**	24	40	
30	65.550	62.045	21.150	44	42	25	
31	65.115	62.165	19.375	44	47	10	
32	64.565	62.380	16.645	44	47	15	
33	69.685	64.490	26.400	81	48	55	
34	95.180	92.925	20.590	105	27	0	
35	94.870	92.920	19.115	105	27	0	
36	94.445	92.930	16.850	105	27	30	

400 S Bridge Survey						

Prism Height:		6 ft					
Station 3	Height	7.440		Expansion Gap		7.5	inches
		Dist	**Hz**	**Vert**			
Prism	Reference	90.860	90.845	-1.440			
				Hz Angle			
Target #	**Dist**	**Hz**	**Vert**	**Deg**	**Min**	**Sec**	
20				278	29	35	
21				278	36	55	
22	95.130	93.365	18.235	297	53	25	
23	94.700	93.290	16.285	297	54	20	
24	94.320	93.215	14.385	297	55	30	
25	74.700	70.780	23.880	320	57	25	
26	74.585	72.075	19.185	356	47	10	
27	74.195	72.215	17.025	356	43	0	
28	73.695	72.390	13.800	356	30	55	
29							
Station 4	Height	6.790		Expansion Gap		5.6875	inches
		Dist	**Hz**	**Vert**			
Prism	Reference	126.325	126.320	-0.790			
				Hz Angle			
Target #	**Dist**	**Hz**	**Vert**	**Deg**	**Min**	**Sec**	
10				326	36	5	
11	72.960	70.500	18.790	354	37	55	
12	72.440	70.670	15.930	354	49	45	
13	72.025	70.875	12.825	355	0	40	
14	58.715	53.895	23.295	30	46	40	
15	72.465	70.155	18.165	66	59	40	
16	71.985	70.180	16.005	66	59	25	
17	71.560	70.165	14.055	66	56	15	
18				92	38	50	
19				92	47	40	

400 S Bridge Survey

Date: 23-Feb-12

Prism Height:		6 ft	Avg Temp	38.53846	F	

Station 1	Height	6.455				
		Dist	**Hz**	**Vert**		
Prism	Reference	175.770	175.770	-0.455		
				Hz Angle		
Target #	**Dist**	**Hz**	**Vert**	**Deg**	**Min**	**Sec**
1				227	49	25
2	124.035	122.385	20.145	227	57	10
3	79.380	77.715	16.160	246	58	30
4	79.120	77.800	14.380	246	54	45
5	78.770	77.780	12.450	246	54	40
6	54.280	49.725	21.765	278	28	40
7	55.055	52.220	17.440	323	24	20
8	54.595	52.415	15.280	323	21	15
9	54.015	52.690	11.885	323	16	20
10				6	41	25
Station 2	Height	5.705				
		Dist	**Hz**	**Vert**		
Prism	Reference	176.980	176.980	0.295		
				Hz Angle		
Target #	**Dist**	**Hz**	**Vert**	**Deg**	**Min**	**Sec**
29				**6**	27	5
30	65.515	62.035	21.070	44	46	35
31	65.080	62.160	19.290	44	51	55
32	64.535	62.375	16.560	44	51	35
33	69.670	64.510	26.315	81	51	20
34	95.210	92.975	20.510	105	29	10
35	94.895	92.970	19.025	105	29	20
36	94.480	92.985	16.760	105	29	20

400 S Bridge Survey						

Prism Height:		6 ft				
Station 3	Height	7.195				
		Dist	**Hz**	**Vert**		
Prism	Reference	90.840	90.835	-1.195		
				Hz Angle		
Target #	**Dist**	**Hz**	**Vert**	**Deg**	**Min**	**Sec**
20				278	30	55
21				278	38	25
22	95.170	93.365	18.470	297	57	20
23	94.745	93.290	16.520	297	58	45
24	94.355	93.215	14.620	298	0	0
25	74.775	70.775	24.120	321	2	35
26	74.650	72.080	19.415	356	51	35
27	74.255	72.225	17.255	356	47	10
28	73.745	72.400	14.035	356	34	45
29						
Station 4	Height	6.680				
		Dist	**Hz**	**Vert**		
Prism	Reference	126.245	126.245	-0.680		
				Hz Angle		
Target #	**Dist**	**Hz**	**Vert**	**Deg**	**Min**	**Sec**
10				326	35	10
11	72.975	70.490	18.885	354	38	45
12	72.455	70.660	16.025	354	50	50
13	72.035	70.865	12.920	355	1	30
14	58.735	53.875	23.390	30	47	50
15	72.480	70.145	18.255	67	1	20
16	71.995	70.175	16.100	67	0	55
17	71.570	70.155	14.150	66	57	45
18				92	40	55
19				92	49	10

400 S Bridge Survey	
Date:	24-Mar-12

Prism Height:	6 ft	Avg Temp	70.38095	

Station 1	Height	6.410				
		Dist	**Hz**	**Vert**		
Prism	Reference	175.840	175.840	-0.410		
				Hz Angle		
Target #	**Dist**	**Hz**	**Vert**	**Deg**	**Min**	**Sec**
1				227	51	30
2	124.055	122.400	20.195	227	59	5
3	79.405	77.730	16.215	247	0	0
4	79.140	77.810	14.430	246	55	55
5	78.785	77.790	12.500	246	55	55
6	54.300	49.725	21.815	278	30	0
7	55.075	52.220	17.490	323	25	30
8	54.605	52.410	15.330	323	22	35
9	54.025	52.690	11.940	323	17	40
10				6	43	20
Station 2	Height	5.615				
		Dist	**Hz**	**Vert**		
Prism	Reference	177.030	177.030	0.385		
				Hz Angle		
Target #	**Dist**	**Hz**	**Vert**	**Deg**	**Min**	**Sec**
29				**6**	25	15
30	65.555	62.035	21.180	44	44	25
31	65.120	62.160	19.405	44	49	30
32	64.575	62.380	16.680	44	49	35
33	69.705	64.495	26.435	81	51	20
34	95.215	92.955	20.620	105	29	25
35	94.900	92.950	19.135	105	29	35
36	94.480	92.960	16.880	105	30	0

400 S Bridge Survey						
Prism Height:		6 ft				

Station 3	Height	7.285				
		Dist	**Hz**	**Vert**		
Prism	Reference	90.860	90.850	-1.285		
				Hz Angle		
Target #	**Dist**	**Hz**	**Vert**	**Deg**	**Min**	**Sec**
20				278	29	30
21				278	36	50
22	95.155	93.370	18.355	297	54	55
23	94.730	93.300	16.405	297	56	5
24	93.345	93.225	14.505	297	57	20
25	74.725	70.770	24.000	321	0	35
26	74.610	72.065	19.305	356	50	0
27	74.220	72.210	17.150	356	45	50
28	73.710	72.385	13.920	356	33	5
Station 4	Height	6.615				
		Dist	**Hz**	**Vert**		
Prism	Reference	126.360	126.360	-0.615		
				Hz Angle		
Target #	**Dist**	**Hz**	**Vert**	**Deg**	**Min**	**Sec**
10				326	36	0
11	72.990	70.485	18.950	354	40	15
12	72.465	70.655	16.095	354	51	45
13	72.045	70.865	12.990	355	1	40
14	58.760	53.875	23.455	30	49	50
15	72.520	70.165	18.330	67	3	55
16	72.025	70.185	16.165	67	3	20
17	71.595	70.170	14.215	66	59	40
18				92	42	25
19				92	50	25

400 S Bridge Survey

Date: 5-May-12

Prism Height: 6 ft Avg Temp 50.4

Station 1	Height	6.310				
		Dist	**Hz**	**Vert**		
Prism	Reference	176.010	176.010	-0.310		
				Hz Angle		
Target #	**Dist**	**Hz**	**Vert**	**Deg**	**Min**	**Sec**
1				227	49	10
2	124.070	122.395	20.300	227	56	30
3	79.410	77.720	16.300	246	57	20
4	79.155	77.815	14.525	246	53	55
5	78.800	77.785	12.595	246	53	45
6	54.335	49.725	21.905	278	28	10
7	55.095	52.215	17.585	323	22	0
8	54.630	52.410	15.425	323	22	0
9	54.040	52.685	12.030	323	16	55
10				6	42	20
Station 2	Height	5.670				
		Dist	**Hz**	**Vert**		
Prism	Reference	177.230	177.230	0.330		
				Hz Angle		
Target #	**Dist**	**Hz**	**Vert**	**Deg**	**Min**	**Sec**
29				**6**	20	50
30	65.535	62.050	21.100	44	39	30
31	65.105	62.170	19.325	44	45	5
32	64.560	62.390	16.600	44	44	50
33	69.675	64.505	26.350	81	44	55
34	95.125	92.950	20.535	105	23	35
35	94.875	92.945	19.045	105	23	30
36	94.455	92.955	16.785	105	24	0

400 S Bridge Survey						
Prism Height:		6 ft				

Station 3	Height	7.245				
		Dist	**Hz**	**Vert**		
Prism	Reference	90.810	90.805	-1.245		
				Hz Angle		
Target #	**Dist**	**Hz**	**Vert**	**Deg**	**Min**	**Sec**
20				278	30	15
21				278	38	15
22	95.165	93.370	18.390	297	56	45
23	94.735	93.300	16.440	297	58	20
24	94.355	93.225	14.535	297	59	25
25	74.750	70.780	24.035	321	2	10
26	74.625	72.080	19.340	356	51	40
27	74.235	72.220	17.175	356	47	15
28	73.730	72.395	13.955	356	34	35
Station 4	Height	6.595				
		Dist	**Hz**	**Vert**		
Prism	Reference	126.301	126.305	-0.595		
				Hz Angle		
Target #	**Dist**	**Hz**	**Vert**	**Deg**	**Min**	**Sec**
10				326	29	15
11	73.005	70.495	18.975	354	32	55
12	72.480	70.665	16.115	354	44	15
13	72.055	70.870	13.010	354	54	45
14	58.785	53.890	23.480	30	40	55
15	72.520	70.165	18.340	66	54	40
16	72.030	70.190	16.185	66	54	0
17	71.605	70.175	14.235	66	50	55
18				92	34	5
19				92	39	10

400 S Bridge Survey

Date: 1-Jun-12

Prism Height: 6 ft Avg Temp 80.71429

Station 1	Height	6.530				
		Dist	**Hz**	**Vert**		
Prism	Reference	175.960	175.960	-0.530		
				Hz Angle		
Target #	**Dist**	**Hz**	**Vert**	**Deg**	**Min**	**Sec**
1				227	55	40
2	124.005	122.370	20.085	228	2	55
3	79.390	77.740	16.090	247	6	30
4	79.140	77.835	14.310	247	2	40
5	78.780	77.800	12.385	247	2	30
6	54.335	49.815	21.695	278	38	20
7	55.180	52.375	17.370	323	26	55
8	54.725	52.565	15.210	323	24	5
9	54.150	52.845	11.820	323	19	10
10				6	40	0
Station 2	Height	5.765				
		Dist	**Hz**	**Vert**		
Prism	Reference	177.020	177.020	0.235		
				Hz Angle		
Target #	**Dist**	**Hz**	**Vert**	**Deg**	**Min**	**Sec**
29				**6**	24	35
30	65.495	62.035	21.010	44	43	45
31	65.065	62.160	19.230	44	49	5
32	64.525	62.380	16.505	44	49	5
33	69.635	64.490	26.265	81	50	5
34	95.170	92.950	20.445	105	28	30
35	94.870	92.955	18.960	105	28	30
36	94.450	92.960	16.700	105	28	30

400 S Bridge Survey						
Prism Height:		6 ft				
Station 3	Height	7.230				

		Dist	Hz	Vert		
Prism	Reference	90.865	90.860	-1.230		
				Hz Angle		
Target #	**Dist**	**Hz**	**Vert**	**Deg**	**Min**	**Sec**
20				278	28	25
21				278	35	10
22	95.175	93.375	18.420	297	53	30
23	94.750	93.305	16.470	297	54	50
24	94.365	93.230	14.570	297	56	15
25	74.750	70.770	24.070	320	58	50
26	74.625	72.065	19.365	356	48	40
27	74.235	72.210	17.210	356	44	30
28	73.725	72.385	13.985	356	31	45
29						
Station 4	Height	6.660				
		Dist	Hz	Vert		
Prism	Reference	126.390	126.390	-0.660		
				Hz Angle		
Target #	**Dist**	**Hz**	**Vert**	**Deg**	**Min**	**Sec**
10				326	35	25
11	72.990	70.490	18.940	354	39	40
12	72.470	70.660	16.075	354	51	5
13	72.045	70.865	12.970	355	1	40
14	58.765	53.885	23.440	30	48	30
15	72.525	70.175	18.300	67	2	25
16	72.030	70.200	16.145	67	1	50
17	71.605	70.180	14.195	66	58	20
18				93	53	15
19				94	0	40

400 S Bridge Survey

Date: 26-Jun-12

Prism Height: 6 ft Avg Temp 85.14286

Station 1	Height	6.515				

		Dist	Hz	Vert		
Prism	Reference	175.700	175.700	-0.515		
				Hz Angle		
Target #	**Dist**	**Hz**	**Vert**	**Deg**	**Min**	**Sec**
1				227	50	55
2	124.065	122.425	20.110	227	58	10
3	79.390	77.740	16.105	246	58	50
4	79.130	77.820	14.330	246	55	25
5	78.775	77.795	12.395	246	55	25
6	54.260	49.730	21.710	278	28	45
7	55.040	52.225	17.385	323	25	30
8	54.585	52.415	15.225	323	22	35
9	54.005	52.695	11.830	323	17	40
10				6	43	45
Station 2	Height	5.825				
		Dist	**Hz**	**Vert**		
Prism	Reference	176.945	176.945	0.175		
				Hz Angle		
Target #	**Dist**	**Hz**	**Vert**	**Deg**	**Min**	**Sec**
29				**6**	24	10
30	65.470	62.020	20.975	44	44	10
31	65.045	62.145	19.200	44	49	25
32	64.505	62.365	16.470	44	49	15
33	69.610	64.480	26.230	81	51	10
34	95.170	92.960	20.405	105	29	50
35	94.860	92.955	18.925	105	30	10
36	94.445	92.965	16.660	105	30	10

400 S Bridge Survey						
Prism Height:		6 ft				
Station 3	Height	7.420				
		Dist	**Hz**	**Vert**		

Prism	Reference	90.820	90.810	-1.420		
				Hz Angle		
Target #	**Dist**	**Hz**	**Vert**	**Deg**	**Min**	**Sec**
20				278	30	40
21				278	37	10
22	95.145	93.375	18.245	297	55	35
23	94.715	93.305	16.295	297	56	50
24	94.340	93.235	14.395	297	58	10
25	74.690	70.765	23.895	321	0	35
26	74.575	72.060	19.195	356	50	35
27	74.190	72.205	17.035	356	46	35
28	73.685	72.380	13.815	356	33	35
Station 4	Height	6.755				
		Dist	**Hz**	**Vert**		
Prism	Reference	126.250	126.245	-0.755		
				Hz Angle		
Target #	**Dist**	**Hz**	**Vert**	**Deg**	**Min**	**Sec**
10				326	35	15
11	72.965	70.490	18.835	354	39	20
12	72.445	70.665	15.975	354	51	0
13	72.030	70.870	12.870	355	1	25
14	58.720	53.885	23.340	30	48	45
15	72.495	70.175	18.200	67	2	30
16	72.005	70.195	16.045	67	2	0
17	71.580	70.180	14.095	66	58	25
18				92	41	25
19				92	49	5

400 S Bridge Survey

Date: 12-Jul-12

Prism Height: 6 ft Avg Temp 92.5

Station 1	Height	6.580				
		Dist	**Hz**	**Vert**		
Prism	Reference	175.765	175.765	-0.580		
				Hz Angle		

Target #	Dist	Hz	Vert	Deg	Min	Sec
1				227	49	55
2				227	57	10
3	79.385	77.740	16.080	246	57	35
4	79.125	77.820	14.300	246	54	5
5	78.780	77.800	12.370	246	53	45
6	54.255	49.730	21.685	278	27	40
7	55.030	52.220	17.365	323	23	15
8	54.570	52.410	15.200	323	20	35
9	53.995	52.690	11.805	323	15	45
10				6	41	35
Station 2	Height	5.840				
		Dist	**Hz**	**Vert**		
Prism	Reference	176.935	176.935	0.160		
				Hz Angle		
Target #	**Dist**	**Hz**	**Vert**	**Deg**	**Min**	**Sec**
29				**6**	24	10
30	65.440	62.005	20.720	44	44	45
31	65.015	62.130	19.145	44	49	45
32	64.470	62.345	16.415	44	49	45
33	69.590	64.485	26.165	81	51	40
34	95.160	92.960	20.355	105	29	40
35	94.860	92.965	18.865	105	29	30
36	94.440	92.970	16.605	105	29	35

400 S Bridge Survey						
Prism Height:		6 ft				
Station 3	Height	7.575				
		Dist	**Hz**	**Vert**		
Prism	Reference	90.805	90.790	-1.575		
				Hz Angle		
Target #	**Dist**	**Hz**	**Vert**	**Deg**	**Min**	**Sec**

20				278	26	20
21				278	33	5
22	95.120	93.385	18.100	297	51	5
23	94.705	93.315	16.155	297	52	40
24	94.325	93.245	14.255	297	53	55
25	74.650	70.770	23.755	320	55	55
26	74.535	72.055	19.055	356	46	5
27	74.150	72.200	16.890	356	41	45
28	73.655	72.375	13.670	356	28	55
Station 4	Height	6.850				
		Dist	**Hz**	**Vert**		
Prism	Reference	126.385	126.385	-0.850		
				Hz Angle		
Target #	**Dist**	**Hz**	**Vert**	**Deg**	**Min**	**Sec**
10				326	34	0
11	72.935	70.485	18.735	354	38	45
12	72.415	70.655	15.870	354	50	20
13	72.000	70.860	12.765	355	0	45
14	58.680	53.885	23.235	30	48	30
15	72.470	70.175	18.090	67	1	45
16	71.985	70.200	15.935	67	1	20
17	71.565	70.185	13.990	66	57	50
18				92	40	35
19				92	47	50
		3.000				

APPENDIX B: FULL-DAY SURVEY DATA

B-1: SPAN 1 RAW DATA

Time:	9:20 AM

	SE
Temp	35.5

Span 1				Hz Angle		
Target	Dist	Hz	Vert	Deg	Min	Sec
3	79.390	77.705	16.275	258	42	20
4	79.130	77.795	14.495	258	38	25
5	78.780	77.770	12.570	258	38	25
6	54.320	49.720	21.875	290	12	25
7	55.085	52.215	17.550	335	8	10
8	54.620	52.405	15.395	335	5	10
9	54.030	52.680	12.000	335	0	25

Time:	10:30 AM

	SE
Temp	43.0

Span 1				Hz Angle		
Target	Dist	Hz	Vert	Deg	Min	Sec
3	79.400	77.715	16.285	258	42	35
4	79.135	77.795	14.505	258	38	50
5	78.785	77.775	12.580	258	38	45
6	54.330	49.725	21.885	290	13	5
7	55.090	52.215	17.560	335	9	10
8	54.625	52.410	15.405	335	6	15
9	54.035	52.685	12.010	335	1	25

Time:	11:30 AM

	SE
Temp	57.5

Span 1				Hz Angle		
Target	Dist	Hz	Vert	Deg	Min	Sec
3	79.405	77.715	16.285	258	42	5
4	79.145	77.805	14.510	258	37	40
5	78.775	77.765	12.570	258	37	35
6	54.325	49.720	21.885	290	11	40
7	55.090	52.215	17.560	335	7	30
8	54.620	52.405	15.400	335	5	25
9	54.030	52.680	12.010	335	0	10

Time:	12:30 PM

	SE Temp	61.5

Span 1				Hz Angle		
Target	Dist	Hz	Vert	Deg	Min	Sec
3	79.410	77.715	16.300	258	42	55
4	79.155	77.810	14.520	258	39	0
5	78.795	77.780	12.590	258	38	45
6	54.335	49.725	21.895	290	12	50
7	55.100	52.220	17.580	335	8	20
8	54.635	52.410	15.420	335	5	25
9	54.040	52.685	12.025	335	0	35

Time:	1:30 PM

	SE Temp	70.5

Span 1				Hz Angle		
Target	Dist	Hz	Vert	Deg	Min	Sec
3	79.405	77.710	16.300	258	42	45
4	79.155	77.810	14.520	258	38	50
5	78.790	77.775	12.590	258	38	50
6	54.330	49.720	21.900	290	12	55
7	55.095	52.215	17.575	335	8	25
8	54.630	52.405	15.415	335	5	50
9	54.040	52.685	12.025	335	0	55

Time:	2:30 PM

	SE Temp	69.5

Span 1				Hz Angle		
Target	Dist	Hz	Vert	Deg	Min	Sec
3	79.405	77.720	16.265	258	42	30
4	79.140	77.805	14.480	258	38	50
5	78.790	77.785	12.555	258	38	50
6	54.315	49.720	21.860	290	12	35
7	55.080	52.215	17.540	335	8	20
8	54.615	52.405	15.380	335	5	35
9	54.030	52.685	11.990	335	0	35

Time:	3:30 PM					
		SE Temp	68.5			
Span 1				Hz Angle		
Target	Dist	Hz	Vert	Deg	Min	Sec
3	79.400	77.720	16.260	258	42	55
4	79.130	77.795	14.485	258	39	15
5	78.785	77.780	12.550	258	39	10
6	54.315	49.720	21.860	290	13	20
7	55.085	52.220	17.540	335	9	0
8	54.620	52.410	15.380	335	6	5
9	54.035	52.685	11.990	335	1	5

Time:	4:30 PM					
		SE Temp	66.5			
Span 1				Hz Angle		
Target	Dist	Hz	Vert	Deg	Min	Sec
3	79.400	77.720	16.240	258	42	25
4	79.135	77.800	14.460	258	38	40
5	78.785	77.780	12.530	258	38	30
6	54.305	49.720	21.845	290	12	25
7	55.075	52.215	17.515	335	8	40
8	54.610	52.405	15.355	335	5	50
9	54.025	52.685	11.965	335	0	55

Time:	5:30 PM					
		SE Temp	60.0			
Span 1				Hz Angle		
Target	Dist	Hz	Vert	Deg	Min	Sec
3	79.405	77.725	16.245	258	42	30
4	79.135	77.800	14.465	258	38	45
5	78.790	77.785	12.535	258	38	35
6	54.305	49.720	21.845	290	12	50
7	55.075	52.215	17.515	335	9	5
8	54.615	52.410	15.360	335	6	30
9	54.030	52.685	11.970	335	1	30

Time:	6:30 PM

	SE
Temp	52.0

Span 1				Hz Angle		
Target	Dist	Hz	Vert	Deg	Min	Sec
3	79.400	77.720	16.250	258	42	50
4	79.140	77.805	14.470	258	38	45
5	78.795	77.790	12.540	258	38	30
6	54.310	49.725	21.845	290	12	20
7	55.075	52.215	17.520	335	8	0
8	54.610	52.405	15.355	335	5	10
9	54.030	52.685	11.970	335	0	10

B-2: SPAN 2 RAW DATA

Time:	8:00 AM

Prism:	388.340	388.335	-2.125		Hz Angle	
Target	Dist	Hz	Vert	Deg	Min	Sec
7	207.960	207.375	15.545	342	17	35
8	207.965	207.535	13.380	342	19	35
9	208.020	207.780	9.990	342	22	15
10	183.665	182.445	21.125	3	17	35
11	187.170	186.375	17.220	26	33	40
12	187.220	186.665	14.355	26	34	5
13	187.300	186.960	11.245	26	33	30
14	198.975	197.785	21.730	38	33	5

Time:	9:20 AM

Prism:	388.340	388.335	-2.120		Hz Angle	
Target	Dist	Hz	Vert	Deg	Min	Sec
7	207.960	207.380	15.550	342	17	45
8	207.970	207.535	13.390	342	19	55
9	208.020	207.780	10.000	342	22	25
10	183.660	182.440	21.130	3	17	55
11	187.165	186.370	17.220	26	34	0
12	187.215	186.665	14.365	26	34	25
13	187.295	186.955	11.255	26	34	10
14	198.970	197.780	21.730	38	33	25

Time:	10:30 AM

Prism:	388.280	388.270	-2.100		Hz Angle	
Target	Dist	Hz	Vert	Deg	Min	Sec
7	207.965	207.380	15.560	342	17	40
8	207.970	207.535	13.395	342	19	35
9	208.020	207.780	10.000	342	22	15
10	183.665	182.445	21.135	3	17	30
11	187.170	186.375	17.230	26	33	55
12	187.220	186.665	14.360	26	33	5
13	187.300	186.965	11.260	26	32	50
14						

Time:	11:30 AM

Prism:	388.275	388.270	-2.095		Hz Angle	
Target	Dist	Hz	Vert	Deg	Min	Sec
7	207.950	207.370	15.545	342	17	40
8	207.965	207.535	13.385	342	19	40
9	208.020	207.780	9.980	342	22	5
10	183.660	182.440	21.130	3	17	35
11	187.165	186.370	17.210	26	33	50
12	187.215	186.660	14.355	26	34	5
13	187.295	186.960	11.235	26	33	45
14	198.960	197.775	21.710	38	33	20

Time:	12:30 PM

Prism:	388.275	388.270	-2.145		Hz Angle	
Target	Dist	Hz	Vert	Deg	Min	Sec
7	207.950	207.365	15.540	342	17	30
8	207.955	207.525	13.380	342	19	30
9	208.015	207.775	9.990	342	22	5
10	183.660	182.440	21.125	3	17	30
11	187.170	186.375	17.220	26	33	40
12	187.220	186.665	14.360	26	34	5
13	187.300	186.960	11.250	26	33	50
14	198.965	197.775	21.725	38	32	45

Time:	1:30 PM

Prism:	388.270	388.265	-2.120		Hz Angle	
Target	Dist	Hz	Vert	Deg	Min	Sec
7	207.955	207.370	15.545	342	17	35
8	207.960	207.525	13.390	342	19	30
9	208.005	207.765	9.995	342	22	5
10	183.665	182.435	21.125	3	17	30
11	187.170	186.375	17.215	26	33	50
12	187.220	186.665	14.355	26	34	5
13	187.300	186.960	11.245	26	33	55
14	198.965	197.775	21.715	38	33	20

Time:	2:30 PM

Prism:	388.275	388.270	-2.145		Hz Angle	
Target	Dist	Hz	Vert	Deg	Min	Sec
7	207.955	207.375	15.535	342	17	35
8	207.965	207.535	13.385	342	19	25
9	208.010	207.770	9.980	342	22	0
10	183.655	182.435	21.120	3	17	30
11	187.165	186.370	17.225	26	33	45
12	187.215	186.665	14.360	26	34	10
13	187.300	186.960	11.260	26	33	50
14	198.965	197.775	21.725	38	33	15

Time:	3:30 PM

Prism:	388.275	388.270	-2.135		Hz Angle	
Target	Dist	Hz	Vert	Deg	Min	Sec
7	207.960	207.380	15.540	342	17	25
8	207.970	207.540	13.380	342	19	25
9	208.025	207.785	9.985	342	21	55
10	183.655	182.435	21.125	3	17	25
11	187.170	186.375	17.220	26	33	40
12	187.220	186.665	14.365	26	34	5
13	187.300	186.960	11.265	26	33	45
14	198.960	197.770	21.730	38	33	5

Time:	4:30 PM

Prism:	388.270	388.265	-2.140		Hz Angle	
Target	Dist	Hz	Vert	Deg	Min	Sec
7	207.960	207.375	15.550	342	17	20
8	207.955	207.525	13.385	342	19	20
9	208.020	207.780	9.985	342	21	55
10	183.655	182.435	21.120	3	17	20
11	187.165	186.370	17.225	26	33	35
12	187.215	186.665	14.355	26	34	0
13	187.295	186.960	11.255	26	33	45
14	198.960	197.770	21.735	38	33	5

Time:	5:30 PM

Prism:	388.275	388.270	-2.115		Hz Angle	
Target	Dist	Hz	Vert	Deg	Min	Sec
7	207.955	207.375	15.545	342	17	50
8	207.970	207.540	13.380	342	19	30
9	208.025	207.785	9.995	342	22	10
10	183.660	182.440	21.120	3	17	35
11	187.170	186.375	17.220	26	34	0
12	187.215	186.665	14.360	26	34	15
13	187.300	186.965	11.255	26	34	0
14	198.970	197.780	21.725	38	33	25

Time:	6:30 PM

Prism:	388.275	388.270	-2.150		Hz Angle	
Target	Dist	Hz	Vert	Deg	Min	Sec
7	207.955	207.370	15.540	342	17	45
8	207.965	207.535	13.370	342	19	40
9	208.025	207.785	9.995	342	22	15
10	183.660	182.440	21.125	3	17	35
11	187.170	186.375	17.215	26	34	0
12	187.300	186.665	14.355	26	34	30
13	187.300	186.960	11.250	26	34	5
14	198.970	197.775	21.735	38	33	30

Time:	7:00 PM

Prism:	388.275	388.270	-2.095		Hz Angle	
Target	Dist	Hz	Vert	Deg	Min	Sec
7	207.955	207.370	15.540	342	17	20
8	207.980	207.550	13.385	342	19	10
9	208.025	207.785	9.975	342	22	0
10						
11	187.170	186.375	17.225	26	33	45
12	187.220	186.665	14.365	26	34	5
13	187.300	186.960	11.260	26	33	50
14						

B-3: SPAN 3 RAW DATA

		NE Temp	32.5			
Span 3		9:20 AM		Hz Angle		
Target	Dist	Hz	Vert	Deg	Min	Sec
11	72.940	70.490	18.740	354	32	30
12	72.425	70.665	15.880	354	43	45
13	72.010	70.870	12.775	354	54	15
14	58.690	53.890	23.245	30	41	0
15	72.445	70.150	18.105	66	54	30
16	71.965	70.175	15.950	66	54	10
17	71.545	70.160	14.005	66	50	45

7.375046

0.290356 in.

		NE Temp	43.5			
Span 3		10:30 AM		Hz Angle		
Target	Dist	Hz	Vert	Deg	Min	Sec
11	72.965	70.495	18.835	354	32	20
12	72.445	70.665	15.975	354	43	35
13	72.025	70.870	12.865	354	54	5
14	58.725	53.890	23.335	30	40	55
15	72.475	70.155	18.200	66	54	35
16	71.990	70.180	16.045	66	54	0
17	70.565	70.160	14.095	66	50	45

		NE Temp	52.5			
Span 3		11:30 AM		Hz Angle		
Target	Dist	Hz	Vert	Deg	Min	Sec
11	72.945	70.490	18.760	354	32	30
12	72.425	70.660	15.900	354	44	5
13	72.010	70.865	12.795	354	54	20
14	58.695	53.885	23.265	30	41	15
15	72.460	70.155	18.125	66	54	35
16	71.970	70.175	15.975	66	54	20
17	71.550	70.160	14.025	66	51	0

		NE Temp	59.0			
Span 3		12:30 PM		Hz Angle		
Target	Dist	Hz	Vert	Deg	Min	Sec
11	72.945	70.495	18.760	354	32	5
12	72.430	70.660	15.900	354	43	40
13	72.015	70.870	12.795	354	54	5
14	58.695	53.890	23.260	30	40	55
15	72.460	70.160	18.130	66	54	45
16	71.975	70.180	15.975	66	54	5
17	71.555	70.165	14.025	66	51	0

		NE Temp	63.5			
Span 3		1:30 PM		Hz Angle		
Target	Dist	Hz	Vert	Deg	Min	Sec
11	72.990	70.490	18.935	354	32	45
12	72.465	70.660	16.070	354	43	50
13	72.045	70.870	12.965	354	53	50
14	58.760	53.885	23.430	30	40	50
15	72.505	70.160	18.300	66	54	0
16	72.020	70.185	16.145	66	53	50
17	71.590	70.170	14.195	66	50	15

		NE Temp	67.5			
Span 3		2:30 PM		Hz Angle		
Target	Dist	Hz	Vert	Deg	Min	Sec
11	72.990	70.495	18.935	354	32	35
12	72.465	70.665	16.070	354	44	25
13	72.045	70.870	12.965	354	54	35
14	58.765	53.890	23.435	30	41	30
15	72.510	70.160	18.300	66	54	40
16	72.020	70.185	16.145	66	54	30
17	71.590	70.165	14.195	66	50	45

		NE Temp	62.0			
Span 3		3:30 PM		Hz Angle		
Target	Dist	Hz	Vert	Deg	Min	Sec
11	72.975	70.490	18.870	354	32	30
12	72.455	70.660	16.015	354	44	15
13	72.035	70.870	12.905	354	55	10
14	58.735	53.885	23.370	30	41	40
15	72.490	70.160	18.235	66	55	10
16	72.005	70.185	16.085	66	55	10
17	71.575	70.170	14.135	66	51	35

		NE Temp	61.5			
Span 3		4:30 PM		Hz Angle		
Target	Dist	Hz	Vert	Deg	Min	Sec
11	72.970	70.490	18.870	354	31	50
12	72.455	70.660	16.010	354	43	25
13	72.040	70.875	12.905	354	53	55
14	58.740	53.890	23.370	30	41	5
15	72.495	70.160	18.240	66	54	10
16	72.010	70.190	16.080	66	54	0
17	71.580	70.170	14.130	66	50	50

		NE Temp	56.5			
Span 3		5:30 PM		Hz Angle		
Target	Dist	Hz	Vert	Deg	Min	Sec
11	72.960	70.495	18.810	354	32	55
12	72.440	70.660	15.950	354	43	55
13	72.025	70.870	12.840	354	54	25
14	58.710	53.885	23.310	30	41	35
15	72.475	70.160	18.175	66	55	10
16	71.990	70.185	16.020	66	54	55
17	71.565	70.170	14.065	66	51	30

		NE Temp 49.0				
Span 3		6:30 PM		Hz Angle		
Target	Dist	Hz	Vert	Deg	Min	Sec
11	72.960	70.490	18.810	354	32	55
12	72.440	70.660	15.955	354	43	50
13	72.025	70.870	12.845	354	53	55
14	58.715	53.890	23.315	30	40	15
15	72.475	70.160	18.175	66	53	20
16	71.995	70.190	16.020	66	53	10
17	71.570	70.170	14.070	66	49	50